DESIGN, FABRICATION, AND MANIPULATION OF A MULTI-DEGREE OF FREEDOM MICRO-MANIPULATOR FOR LARGE-RANGE, THREE-DIMENSIONAL OPERATION ON ATOMIC FORCE MICROSCOPE

By

PARTH PATEL

A thesis submitted to the

School of Graduate Studies

Rutgers, The State University of New Jersey

in partial fulfillment of the requirements

for the degree of

Master of Science

Graduate Program in Mechanical and Aerospace Engineering

Written under the direction of

Qingze Zou

and approved by

_____

_____

_____

New Brunswick, New Jersey

May, 2019

ABSTRACT OF THE THESIS

Design, Fabrication, and Manipulation of a multi-degree of freedom micro-manipulator for large-range, three-dimensional operation on Atomic Force Microscope

by Parth Patel

Thesis Director: Qingze Zou

AFM (Atomic Force Microscope) has become an enabling tool in a wide range of areas ranging from biology, material sciences to other nanosciences and nanoengineering areas. However, currently AFM operation has been limited to a relatively small sample area (below around 0.1 mm by 0.1 mm) and 2-D samples only. On the contrary, froniter and emerging applications in areas such as biology demands and require an AFM capable of imaging and/or measuring properties of samples over a much larger range (in mm size or even larger), and on 3-dimensional samples such as 3-D organoid cell culture.

This M.S. research work is focused on the creation of a multi-degree of freedom micro-manipulator for large-range, 3-dimensional operation of a sample on AFM. Particularly, the needs and constraints arising from integrating the AFM system to an inverted optical microscope for (optical-AFM) coordinated operation are accounted for and addressed in the design and fabrication of the manipulator. A robust stage with minimal noise and vibration needs to be designed to fulfill the goal of micro-manipulation with maximum possible accuracy. During this a '3-DOF RSR (Revolute-Spherical-Revolute) Parallel Delta manipulator' combined with '2-DOF RR (Revolute)

Serial perpendicular axis manipulator', kinematic mechanisms are coupled together to achieve micro-manipulation. High accuracy with high dynamic characteristics of parallel manipulator provides precise positioning by translation motion and two revolute joints facilitates precise orientation by rotational motion. The decoupling of the translation motion from the rotational motion of the sample helps in making a system independent to other while allowing simultaneous operation. The use of small disk design for sample holder to rotate sample, minimizes the disturbances to the solution. Design, kinematic analysis, fabrication, motion simulation, and preliminary motion control in experiments for the independent and combined configuration are covered in this research work.

Dedication

I would like to dedicate this thesis to my family and friends for their help and support.

Table of Contents

List of Tables

List of Figures

Chapter 1

Introduction

This chapter briefly describes Atomic force microscopy (AFM) and Optical Microscopy (OM) - two basic yet powerful nondestructive observation and measurement techniques. It is necessary to understand the working principles of the microscopy techniques to identify the advantages and reveal the underlying disadvantages of individual techniques. Various research work have already been undertaken to resolve and overcome some individual limitations for specific purposes. Furthermore, several work also brings attention to combining both techniques to merge their few advantages[1, 28]. Focus of this chapter is to highlight the limitations and implications of individual working of AFM and combining it with OM.

1.1 Microscopy: Methods for Non-destructive Cell Imaging

1.1.1 Atomic Force Microscopy

1.1.1.1 Working Principle

Atomic Force Microscope uses a very sharp probe which senses the inter-atomic force interaction with the substrate [28]. AFM prob tip is generally fabricated as an integral part of thin film cantilever. The change in force generated during the engagement with the sample is recorded when the probe tip scans the sample in planar surface (i.e. x and y directions). These forces are transduced in the form of error signal in the feedback circuit. This transduction is undertaken by the means of deflection of the cantilever beam generated due to the force interaction of the probe tip with the substrate, which changes the position sensor output and hence generating an error signal. Mostly these forces are in nano units. Most of the AFM instruments use optical methods for the

position sensing output. Thus, a 3-dimensional image of the sample can be obtained in a non-destructive manner.
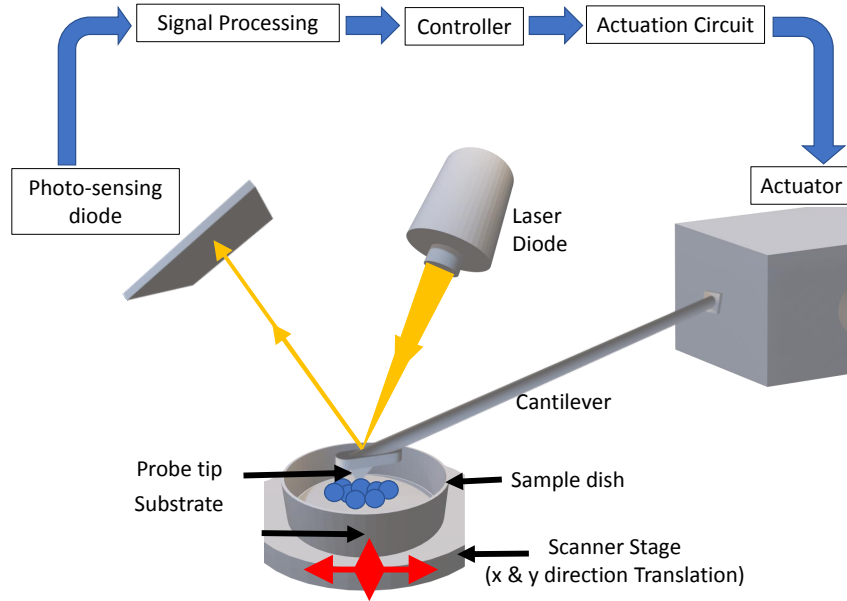
Figure 1.1: General working Principle of AFM

There are several imaging modes available while working with AFM some of which are as follows:

1. **Contact mode:** Most widely used imaging mode to measure sample topography.

2. **Constant-height mode:** In this mode, the sample is scanned horizontally and deflection is measured and recorded.

3. **Constant-deflection mode:** Sample height is constantly adjusted in this mode to maintain constant deflection of the cantilever, using a feedback loop.

4. **Tapping mode:** In this mode, probe is externally excited along with monitoring amplitude and phase of the cantilever near the resonance frequency of the cantilever. [28, 29]

1.1.1.2   Advantages

1. High resolution scanning probe microscope in order of nanometers more than 11000 times better than optical diffraction limit;

2. Direct contact with the substrate using a probe tip and piezoelectric components facilitates accurate and precise scanning;

3. Provides three dimensional surface profile without any specific requirements for treating the sample which damages the sample;

4. Mostly, it can work in ambient air or liquid environment.

1.1.1.3   Limitations

1. Slow rate of scanning during AFM imaging often leads to thermal drift in the image, making less suitable for measuring dynamic samples as mentioned in [30]. Various approaches have been made to achieve high-speed imaging on AFM [31].

2. Effects of non-linearity, hysteresis, creep of the piezoelectric material, and cross-talk between the x, y, and z axes.

3. AFM system has limited scanning capabilities of an image with a maximum height of 10-20 μm and scanning area of about 150×150 μm.

1.1.1.4   Critical Factors for AFM

1. The size and shape of the AFM probe plays an important role in determining the image contrast. Figure 1.2a on page 4, explains the motion of the probe tip over the sample on a sample holder. Figure 1.2a on page 4, explains the data loss due to the probe tip shape. This can be overcome up to a certain limit using thinner probe tip as shown in figure 1.3 on page 4 because of the nanofabrication capabilities.

(a) Intermediate Position of the Probe tip for given sample

(b) Loss of data due to probe shape
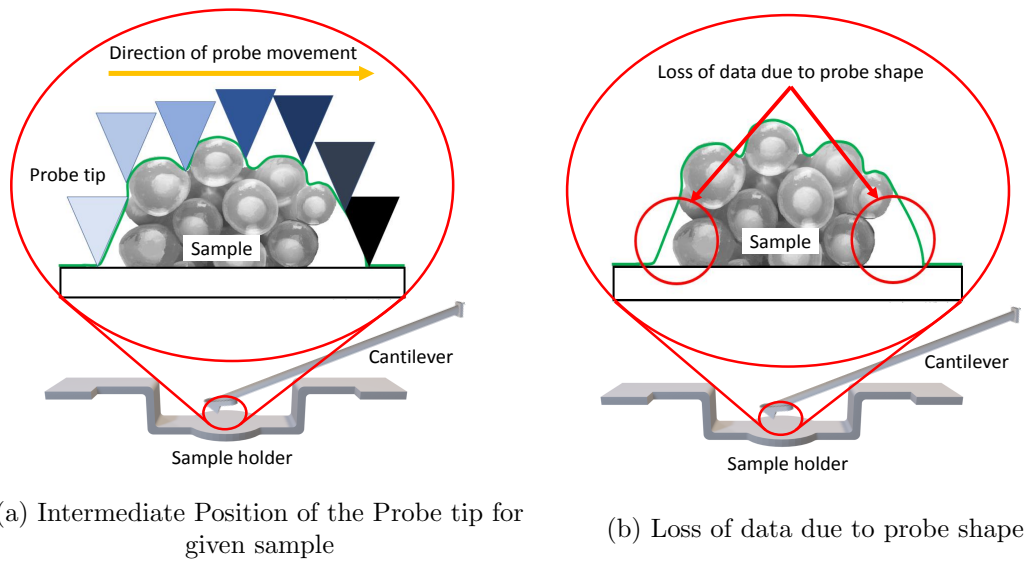
Figure 1.2: Limitation due to probe shape
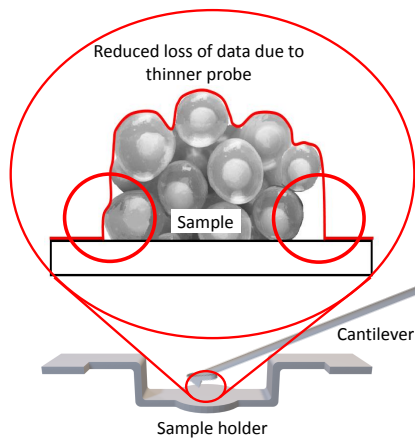
Figure 1.3: Reduced loss of data due to thinner probe tip

2. Accurate and highly efficient motion measurement is very important in nanoscale manipulation. Common tools and techniques: High-precision linear potentiometers and capacitance displacement sensors;

3. When measuring a nanoscale motion using AFM; if measurement speed is low it may shift the results with time;

4. Measurement resulting in voltage undergoes various calculations and computations which also influences the measurement precision

1.1.2 Optical Microscopy

1.1.2.1 Working Principle

Optical microscopes works on the principle of using visible light and system of lenses to enlarge the small substrates by considerable factor. Using earliest versions of Optical microscopes substrates would be directly observed by the user with visible light. Figure 1.4 on page 5 shows the path of light travelled from source to user via substrate and lenses. Initially, Photographic films were used to capture the images which was then replaced by other modern technologies. These days, it is very common to project digital images on a computer screen directly. Variants of optical microscopes have been developed for distinct purposes [1].
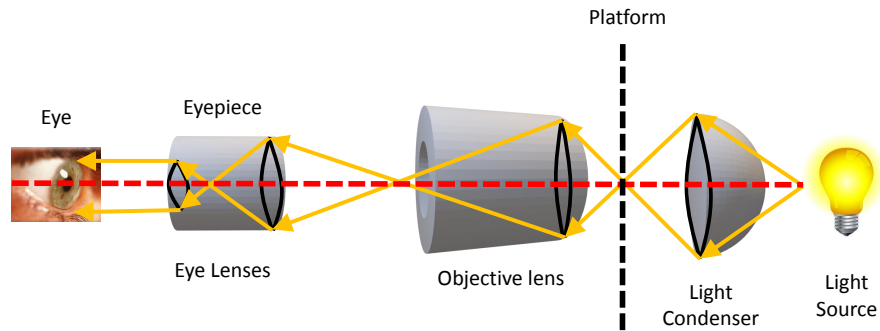
Figure 1.4: General working Principle of Optical Microscope

1.1.2.2 Advantages

1. Inexpensive when compared with the other high-resolution measurement techniques like transmission/scanning electron microscope (TEM/SEM);

2. Simple and direct imaging process, eliminating transformation on information;

3. Along with the in-plane properties, 3D coupling properties can also be measured.

4. Various optical techniques are now being used to modify or stimulate samples of interest.

1.1.2.3 Limitations

1. **Resolution:**

   Minimum resolution (d) of an optical microscopy is limited by its aperture size [1].

   $$d = 0.61 \frac{\lambda_0}{NA} \tag{1.1}$$

   where λ_0 is the wavelength in vacuum, and NA is the numerical aperture of the optical component. (Maximum 1.3-1.4). Thus, the resolution limit is usually around $\lambda_0/2$ (about 200 nm) for conventional optical microscopy

   This limitations were overcome up to certain extent by the use of multiple scattering of light which improves the resolution up to about 100 nm [1].

2. **Near-Field Scanning Optical Microscopy: limitations**

   Near field scanning optical microscopy (NSOM) breaks the Abbe's diffraction limit (optical spreading out of each image point in diffraction disk). It uses a probe which is placed very close to the specimen surface. High spatial, spectral, and temporal resolving power are used to conduct the surface inspection [1].

   Limitations of this technology are:

   (i) limited resolution, limited by the size of the probe aperture,

   (ii) significantly low working distance and extremely shallow depth of field,

   (iii) limited to surface study,

   (iv) not conducive for studying soft materials,

   (v) long scan times for large sample areas.

3. **Difficulties in 3D motion measurement with high resolution**

   (i) Sensor drift and non-linearity caused while maneuvering a stage with sub-nanometer accuracy throughout the entire work-space of stage poses difficulties;

(ii) kinematic transformation between the coordinate frame of the stage measurement system and that of the object being controlled is not perfectly understood;

(iii) Uncertainties induced by mechanical forces and thermal variations affects the alignment and calibration causing in system time variance. Optimal feedback would be required to deal with the direct metrology and find the relative position and orientation of the object that are subjected to 3D positioning, alignment and engagement.

1.2 Summary for application fields and advantages

Following table summarizes the applications and advantages of the optical and Atomic force microscopy [1].

Type of Microscopy	Application fields	Advantages
Atomic Force Microscopy	Nanobiology[1, 30, 32] Nanaomaterials Nanoelectric Devices	(1) High Resolution (2) Precise scanning (3) 3D surface profile (4) Work in air and liquid medium
Optical Microscopy	2D Motion Measurement 3D Motion Measurement Shape reconstruction	(1) Inexpensive (2) Simple and direct (3) Fit for 2D and 3D measurements

Table 1.1: Applications and Advantages of Optical and Atomic Force Microscopy [1]

1.3 Technical challenges and focus of work

Possible avenues for using both AFM and OM together have been proposed and discussed in several research works [1] and literature review [33].

The technical challenges addressed in this research work related to individual issues and conjunction of microscopy techniques are as follows:

1. **3D Manipulation:**

   While working with the conventional AFM, the stages moves in x, y and z directions only with limited range of motion. This research work proposes to use two rotational axis for orientation of sample in desired direction for improved and detailed scanning results. This can also overcome the limitation for the data loss due to the probe tip shape configuration as mentioned in figure 1.2.

2. **Increased Range of motion:**

   As discussed in the limitations section of AFM, the current movement of the stage is limited to micrometers range. The goal is to increase this working range to millimeters.

3. **Robust Stage:**

   A robust custom-made stage is required for most of the optically interfaced AFMs, to support the instrument and minimize the mechanical noise

4. **Optical focus of the inverted microscope:**

   Optical focus of the inverted microscope is limited up to to a certain height from the stage due to depth of focus depending on the lens used for magnification.

5. **Opacity of the stage holders:**

   Incorporation of top down optical access into AFM designs for optical access is another difficulty that is posed while dealing with combining these two techniques.

6. **Space constraints:**

   The stage designed must also consider the requirements of the desired movement. While combining the two microscopy techniques it is important to consider most of the parts related to individual tools, neglecting this parts would result in the risk of interference.

Chapter 2

Design Methodology

A step by step detailed procedure of the design methodology used to come up with the final version of the manipulator will be discussed in this chapter. Initially, the working environment and critical parameters that are to be considered for the design would be discussed in detail. During this step all the components that interacts with the manipulator were identified and limitations and constraints of it were discussed.

Furthermore, targets are established, because it is very important to begin with the clear idea of desired output while designing a manipulation system. Hence, in this step most of the inputs were taken from the laboratory and research advisor to select the optimal desired output.

Moving forward various robotic manipulators were reviewed and analyzed for their characteristics and performance parameters. This proved to be very critical and helpful for selection of the final configuration concept and determining the link dimensions. While considering the link dimensions an iterative process was conducted to meet the established target.

The entire design methodology is outlined in the following figure 2.1.

Defining working environment and identifying critical parameters → Establish target specifications → Generate and evaluate concepts → Select final concept for modelling configuration
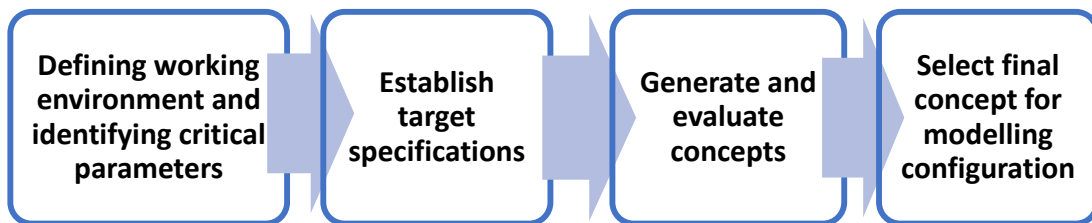
Figure 2.1: Outline for design methodology

2.1 Defining working environment and identifying critical parameters

2.1.1 Identifying the system - AFM and OIM

Initially, the Atomic force microscope (AFM) and Optical Inverse Microscope (OIM) setup to be used in conjunction were identified as shown in the following table 2.1 :

Type of Microscope	Setup in Lab
Atomic force microscope	Dimension Icon head - Atomic Force Microscope system with ScanAsyst from Bruker [34].
Optical Inverse Microscope	Inverted Microscope Diaphot 200 from Nikon Corporation, Japan [35].

Table 2.1: AFM and OIM Setup in Laboratory

(a) Dimension Icon head - Atomic Force Microscope system with ScanAsyst from Bruker [36]

(b) Inverted Microscope Diaphot 200 from Nikon Corporation [37]

Figure 2.2: AFM and OIM Setup in Laboratory

2.1.2 Defining the manipulator - components

1. **Sample:** The micro/nano particles that are to be analyzed using AFM and OIM.

2. **Sample Holder:** A base for the sample (i.e. micro/nano particles) used as a substrate, in order to grow and/or examine sample properties and characteristics.

3. **Petri Dish:** A shallow, circular, transparent dish with a flat lid, used for the culture of microorganisms.

4. **Stage:** Flat surface on which the Petri Dish is supported.

Goal of defining these components is to clearly identify their role in the functioning of the system and modify it for the extension of its application. As shown in the figure 2.3a the sample is placed directly on the petri dish or allowed to grow on the surace of petri dish directly. The modified version of it is proposed in the figure 2.3b in which the sample is placed on the sample holder so that the medium in the petri dish remains undisturbed. Simultaneously, the sample can be free for independent manipulation while still remaining inside the medium.

(a) Current manipulation setup for the AFM

(b) Modified manipulation setup for the AFM with increased degree of freedom
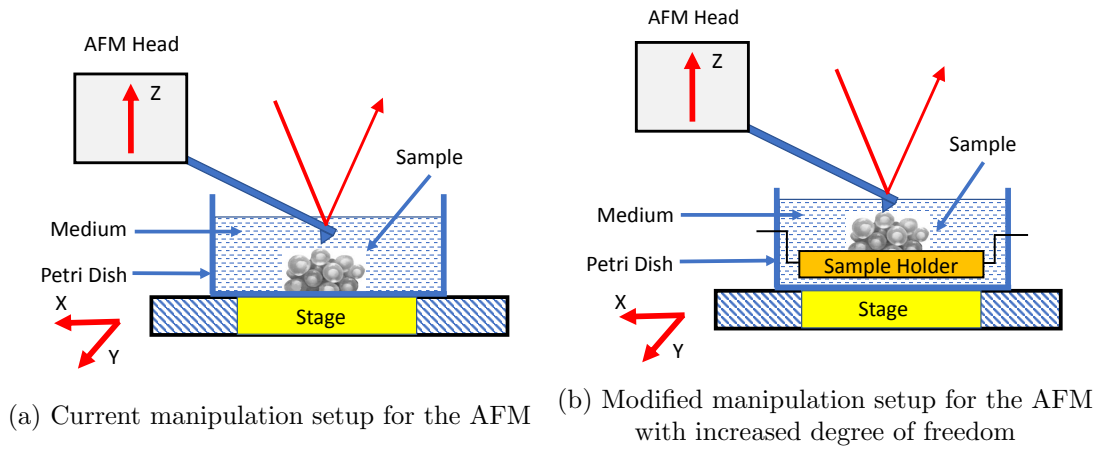
Figure 2.3: Current and modified manipulation setup for the AFM

2.1.3 Identifying and analyzing the parts of AFM and OIM interacting with the manipulator

1. In order to know the working environment for the stage the AFM and OIM, the parts of AFM and OIM that interacts with the sample directly were identified. They are as shown in the table 2.2 and figure 2.4.

Microscope	Interacting Part
Atomic Force Microscope	(1) Optics (2) Scanner head
Inverted Optical Microscope	(1) Platform

Table 2.2: AFM and OIM parts interacting with manipulator

(a) AFM parts
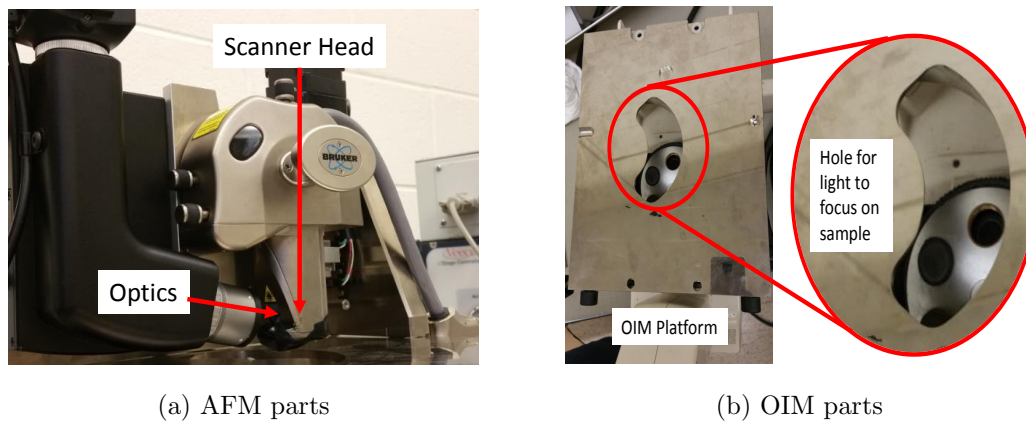
(b) OIM parts

Figure 2.4: AFM and OIM parts interacting with manipulator

2. For examining the space constraints the AFM in entirety was studied. See the following figure 2.5
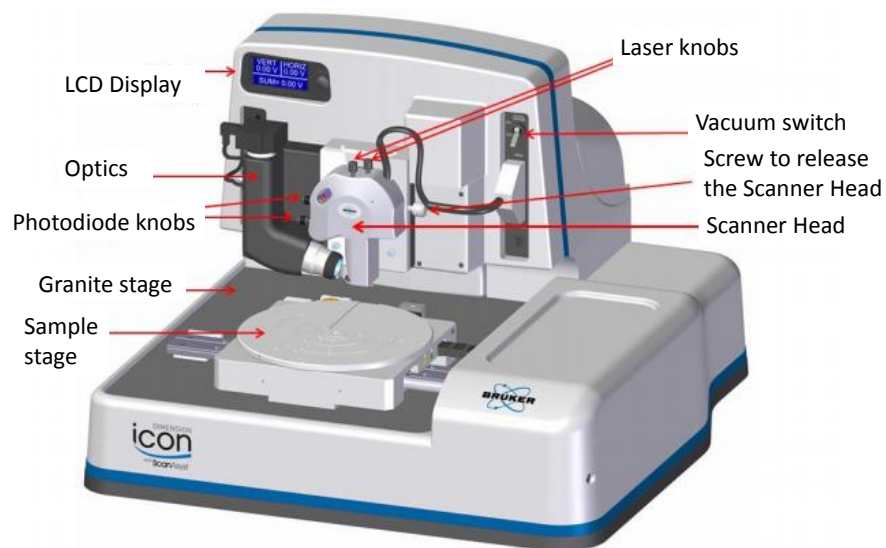
Figure 2.5: AFM parts with labelling [6]

3. Furthermore, all the parts were disassembled and individually measured as shown in the figure 2.6.
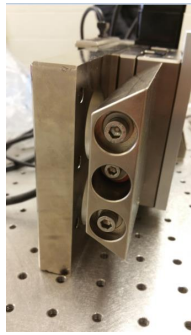
(a) AFM Icon head linear guide

(b) AFM Icon head

(c) Measuring AFM Icon head probe tip

Figure 2.6: AFM and parts disassembled and measured

4. After measuring the parts individually an analysis of the complete setup (i.e. temporarily assembled AFM and OIM) was done, to identify the space constraints which are shown in the figure 2.7 and figure 2.8.
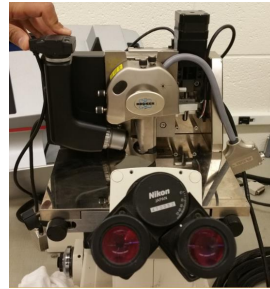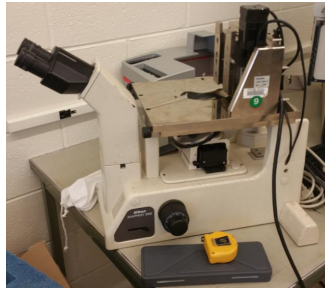
Figure 2.7: Temporary assembly of AFM and OIM
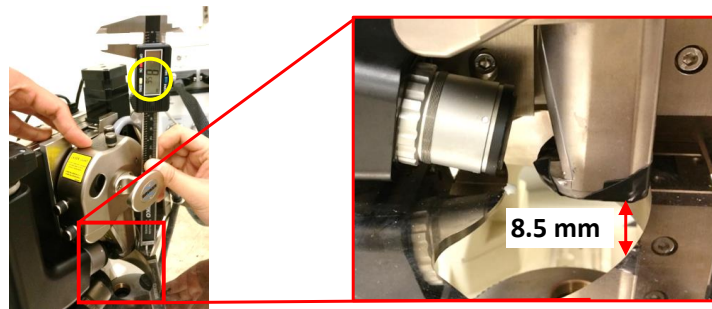
Figure 2.8: Space constraint in z-direction

5. In order to understand the dynamic relation of the OIM and the AFM parts, all the parts that were individually measured, were then modelled in the CAD software (SOLIDWORKS). Additionally, since the space in z-direction was very tight a rough idea of a support block was proposed to elevate the dimension Icon head by $\approx$ 33 mm. See the figure 2.9 for the proposed support block and figure 2.10 for the increase in z-direction constraint because of the support block.
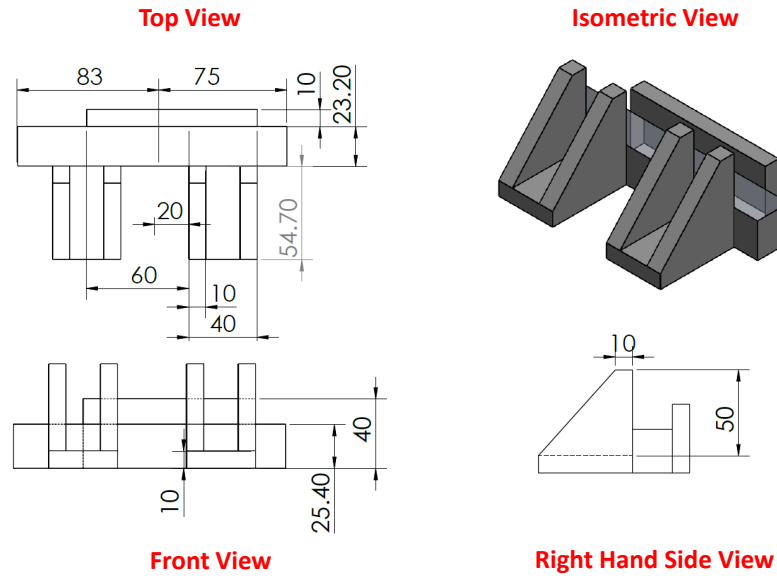
Figure 2.9: Proposed rough design for support block to elevate the scanner head
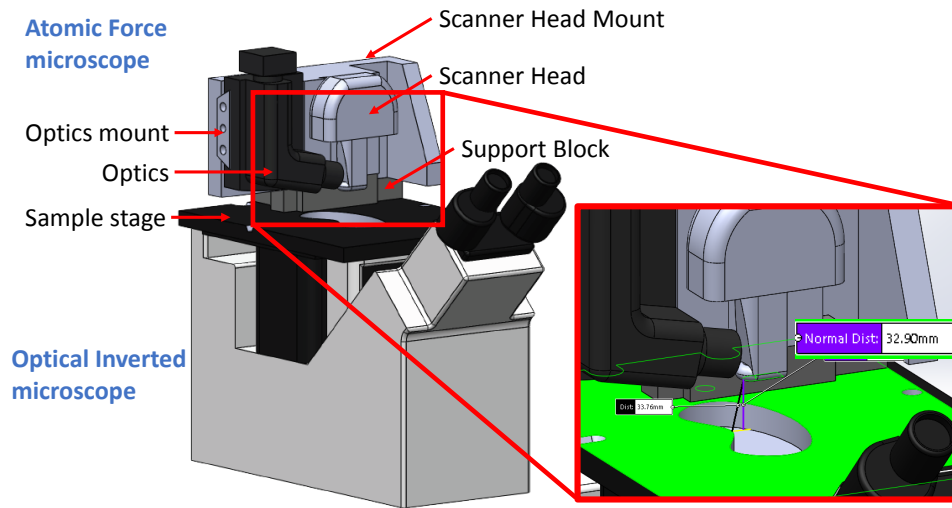
Figure 2.10: Increase in z-direction constraint because of the support block

2.2 Establishing target specification

2.2.1 Defining the end-effector - desired manipulation

Subsection 1.3 discusses about the technical challenges for the 3D manipulation of the stage for a combined system of AFM and OIM. This section gives the details of the manipulation desired as an output and establish the target specification. See the following table 2.3.

Component	Type of manipulation	Variables assigned
Stage	3-Axis Linear manipulation	(x, y, z)
Sample	2-Axis Rotational manipulation	(ϕ, ψ)

Table 2.3: End-effector - components and its desired manipulation

See the following figure 2.11 for detailed explanation of the expected outcome. It is to show the sample on the sample holder acts as the end-effector and in order to manipulate the sample, the sample holder is targeted to have 3-axis linear manipulation and 2-axis rotational manipulation
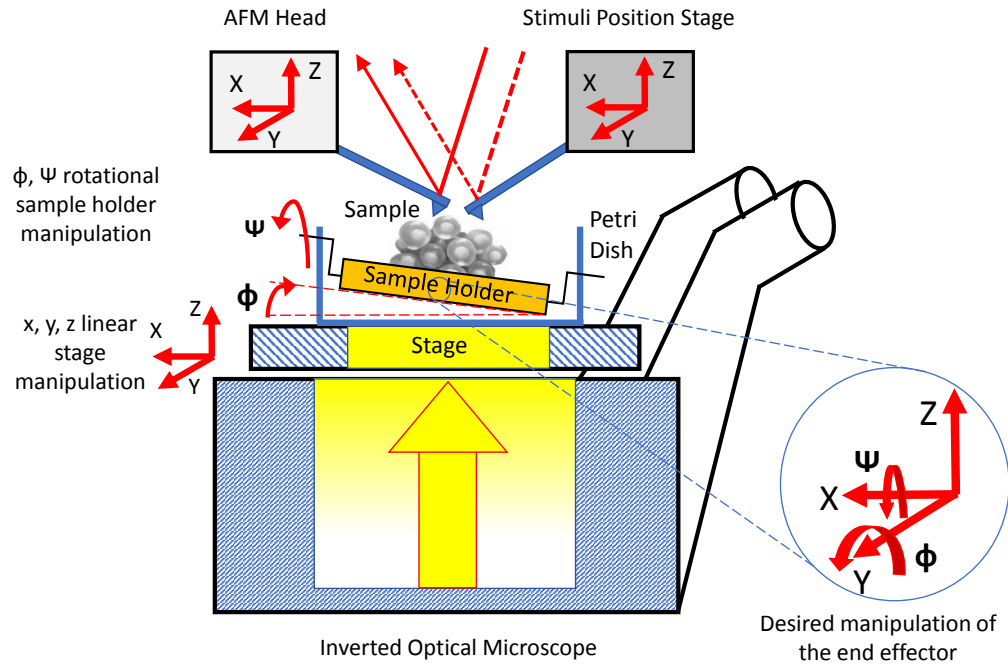
Figure 2.11: Defining the end-effector - components and desired output

2.2.2 Defining the end-effector - desired accuracy for manipulation

Type of manipulation	Variables assigned	Desired accuracy
3-Axis Linear manipulation	(x, y, z)	**5-10 μm**
2-Axis Rotational manipulation	(ϕ,ψ)	1°

Table 2.4: Desired accuracy for manipulation

2.2.3 Defining the end-effector - target work space

Considering the area of Optical focus of the OIM as shown in the figure 2.12, and the space constrain in z-direction because of the AFM scanner head as discussed in 2.1.3 the desired work space was established as shown in the following figure 2.13.
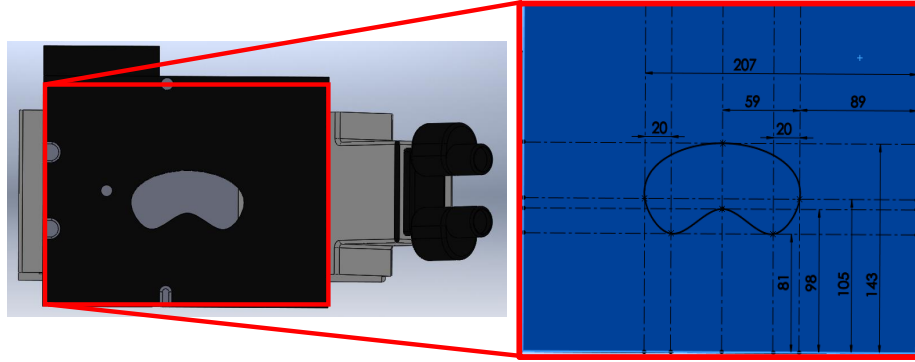
Figure 2.12: Area on OIM platform available for focus
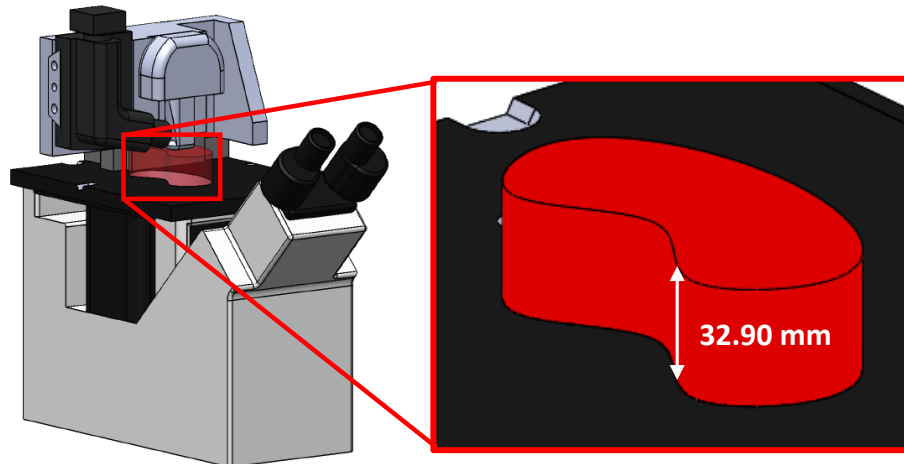
Figure 2.13: Target work space

Establishing, X-axis parallel to the horizontal in figure 2.12 we define the target range as X-axis range - 62mm, Y-axis Range - 207 mm and Z-axis range from 237 mm (height of the top of platform to the base of the OIM) to 270 mm.

2.3 Generation and evaluation of concepts

For obtaining a solution to having a large range, 3D operation on atomic force microscope, a manipulator structure should be carefully selected. To do his various series and parallel robots characteristics were reviewed [2, 3, 38]. A brief discussion of the types of robots their performance characteristics and parameters will be done in this section.

2.3.1 Defining - types of manipulator structures

A manipulator which are re-programmable and performs variable motions in a programmed manner can be defined as a robot. A classification of robots based upon their kinematic structure shall be discussed in this work primarily. There are two types of robots based upon their topological formation. These are as follows:

1. **Series manipulator:** If the kinematic structure consists of open loop chain, it can be defined as a series manipulator. An example is as shown in figure 2.14a.

2. **Parallel manipulator:** Kinematic structure formed by the closed loop links then it can be defined as a parallel manipulator.

3. **Hybrid manipulator:** A manipulator having both open and closed loop chains are defined as hybrid manipulator.

2.3.2 Characteristics of manipulators based on their structure

The most critical parameter while selecting a manipulator structure for this research work is accuracy. For this application parallel manipulators are the best selection because of their advantages over serial robots. As summarized in the following table 2.5, parallel manipulators offers higher precision, better stiffness, low inertia, higher

(a) Series PPR manipulator designed for shoot peening mechanism [39]

(b) 3-RRS Parallel Manipulator [40]
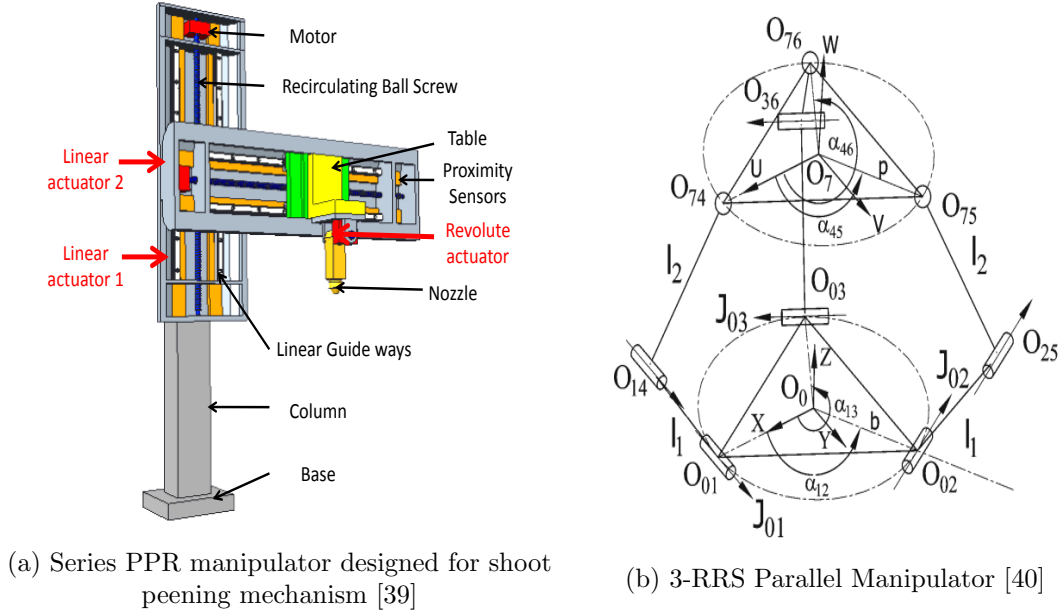
Figure 2.14: Example of series and parallel manipulators

operating speeds and accelerations. However, parallel manipulators are difficult to design because of their complex kinematics and actuation [2].

Even though theoretically parallel manipulators are more accurate than the serial manipulator, practically serial manipulators are widespread in industrial application because of the ease of manufacturing and calibration techniques [38]. Mechanical design, fabrication and calibration are key factors in the accuracy although the optimal kinematic design plays an important role. It is easy to conclude that for the application of ultra precision positioning parallel manipulators serves the purpose best [2, 38].

2.4   Selection of concepts

2.4.1   Selection of the structure

Based on the arguments made in the previous subsection 2.3.2, it was decided to use a parallel manipulator for the precision linear motions. For the rotational motions it was decided to use the serial manipulation by a pair of revolute joints. This can be summarized as shown in the following table 2.3

Parameter	Serial Manipulator	Parallel Manipulator
Workspace	**Large**	Small and complex
Position Error	Accumulates	**Averages**
Force Error	**Averages**	Accumulates
Maximum force	Limited by minimum actuator force	**Summation of all actuator forces**
Stiffness	Low	**High**
Dynamic Characteristics	Poor, especially with increasing the size	**Very high**
Inertia	Large	**Small**
Payload/Weight ratio	Low	**High**
Speed and Acceleration	Low	**High**
Accuracy	Low	**High**
Calibration	**Relatively Simple**	Complicated
Workspace/Robot size ratio	**High**	Low
Preferred application	Gross motion	**Precise Positioning**

Table 2.5: Characteristics of serial and parallel manipulators [2, 3]

Type of Manipulation	Variables assigned	Desired accuracy	Selected structure
3-Axis Linear manipulation	(x, y, z)	**5-10 μm**	Parallel
2-Axis Rotational manipulation	(ϕ,ψ)	1°	Serial

Table 2.6: Selected structure for manipulation

2.4.1.1 Selection of the model for parallel manipulator structure

There have been extensive work done in the field of developing parallel robots for industrial applications. A brief discussion about the history of the parallel manipulators with their applications was studied[3]. Most, widely adopted types of Parallel manipulators are (i) Hexapods and (ii) Delta Robots [3].An example of each is as shown in figure 2.15.

Parallel manipulators can be classified as (i)symmetrical or (ii)asymmetrical. For a parallel manipulator to be symmetric it has to fulfill the following conditions:

1. Number of links must be equal to the number of degrees-of-freedom (DOF) of the moving platform.

(a) Hexapods for ultra precision positioning [3]

(b) Ultra-fast pick and place robot
ABB-Flex Picker IRB 340 [3]

Figure 2.15: Examples of Hexapods and Delta manipulators

2. The arrangement of all the links in the manipulator must be in an identical pattern.

3. Location and number of actuators are same.

If a manipulator fail to fulfill all the conditions for symmetric parallel manipulator it is said to be asymmetrical parallel manipulator.

Furthermore, on the basis of their motion characteristics as (i) Planar, (ii) Spherical and (iii) Spatial which is described further in details in table 2.7 on page number 20 [3, 4].

Type of Manipulator	Description
Planar	In this manipulator more than one parallel links connects to a common platform and moves in planes parallel to one another
Spherical	Spherical motion of the joint actuators have a common center coordinate can be classified as spherical manipulators
Spatial	If any one of the links of parallel manipulators shows general spatial motion it becomes spatial manipulator

Table 2.7: Types of parallel manipulators based on motion characteristics [3, 4]

Another critical consideration to be made while selecting the type of parallel manipulator is the actuation of joints. If a joint is directly actuated and controlled, or in direct contact with the end effector it is described as an active joint. All other joints

acts as passive joints which assists the transmission of motion from the joints actuated to the joints connected with the end effector. The types of joint actuation considered for the work are: (i) Prismatic, (ii) Revolute, (iii) Spherical, and (iv) Universal. See the table 2.8 and figure 2.16 on page number 21 for the description of each.

Joint Actuator	Description
Prismatic (P)	Links translates with respect to one another on an axis
Revolute (R)	Links rotates with respect to one another on an axis
Cylindrical (C)	Links rotates and translate with respect to one another on an axis
Spherical (S)	Links rotates with three degrees of freedom about the center of the joint. Also known as a ball-and-socket joint.

Table 2.8: Types of joint actuation [4]

Prismatic
1 Degree of Freedom

Revolute
1 Degree of Freedom

Cylindrical
2 Degrees of Freedom

Spherical
3 Degrees of Freedom
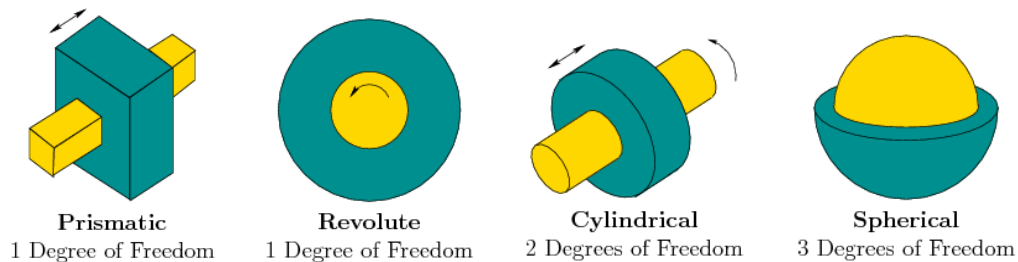
Figure 2.16: Types of 3D joints arising from the 2D surface contact between two bodies [7]

Large number of variations in architectures of manipulators can be achieved by different combinations of joint actuation between links. A substantial work presented in [4] was studied for further narrowing down the selection of the parallel manipulator for the current application. The factors considered were as follows:

1. **Practicality:** It is impractical to have three links or more than three links for current application. Also, legs with two revolute joints in series causes to fold up so it is not a feasible option.

2. **Passive prismatic joints:** Because of the difficulty in controlling the prismatic joints they are avoided.

3. **Symmetry:** All actuated legs are assumed to have the same kinematic structure.

4. **Proper type of motion:** Links resulting in complicated motion shall not be used. Hence, universal joints were discarded.

5. **Manufacturing ease:** Joint actuators shall be easy to fabricate and/or purchase from the market.

6. **Calibration ease for accuracy:** It should be simple to calibrate the joints, reduce generation of possible position errors and precise repeatable motion.

This leads to the configurations - RRS, RSR, RPS, PRS for 3DOF manipulation. After a thorough brainstorming and careful considerations of all the configurations it was decided to use a very famous Delta parallel robot with 3DOF-RSR configuration as shown in figure 2.18. This robot is also called as Clavel's Delta Robot because it was invented by Reymond Clavel in 1985 [41]. A schematic diagram of the Delta robot is shown in figure 2.17.
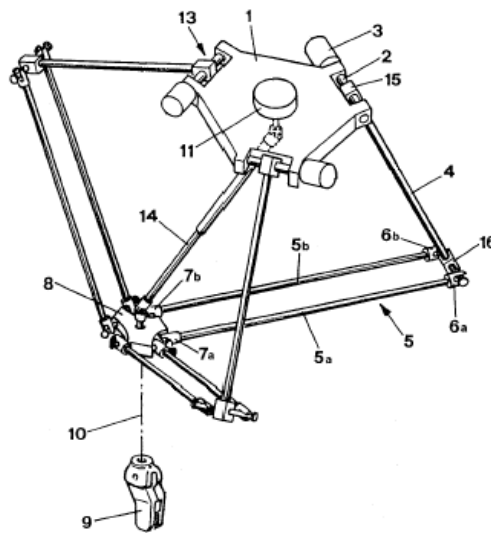
Figure 2.17: Schematic of the Delta robot (from US patent No. 4,976,582)

As shown in the figure 2.17 the delta robot consists of two platforms: the upper fixed platform (1), with three motors (3) mounted on it, and lower moving platform (8), with an end effector (9). The platforms are connected through three arms with

parallelograms; the parallelograms restrain the orientation of the lower platform to be parallel to the working surface. The motors (3) actuates the active revolute joints (2) to set the position of the biceps (4), this sets the passive spherical joints (6) to move since the set of arms (5), are connected at the end effector (8), with active revolute joints (7). This is how the end effector is set in x,y and z coordinates. While the fourth motor (11) is used for rotation of the end effectors [42]. The figure 2.18 shows
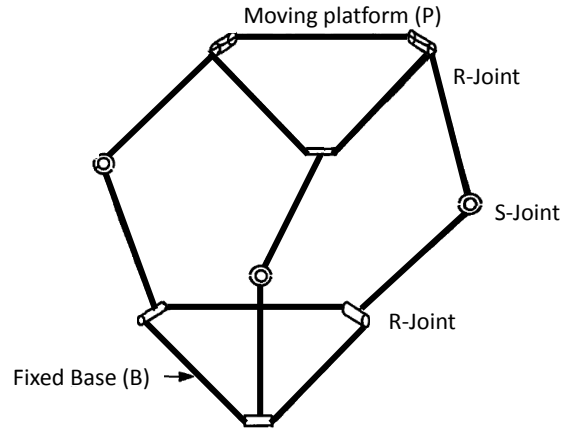
Figure 2.18: Schematic diagram of a 3-RSR parallel manipulator

the 3-RSR parallel configuration which is similar in operation but in inverted fashion. Here, the lower platform is fixed while the upper platform acts as an end effector. This configuration does not includes a rotation at the end effector.

2.4.2   Summary of the final manipulator configuration

The following table 2.9 shows the final selection of the model for parallel manipulator for the linear manipulator and joint actuation for the rotational manipulation.

Type of Manipulation	Variables assigned	Desired accuracy	Selected structure	Model configuration
3-Axis Linear manipulation	(x, y, z)	**5-10 μm**	Parallel	3-RSR i.e. Inverted Clavel's Delta Manipulator
2-Axis Rotary manipulation	(ϕ,ψ)	1°	Serial	Revolute joints used for $\perp^{lr}$ connection of links

Table 2.9: Model configuration for parallel manipulator and serial manipulator

Chapter 3

Kinematics

This chapter will include the kinematic analysis of the 3-DOF RSR Parallel Delta Manipulator and two serial revolute joints. This kinematic analysis also incorporates the direct and inverse kinematics of individual parallel and serial manipulator and a complete set of both the kinematics grouped together in a global coordinate frame. This kinematic analysis helps in generating the workspace and decide the dimensional links as per [5]. Further, a simulation of the links is done in MATLAB for both parallel and serial robot individually and then as a combination of both together.

3.1   Kinematic Analysis for 3-DOF RSR Parallel Delta Manipulator

R. L. Williams in [43] describes the kinematic analysis for Delta parallel manipulator. In this research work the orientation of the 3-DOF RSR Parallel Delta Manipulator is inverted due to which there is change in the kinematic equations from [43].

3.1.1   3-DOF RSR Parallel Delta Manipulator: Description

The labelled diagram of the 3-DOF RSR Parallel Delta Manipulator is shown in figure 3.1 on page number 25. In 3-DOF RSR Parallel Delta Manipulator three lower links or biceps (L) are connected to a fixed base. All these lower links are able to rotate angle θ_i , i = 1,2,3 with the help of motor actuators (B), hence forming a revolute (R) joint. Here, when $\theta = 0$ the lower links becomes coplanar with the fixed base. Furthermore, these three lower links are connected with the upper links or arms (l) by a spherical (S) joint. Finally, all these upper links connects at the moving platform (P) with another revolute (R) joint. This moving triangular platform has the end effector with (x_P, y_P, z_P) coordinates.
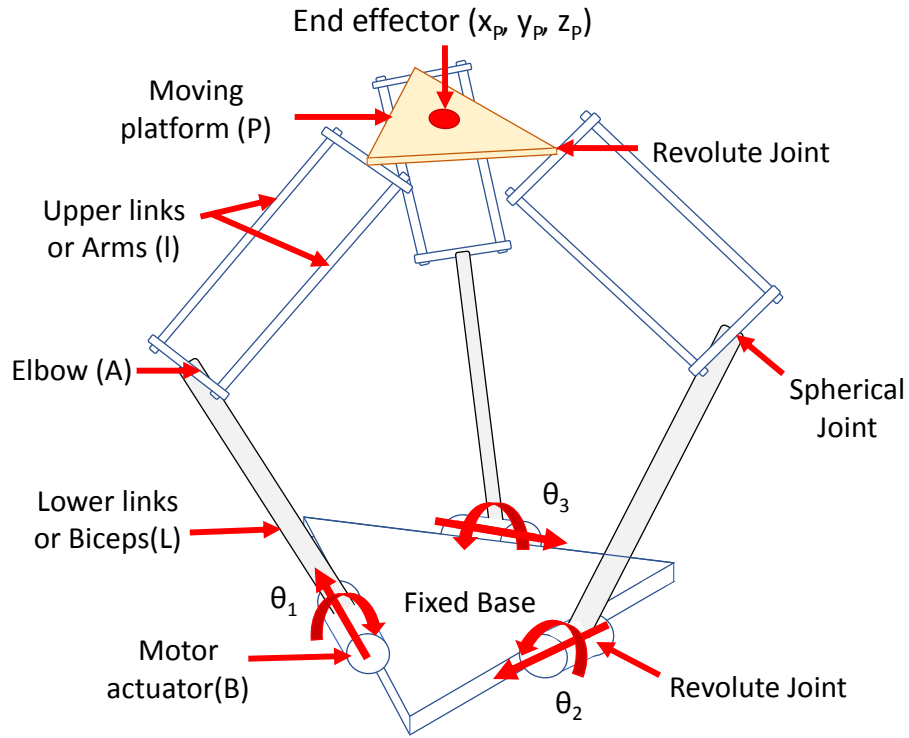
Figure 3.1: Labelled diagram for 3-DOF RSR Parallel Delta Manipulator

The summary of the nomenclature is as shown in the following table 3.1

Identifier	Description
B_i	Revolute joint locations between lower links and fixed base
θ_i	Rotation at the revolute joint actuated by motors
L	Lower links or biceps
A_i	Spherical joint (Elbow joint) locations between lower links and upper links
l	Upper links or arms
P_i	Revolute joint locations between upper links and moving platform
(x_P, y_p, z_p)	End-effector coordinates at moving platform

Table 3.1: Summary of nomenclature for 3-DOF RSR Parallel Delta Manipulator

The figure 3.3 shows the Cartesian coordinates attached to the fixed frame $\{B\}$, with the center of the fixed base as origin. The final coordinate frame is $\{P\}$, with the center of the moving platform as end-effector. The orientation of $\{P\}$ does not changes with respect to the fixed base frame $\{B\}$ so rotation matrix $_P^B R = I_3$ is constant. The nomenclature applied to the diagram is shown in the next figure 3.2. The joint variables are $\Theta = \{\theta_1 \quad \theta_2 \quad \theta_3\}^T$, and the Cartesian variables are $^B P_P = \{x \quad y \quad z\}^T$. This is a symmetric parallel manipulator.
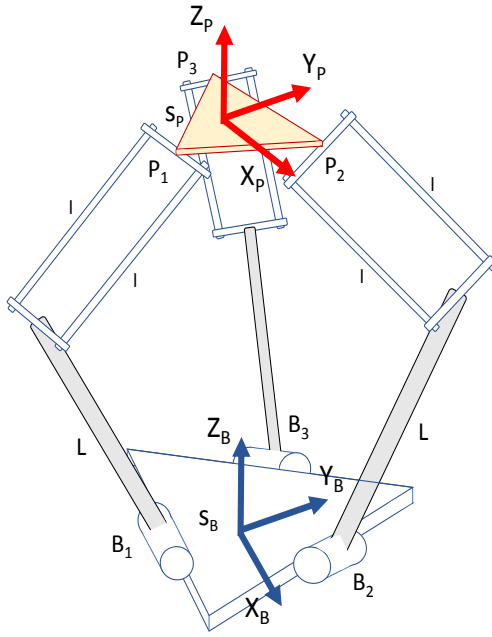
Figure 3.2: 3-DOF RSR Parallel Delta Manipulator Kinematic Diagram with coordinate frames
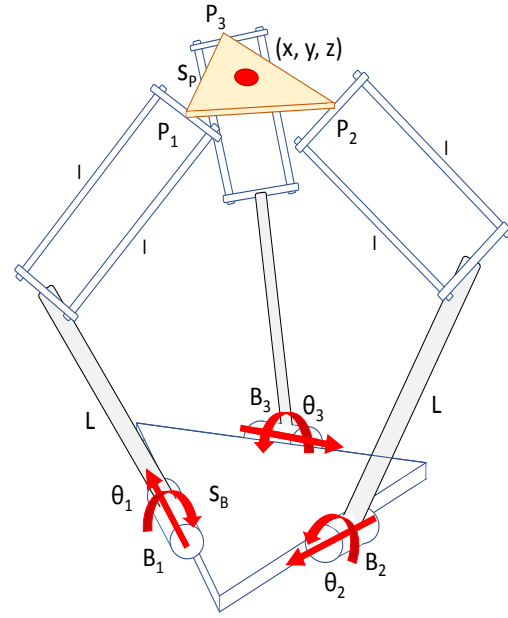
Figure 3.3: 3-DOF RSR Parallel Delta Manipulator with actuators and end-effector

The following figure 3.4 shows the 3-DOF RSR Parallel Delta Manipulator fixed base geometry and figure 3.5 on page number 27 shows the moving platform geometry. This moving triangular platform has the centroid/circumcenter as the end effector with (x_P, y_P, z_P) coordinates because it is an equilateral triangle. The orientation of the moving platform does not changes with respect to the fixed base.

The fixed-base revolute joints B_i are constant in the base frame $\{B\}$ and the platform-fixed revolute joint connection points P_i are constant in base frame $\{P\}$:
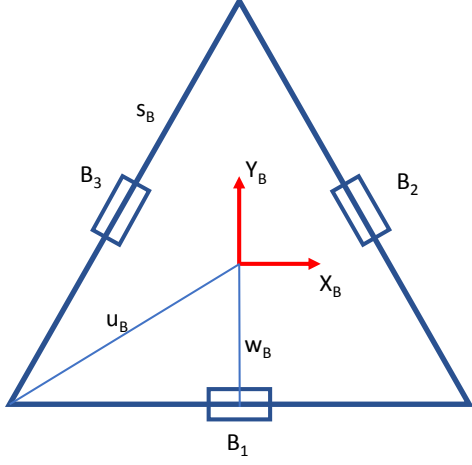
Figure 3.4: Fixed Base geometry
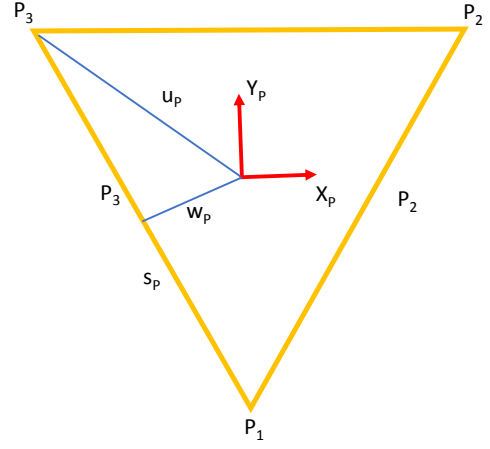
Figure 3.5: Moving Platform geometry

$$\{^{B}B_1\} = \left\{ \begin{array}{c} 0 \\ -w_B \\ 0 \end{array} \right\} \qquad \{^{B}B_2\} = \left\{ \begin{array}{c} \frac{\sqrt{3}}{2}w_B \\ \frac{1}{2}w_B \\ 0 \end{array} \right\} \qquad \{^{B}B_3\} = \left\{ \begin{array}{c} -\frac{\sqrt{3}}{2}w_B \\ \frac{1}{2}w_B \\ 0 \end{array} \right\} \qquad (3.1)$$

$$\{^{P}P_1\} = \left\{ \begin{array}{c} 0 \\ -u_P \\ 0 \end{array} \right\} \qquad \{^{P}P_2\} = \left\{ \begin{array}{c} \frac{s_P}{2} \\ w_P \\ 0 \end{array} \right\} \qquad \{^{P}P_3\} = \left\{ \begin{array}{c} -\frac{s_P}{2} \\ w_P \\ 0 \end{array} \right\} \qquad (3.2)$$

$$\{^{B}b_1\} = \left\{ \begin{array}{c} \frac{s_B}{2} \\ -w_B \\ 0 \end{array} \right\} \qquad \{^{B}b_2\} = \left\{ \begin{array}{c} 0 \\ u_B \\ 0 \end{array} \right\} \qquad \{^{B}b_3\} = \left\{ \begin{array}{c} -\frac{s_B}{2} \\ -w_B \\ 0 \end{array} \right\} \qquad (3.3)$$

where:

$$w_B = \frac{\sqrt{3}}{6}s_B \qquad u_B = \frac{\sqrt{3}}{3}s_B \qquad w_P = \frac{\sqrt{3}}{6}s_P \qquad u_P = \frac{\sqrt{m}}{3}s_P$$

R.L. Williams also discusses the mobility for the revolute-input delta robot [43] by applying the concept of three parallel four-bar mechanisms to the spatial Kutzbach mobility equations.

$$M = 6(N-1) - 5J_1 - 4J_2 - 3J_3$$

where:

M is the mobility, or number of degrees-of-freedom; N is the total number of links, including ground; J_1 is the number of one-DOF joints; J_2 is the number of two-DOF joints; J_3 is the number of three-DOF joints;

$$for, \quad N = 14, \quad J_1 = 15, \quad J_2 = 0, \quad J_3 = 0$$

$$M = 6(14 - 1) - 5(15) - 4(0) - 3(0)$$

$$M = 3DOF$$

3.1.2   3-DOF RSR Parallel Delta Manipulator: Kinematic Analysis

Vector-loop closure equations for 3-RSR Delta manipulator can be written as 3.4 from the kinematic diagram shown in the figure 3.4:
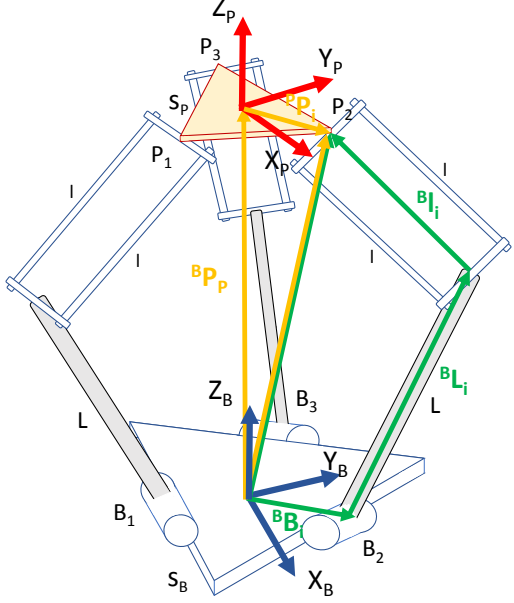
$$\{^B B_i\} + \{^B L_i\} + \{^B l_i\}$$

$$= \{^B P_P\} + [^B_P R_i]\{^P P_i\}$$

$$= \{^B P_P\} + \{^P P_i\} \quad (3.4)$$

for i= 1,2,3

where $[^B_P R_i] = [I_3]$

Since no rotations are allowed by the 3-RSR Delta manipulator

Figure 3.6: Vector loop

Table 3.2: Vector Loop closure equation

The vectors $^B L_i$ are dependent on the joint variables $\Theta = \{\theta_1 \quad \theta_2 \quad \theta_3\}^T$ which are shown in table 3.3 on page number 29.
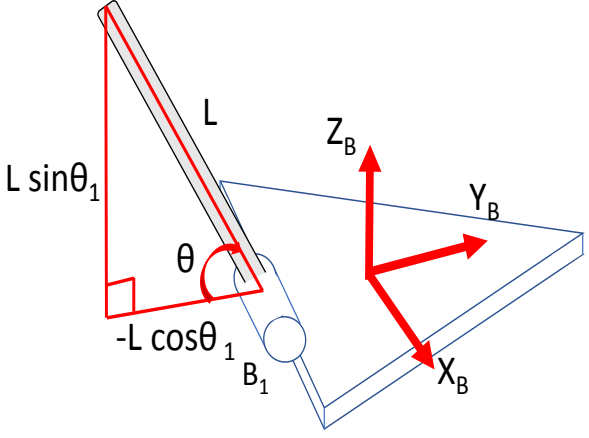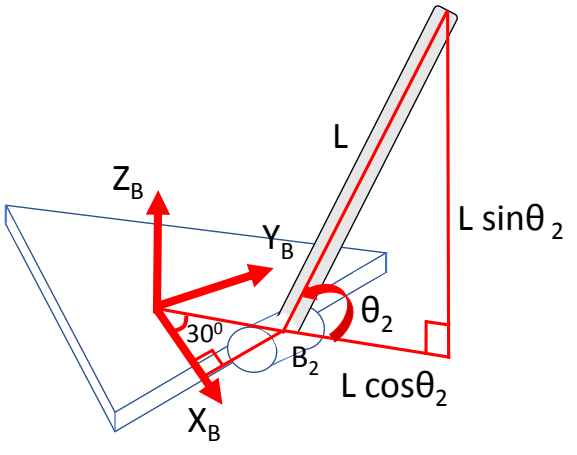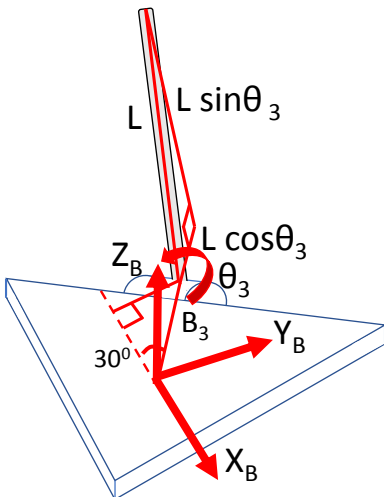
Figure 3.7: Illustration: $^{B}L_1$	$$^{B}L_1 = \left\{ \begin{array}{c} 0 \\ -Lcos\theta_1 \\ Lsin\theta_1 \end{array} \right\} \quad (3.5)$$
Figure 3.8: Illustration: $^{B}L_2$	$$^{B}L_2 = \left\{ \begin{array}{c} \frac{\sqrt{3}}{2}Lcos\theta_2 \\ \frac{1}{2}Lcos\theta_2 \\ Lsin\theta_2 \end{array} \right\} \quad (3.6)$$
Figure 3.9: Illustration: $^{B}L_3$	$$^{B}L_3 = \left\{ \begin{array}{c} -\frac{\sqrt{3}}{2}Lcos\theta_3 \\ \frac{1}{2}Lcos\theta_3 \\ Lsin\theta_3 \end{array} \right\} \quad (3.7)$$

Table 3.3: Link Analysis

Again, rearranging the vector loop closure equation and as the links have constant lengths their magnitude can be rewritten as follows:

$$l_i = \| \{^B l_i\} \| = \| \{^B P_P\} + \{^P P_i\} - \{^B B_i\} - \{^B L_i\} \|$$

$$i = 1, 2, 3 \quad (3.8)$$

squaring on both the sides

$$l_i^2 = \| \{^B l_i\} \|^2 = l_{i_x}^2 + l_{i_y}^2 + l_{i_z}^2 \quad i = 1, 2, 3$$

Substituting all above values into the vector-loop closure equation 3.4 gives:

$$\{^B l_1\} = \begin{Bmatrix} x \\ y + L cos\theta_1 + a \\ z + L sin\theta_1 \end{Bmatrix} \{^B l_2\} = \begin{Bmatrix} x - \frac{\sqrt{3}}{2} L cos\theta_2 + b \\ y - \frac{1}{2} L cos\theta_2 + c \\ z + L sin\theta_2 \end{Bmatrix} \{^B l_3\} = \begin{Bmatrix} x + \frac{\sqrt{3}}{2} L cos\theta_3 - b \\ y - \frac{1}{2} L cos\theta_3 + c \\ z + L sin\theta_3 \end{Bmatrix}$$

$$(3.9)$$

where: $\quad a = w_B - u_P \quad\quad b = \frac{s_P}{2} - \frac{\sqrt{3}}{2} w_B \quad\quad c = w_P - \frac{1}{2} w_B$

And the three constraint equations yield the kinematics equations for the 3-DOF RSR Parallel Delta Manipulator:

$$2L(y + a)cos\theta_1 - 2zlsin\theta_1 + x^2 + y^2 + z^2 + a^2 + L^2 + 2ya - l^2 = 0$$

$$-L(\sqrt{3}(x + b) + y + c)cos\theta_2 - 2zlsin\theta_2 + x^2 + y^2 + z^2 + b^2 + c^2 + L^2 + 2xb + 2yc - l^2 = 0$$

$$L(\sqrt{3}(x - b) + y + c)cos\theta_3 - 2zlsin\theta_3 + x^2 + y^2 + z^2 + b^2 + c^2 + L^2 - 2xb + 2yc - l^2 = 0$$

$$(3.10)$$

The three absolute elbow points are found using $^B A_i =^B B_i +^B L_i$, i=1,2,3:

$$\{^B A_1\} = \begin{Bmatrix} 0 \\ -w_B - L cos\theta_1 \\ L sin\theta_1 \end{Bmatrix}$$

$$\{^B A_2\} = \begin{Bmatrix} \frac{\sqrt{3}}{2}(w_B + L cos\theta_2) \\ \frac{1}{2}(w_B + L cos\theta_2) \\ L sin\theta_2 \end{Bmatrix} \quad \{^B A_3\} = \begin{Bmatrix} -\frac{\sqrt{3}}{2}(w_B + L cos\theta_3) \\ \frac{1}{2}(w_B + L cos\theta_3) \\ L sin\theta_3 \end{Bmatrix} \quad (3.11)$$

3.1.3 3-DOF RSR Parallel Delta Manipulator: Inverse Position Kinematics

Inverse position kinematics (IPK) for 3-DOF RSR Parallel Delta Manipulator is done to find out the revolute joint angles $\Theta = \{\theta_1 \quad \theta_2 \quad \theta_3\}^T$ when given end-effector position $^B P_P = \{x \quad y \quad z\}^T$. The IPK can be given analytically by comparing the constraint equations given in 3.10 with the form:

$$E_i cos\theta_i + F_i sin\theta_i + G_i = 0 \quad i = 1, 2, 3 \tag{3.12}$$

where:

$$E_1 = 2L(y + a)$$

$$F_1 = -2zl$$

$$G_1 = x^2 + y^2 + z^2 + a^2 + L^2 + 2ya - l^2$$

$$E_2 = -L(\sqrt{3}(x + b) + y + c)$$

$$F_2 = -2zl$$

$$G_2 = x^2 + y^2 + z^2 + b^2 + c^2 + L^2 + 2(xb + yc) - l^2$$

$$E_3 = L(\sqrt{3}(x - b) - y - c)$$

$$F_3 = -2zl$$

$$G_3 = x^2 + y^2 + z^2 + b^2 + c^2 + L^2 + 2(-xb - yc) - l^2$$

Now, the equation 3.12 can be solved using Tangent Half-Angle Substitution into the EFG equation:

$$E_i \frac{1 - t_i^2}{1 + t_1^2} + F_i \frac{2t_i^2}{1 + t_i^2} + G_i^2 = 0 \qquad E_i(1 - ti^2) + F_i(2t_i) + G_i(1 + t_i^2) = 0 \tag{3.13}$$

$$(G_i - E_i)t_i^2 + (2F_i)t_i + (G_i + E_i) = 0 \qquad \text{quadratic formula:} t_{i_{1_2}} = \frac{-F_i \pm \sqrt{E_i^2 + F_i^2 - G_i^2}}{G_i - E_i}$$

$$\tag{3.14}$$

Solve for θ_i by inverting the original Tangent Half-Angle Substitution definition:

$$\theta_i = 2tan^-1(t_i) \tag{3.15}$$

The solutions result for two θ_i from $\pm$ in the quadratic formula can be obtained. Both are correct and are shown in the below figure 3.10. Generally the links in the outward positions as shown in figure 3.10a are selected.

(a) Link solution 1   (b) Link solution 2
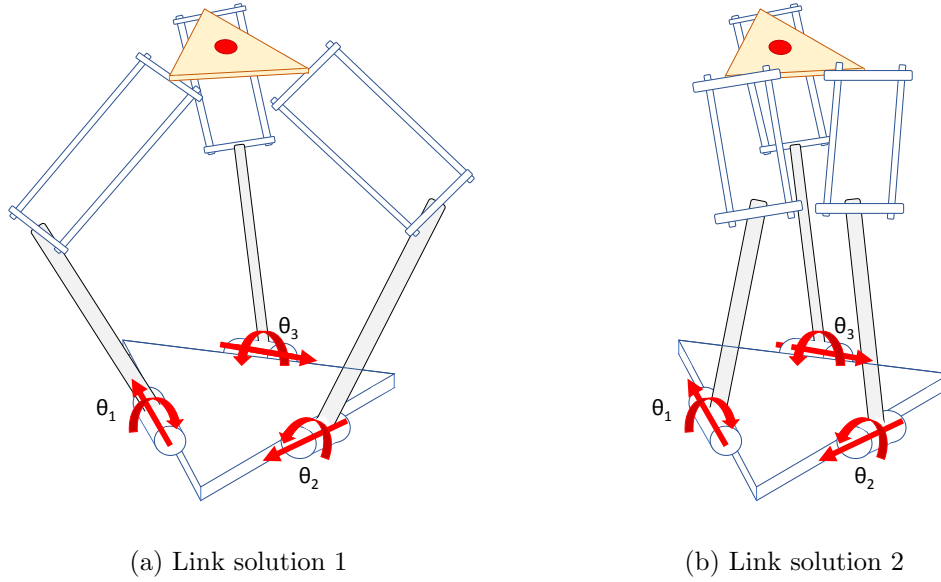
Figure 3.10: Two Inverse kinematic solutions for θ_i from $\pm$ in the quadratic formula

3.1.4 3-DOF RSR Parallel Delta Manipulator: Direct Position Kinematics

Direct position kinematics (DPK) for 3-DOF RSR Parallel Delta Manipulator is done to find out the end-effector position ${}^{B}P_P = \{x \quad y \quad z\}^T$ when given revolute joint angles $\Theta = \{\theta_1 \quad \theta_2 \quad \theta_3\}^T$. The DPK requires the solution of multiple coupled non linear algebraic equations, from the three constraint equation 3.10 applied to the vector loop closure equation 3.4. Generally this gives multiple results.

Due to the only possible translation motion of the 3-DOF RSR Parallel Delta Manipulator there is a simple and straightforward solution for which the correct solution

can be chosen easily. From the given value $\Theta = \{\theta_1 \quad \theta_2 \quad \theta_3\}^T$ we can obtain the absolute vector elbow points using ${}^B A_i = {}^B B_i + {}^B L_i, i = 1, 2, 3$. As shown in the figure below, it has been already been described that the moving platform orientation does not change with the horizontal which gives $[{}^B_P R] = [I_3]$. Since we establish that we can find the three virtual sphere centers from ${}^B A_{i_v} = {}^B A_i - {}^P P_i, i = 1, 2, 3$:
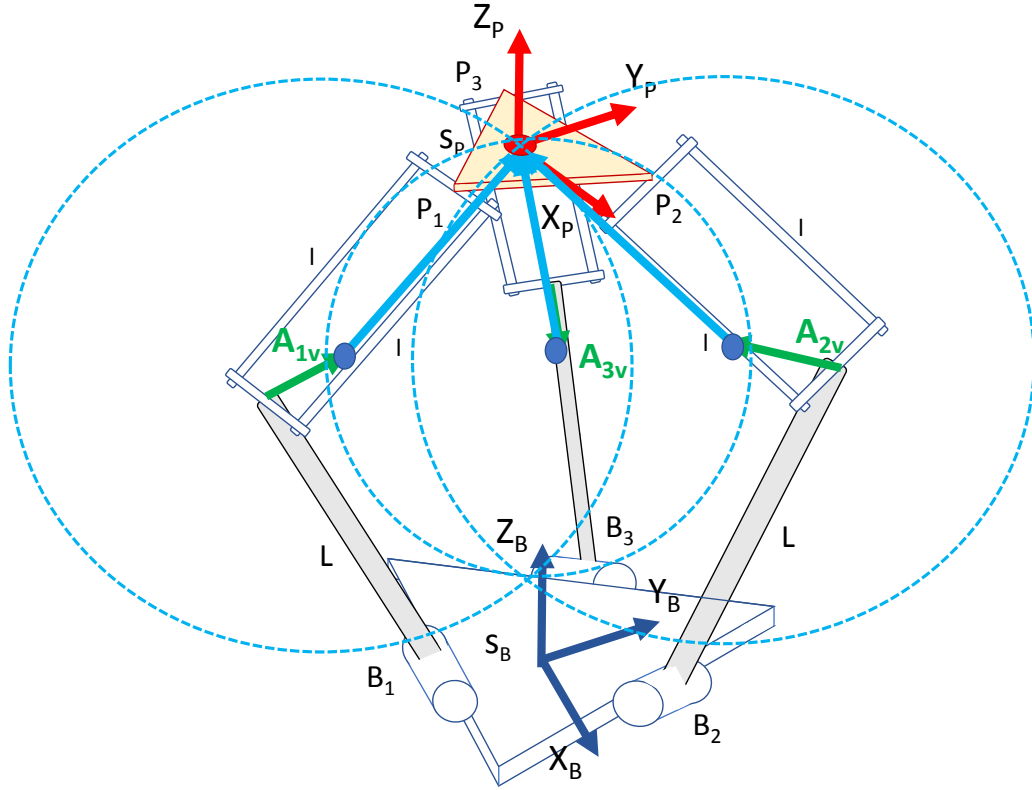
Figure 3.11: 3-DOF RSR Parallel Delta Manipulator DPK Diagram

$$\{{}^B A_{1_v}\} = \left\{ \begin{array}{c} 0 \\ -w_B - L cos\theta_1 + u_P \\ L sin\theta_1 \end{array} \right\}$$

$$\{{}^B A_{2_v}\} = \left\{ \begin{array}{c} \frac{\sqrt{3}}{2}(w_B + L cos\theta_2) - \frac{s_P}{2} \\ \frac{1}{2}(w_B + L cos\theta_2) - w_P \\ L sin\theta_2 \end{array} \right\} \qquad \{{}^B A_{3_v}\} = \left\{ \begin{array}{c} -\frac{\sqrt{3}}{2}(w_B + L cos\theta_3) + \frac{s_P}{2} \\ \frac{1}{2}(w_B + L cos\theta_3) - w_P \\ L sin\theta_3 \end{array} \right\}$$

$$(3.16)$$

The intersection point of the three spheres is the DPK solution for the 3-DOF RSR Parallel Delta Manipulator. Assuming that the sphere is described with the vector center point $\{c\}$ and scalar radius $r, (\{c\}, r)$. Therefore, the DPK unknown point ${}^{B}P_P$ is the intersection of the three spheres as shown in the figure 3.11.

$$(\{{}^{B}A_{i_v}\}, l) \qquad (\{{}^{B}A_{2_v}\}, l) \qquad (\{{}^{B}A_{3_v}\}, l) \tag{3.17}$$

An analytical solution for the intersection point of the three given spheres was studied from [44]. It gives the equations, analytical solution methods and describes imaginary singularities, and multiple solutions that can give error while computing the algorithm.

Furthermore, it also gives the solution to the problem that arises when all the three sphere centers $\{{}^{B}A_{i_v}\}$ have the same height Z.

While, computing the intersection of the spheres it is found that there are two solutions as shown in figure 3.12. It is easy to choose from both the solutions by checking the Z position of the point ${}^{B}P_P = \{x \quad y \quad x\}^T$ for given $\Theta = \{\theta_1 \quad \theta_2 \quad \theta_3\}^T$. Solution 1 Shown in figure 3.12a is selected over 3.12b by eliminating z possibilities below the arms being in horizontal plane parallel to the fixed base and moving platform.

(a) DPK solution 1   (b) DPK solution 2
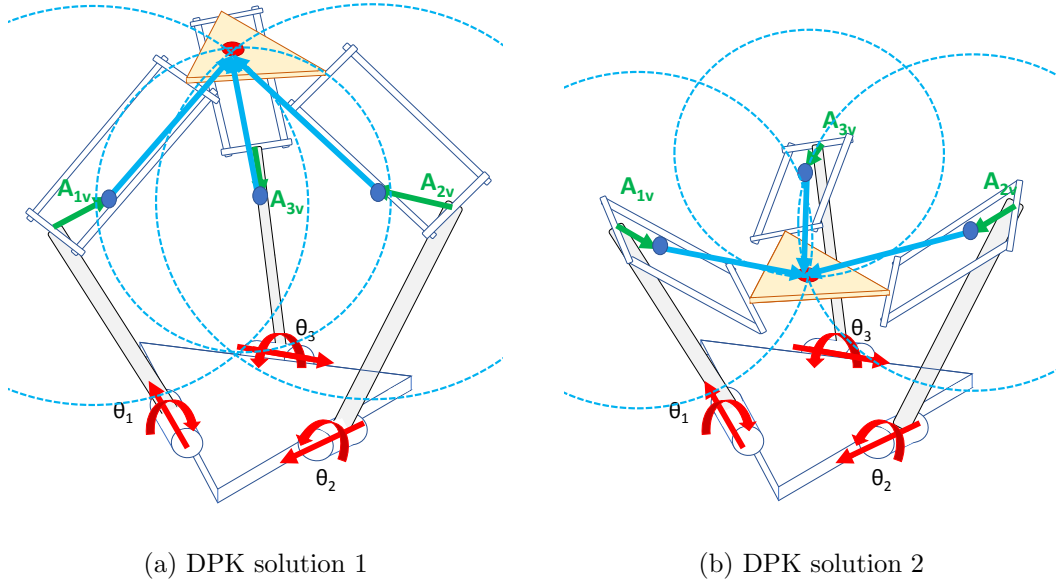
Figure 3.12: Two Direct kinematic solutions from intersection of given spheres

3.1.5 3-DOF RSR Parallel Delta Manipulator: Velocity Kinematics Equations

The derivatives of the three position constraint equations 3.10 gives the velocity kinematics equations for 3-DOF RSR Parallel Delta Manipulator which can be written in Matrix-vector form as shown in 3.18.

$$[A]\{\dot{X}\} = [B]\{\dot{\Theta}\}$$

$$\begin{bmatrix} x & y + a + Lcos\theta_1 & z - Lsin\theta_1 \\ 2(x+b) - \sqrt{3}Lcos\theta_2 & 2(y+c) - Lcos\theta_2 & 2(z - Lsin\theta_2) \\ 2(x-b) + \sqrt{3}Lcos\theta_3 & 2(y+c) - Lcos\theta_3 & 2(z - Lsin\theta_3) \end{bmatrix} \begin{Bmatrix} \dot{x} \\ \dot{y} \\ \dot{z} \end{Bmatrix} = $$
$$\begin{bmatrix} b_{1_1} & 0 & 0 \\ 0 & b_{2_2} & 0 \\ 0 & 0 & b_{3_3} \end{bmatrix} \begin{Bmatrix} \dot{\theta}_1 \\ \dot{\theta}_2 \\ \dot{\theta}_3 \end{Bmatrix}$$

(3.18)

3.1.6 3-DOF RSR Parallel Delta Manipulator: Dimensional synthesis

For the optimal dimensional synthesis of the 3-DOF RSR Parallel Delta Manipulator it is necessary to generate the workspace and compare it with the desired outcome [5, 45]. The total length of the kinematic chain determines the maximum vertical reach. Here total length of kinematic chain is the sum of the lengths of the active link (i.e. Lower links) and the parallelogram link (i.e. Upper links). Link length ratio is defined as ratio of the length of a link attached to the motor at the base plate to the sum of length of links in kinematic chain present between the base plate and the moving plate. The selection of link length ratio helps in determining the workspace [5].

The table 3.4 shows the workspace in XvsZ and YvsZ graphs for 0.25, 0.4, 0.5, 0.6 and 0.75 link length ratio.

It is clear from the work [5] that when the link length ratio is small, the delta robot has a hollow workspace. For smaller link ratios, the height of the workspace, when measured along the axis of the delta robot is small. As the link length ratio increases, the size of the cavity decreases and the cavity disappears at link length ratio of 0.5. So,
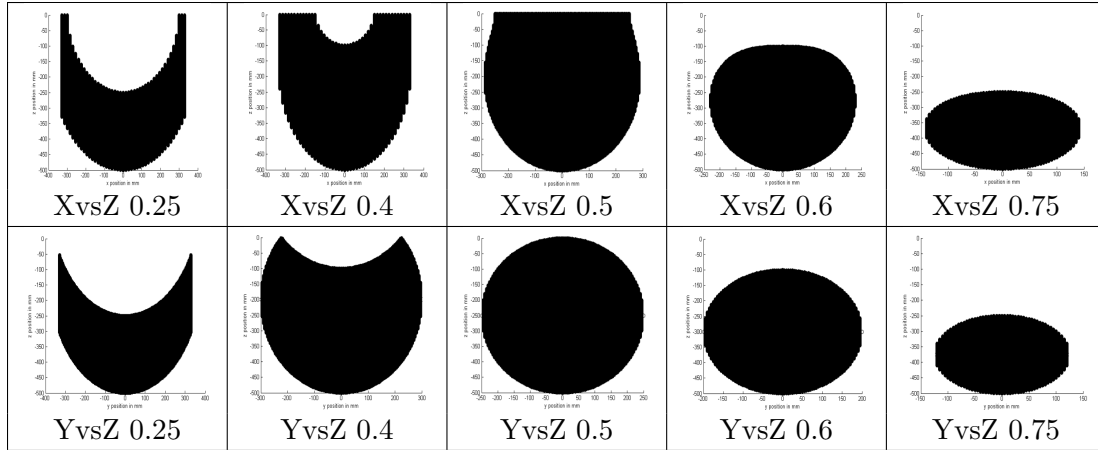
Table 3.4: Effect of link length ratio on the workspace of a Delta Robot [5]

at link length ratio of 0.5, full height is available for the workspace. Again, as the link length ratio increases further, the top most boundary of the workspace starts shifting downwards.

Based on the above comprehensive study of the effect of link lengths, following conclusion was derived for the dimensional synthesis of the link lengths as shown in table 3.5.

Identifier	Description	Value
L	Lower links or bicep length	256
l	Upper links or arm length	178.40
$L/(L+l)$	Link length ratio	0.59
h	Upper links parallelogram width	83.56

Table 3.5: Dimensional synthesis of the link lengths for 3-DOF RSR Parallel Delta Manipulator

Furthermore, desired workspace as discussed in the section 2.2.3, along with the space constraints as discussed in the section 2.1.3, gives the dimensional synthesis of the fixed base and moving platform geometry as shown in table 3.6 on page number 37. This helps in determining all the other derived parameters that are needed for the final workspace generation for the given configuration. These are listed in table 3.7 on

page number 37.

Identifier	Description	Value
D_B	Circumcircle diameter for the base equilateral triangle	400
R_B	Circumcircle radius for the base equilateral triangle	200
s_B	Base equilateral triangle side	692.82
D_P	Circumcircle diameter for the platform equilateral triangle	225
R_P	Circumcircle radius for the platform equilateral triangle	112.5
s_P	Platform equilateral triangle side	194.86

Table 3.6: Dimensional synthesis of the fixed base and moving platform for 3-DOF RSR Parallel Delta Manipulator

Identifier	Description	Value
w_B	Planar distance from {0} to near base side	200
u_B	Planar distance from {0} to a base vertex	400
w_P	Planar distance from {0} to near platform side	56.25
u_P	Planar distance from {0} to a platform vertex	112.5

Table 3.7: Derived values from dimensional synthesis of the 3-DOF RSR Parallel Delta Manipulator

3.1.7   3-DOF RSR Parallel Delta Manipulator: Workspace Generation

An improved numerical search method for the workspace generation for Delta robot is discussed in article [45]. This section will describe the method used for workspace generation which will be helpful in finalizing the optimal link dimensions as proposed in section 3.1.6.

There are various methods with which the workspace of the parallel manipulators can be generated. Most famous methods are (i) Discretization method, (ii) Geometrical method and (iii) Analytical method [45]. Discretization method is the easiest method

in which a grid of nodes with their position and orientations are defined. Then the kinematics analysis for that particular setup is applied to those nodes. Then a check is done to see if the kinematic analysis is solvable, while ensuring that the joints follow all the limitations and interference occurrence is prevented [46].

Discretization methods are expensive methods of computation and the number of nodes provided limits the space. And it is not possible to know if the point provided are valid for generating the nodes. Other method is geometrical method, using which the workspace can be obtained as the intersection of the geometric objects [45]. Analytical method is the most complicated of all but it can distinguish between the multiple solutions easily.

For the 3-DOF RSR Parallel Delta Manipulator, discretization method is used even though it has expensive computation. To verify whether the grid nodes provided are in the workspace we apply the constraint equations 3.10. It can be rearranged and rewritten as:

$$E_i cos\theta_i + F_i sin\theta_i = G_i \quad i = 1, 2, 3$$

$$f_i(xyz) = G_i^2 - (E_i^2 + F_i^2) \leq 0 \quad i = 1, 2, 3 \tag{3.19}$$

It can be further described as shown in the following table 3.8:

Case	Condition
P inside the workspace	$f_i(^B P_P) < 0$
P on the boundary	$f_i(^B P_P) = 0$
P is outside the workspace	$f_i(^B P_P) > 0$

Table 3.8: Conditions related to workspace for the 3-DOF RSR Parallel Delta Manipulator

This method for generating the workspace using grid nodes can be explained using the following algorithm.

1. First of all link dimensions and all the necessary parameters are given as input parameters.

2. Then the grid nodes were generated in terms of the angles of rotations at the lower link ranging from 0 to 90 degrees.

3. Then inverse kinematics was performed on the grid nodes angles to obtain $^{B}P_{P} = \{xxyz\}^{T}$ from it.

4. Furthermore, the resulting end effector points are checked for the conditions related to workspace for the 3-DOF RSR Parallel Delta Manipulator.

5. If the grid nodes satisfies the condition for the point to be in a workspace or on the boundary as per the table 3.8 the grid node is stored in a matrix, else it is discarded.

6. Lastly, the columns of the matrix that are the $^{B}P_{P} = \{xxyz\}^{T}$ satisfying the conditions are plotted to obtain a graphical image of the workspace.

Algorithm 1 summarizes the steps as discussed above. Following table 3.9 shows the output for the workspace generated for the dimensions as discussed in section 3.1.6.

Algorithm 1: Workspace Generation

    Input: Given link dimensions and all the paramters

    Output: Workspace

    Data: Testing conditions related to workspace based on constraint equations

1 Feed all the needed parameters that are proposed in the dimensional synthesis section 3.1.6

2 for $i \leq n$ **do**

3   **if** $(f_i(^{B}P_P) < 0)$ *or* $(f_i(^{B}P_P) = 0)$ **then**

4   Store the $^{B}P_{P} = \{xxyz\}^{T}$ *****   `// Check:  Boundary conditions`

5   **else**

6   Go to next iteration in for loop

7   i=i+1

8 Extract the $^{B}P_{P} = \{xxyz\}^{T}$ stored at *****

9 Plot each $^{B}P_{P} = \{xxyz\}^{T}$
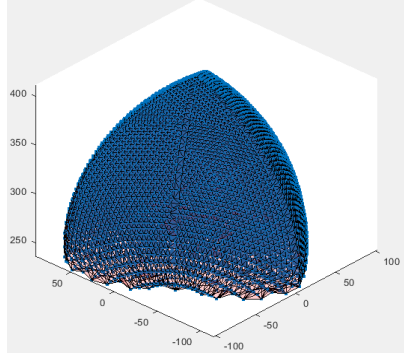
Figure 3.13: Workspace: Top Isometric View
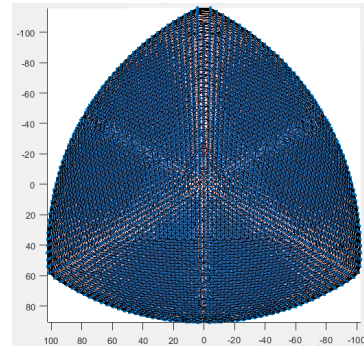
Figure 3.14: Workspace: Top View XvsY
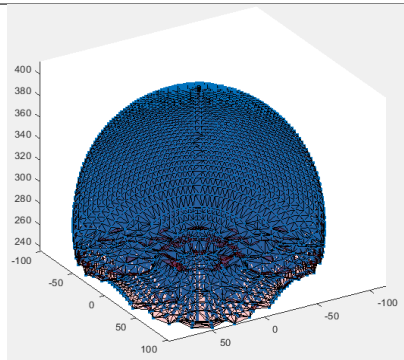
Figure 3.15: Workspace: Bottom Isometric View
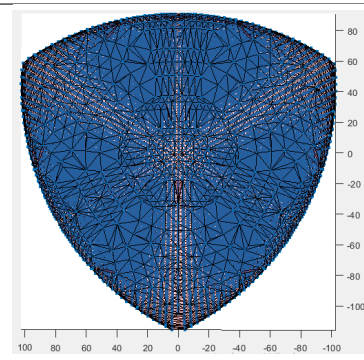
Figure 3.16: Workspace: Bottom View XvsY
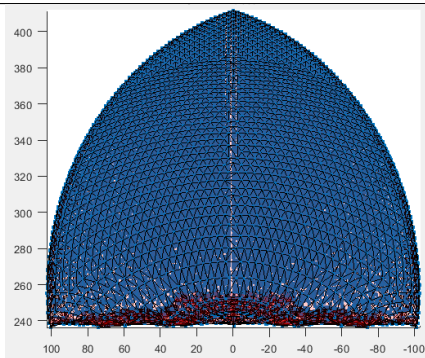
Figure 3.17: Workspace: Front View XvsZ
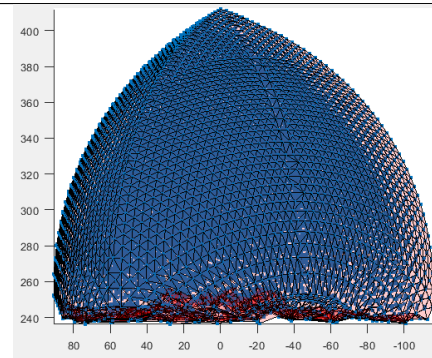
Figure 3.18: Workspace: Side View YvsZ

Table 3.9: Generated workspace in MATLAB

After generating the workspace, an effort was made to create a linkage model of the 3-DOF RSR Parallel Delta Manipulator in Matlab and impose the workspace on it to

get a better view of the workspace in terms of the end-effector.
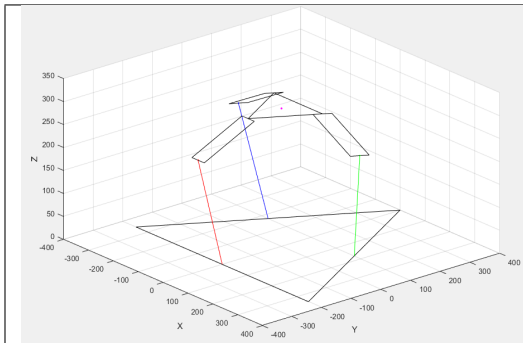
Figure 3.19: Link model: Isometric
View
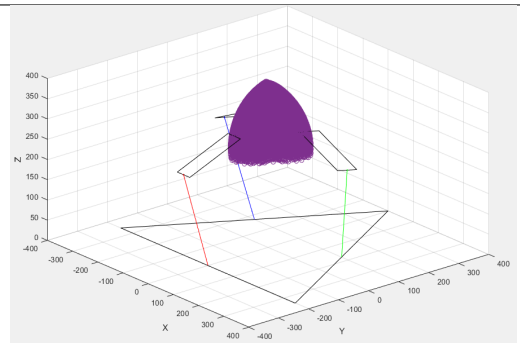
Figure 3.20: Model and Workspace:
Isometric View XYvsZ
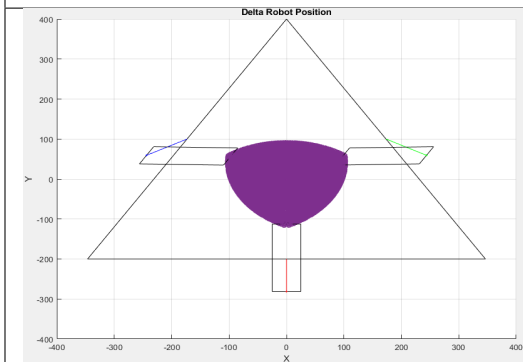
Figure 3.21: Model and Workspace:
Top View XvsY
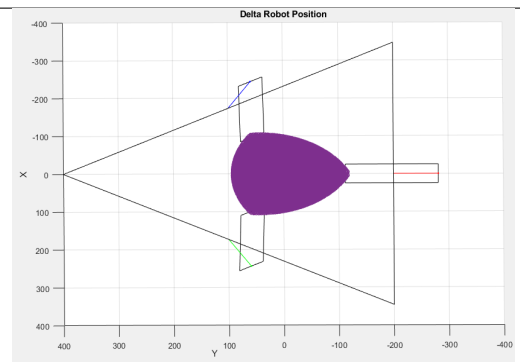
Figure 3.22: Model and Workspace:
Bottom View YvsX
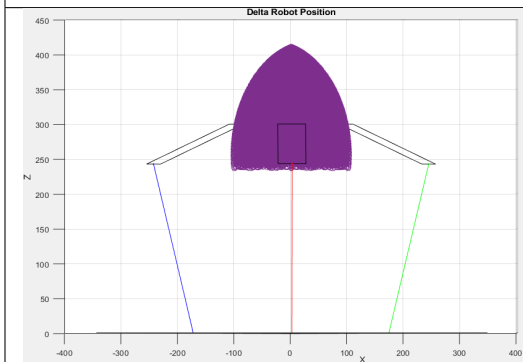
Figure 3.23: Model and Workspace:
Front View XvsZ
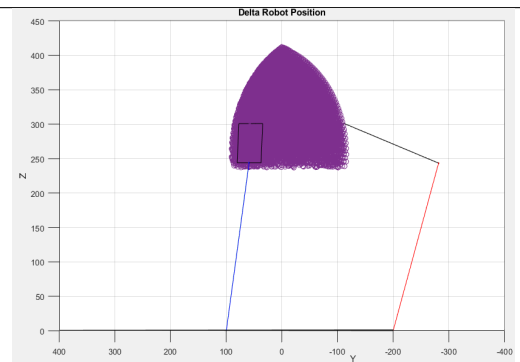
Figure 3.24: Model and Workspace:
Side View YvsZ

Table 3.10: Generated model and workspace in MATLAB

From the workspace generated it is established that the end effector can reach -102

mm to 102 mm in X-axis direction, -115.7 mm to 90.72 mm in Y-axis direction and 237.5 to 411.5 mm in Z direction. Hence, we can say that the range of motion available in X-axis is 204 mm , Y axis is 206.42 mm and Z axis is 174 mm. This XY axis range reduces as the end-effector elevates and at the top most point the workspace shrinks to a single point, taking a dome/bullet head shape. From section 2.2.3 and figure 2.13, on comparing the workspace with the range of available motion it is realized that the target workspace is a subset of the workspace generated 3.9. Hence, this configuration of 3-DOF RSR Parallel Delta Manipulator with the discussed dimensions is accepted for further development.

3.2 Kinematic Analysis for 2-DOF RR Serial $\perp^{lr}$ axis Manipulator

Two revolute joint in series (i.e. RR Linkage) is a very basic concept from spatial mechanism manipulators [47–50]. This section contributes in kinematic analysis of two revolute joints connected with their axis of rotations perpendicular to each other.

3.2.1 2-DOF RR Serial $\perp^{lr}$ axis Manipulator: Description

The labelled diagram of the the two revolute (R) joints in series with their axis perpendicular to each other is shown in figure 3.25. In this 2-DOF RR Serial $\perp^{lr}$ axis Manipulator the wrist is connected to the moving platform via first revolute joint. This revolute joints is driven by a motor actuator and rotation angle is measured as ϕ. Furthermore, the end-effector for this configuration is on the sample holder which is connected to the wrist with the help of 2nd revolute joint. This sample holder is able to rotate angle ψ_i with the help of second motor actuator. Finally, this sample holder submerges in the medium provided in the petri dish which is located at the center of the moving platform as shown in the figure 3.25. Here, it is very important to consider that the moving platform has a cavity underneath the petri dish so that the optical inverse microscope have access to focus on the sample holder (i.e.transparent).
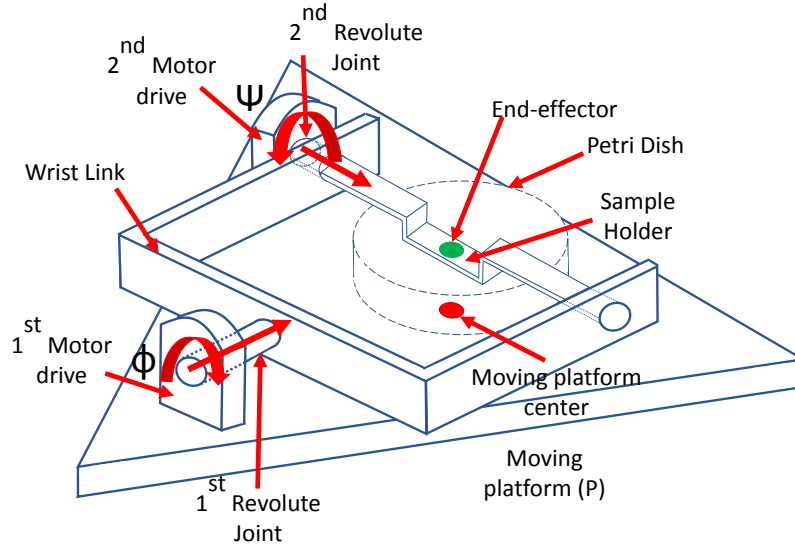
Figure 3.25: Labelled diagram for 2-DOF RR Serial $\perp^{lr}$ axis Manipulator

The figure 3.26 shows the Cartesian coordinates attached to the moving platform $\{P\}$ with the center of the equilateral triangle as origin. The final coordinate frame is $\{E\}$, with the center of the sample holder as end-effector. The nomenclature applied to the diagram is shown in the figure 3.27. This nomenclature is summarized in the table 3.11 on page number 45. The orientation of $\{E\}$ depends on the rotations provided by the two revolute joints. The joint variables are ϕ and ψ respectively.
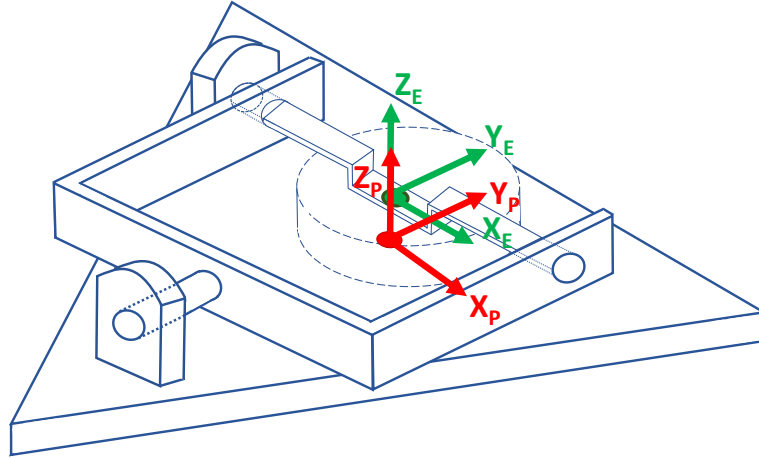
Figure 3.26: 2-DOF RR Serial $\perp^{lr}$ axis Manipulator Kinematic Diagram with coordinate frames
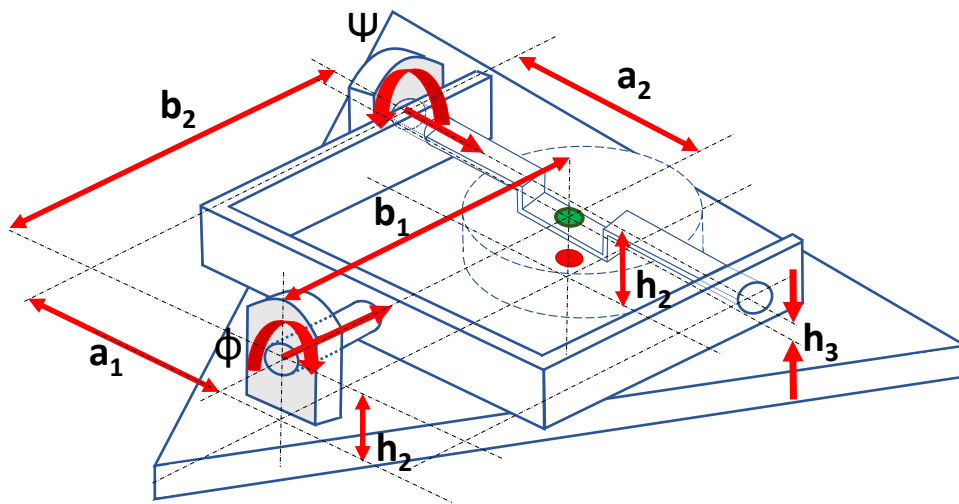
Figure 3.27: 2-DOF RR Serial $\perp^{lr}$ axis Manipulator with nomenclature

Identifier	Description	Axial Direction	Value
h_2	Height from end effector of 3-RSR Parallel Delta manipulator (i.e. center of moving platform) to first revolute joint	Z	30mm
ϕ	Rotation of first revolute joint provided by the actuating motor	Y	-
b_1	Distance of first revolute joint plane from end effector of 3-RSR Parallel Delta manipulator in	Y	70mm
a_1	Distance of second revolute joint's rotation plane from first revolute joint's rotational axis	X	51.075mm
ψ	Rotation of second revolute joint provided by the actuating motor	-	-
b_2	Distance of sample holder end-effector from second revolute joint's rotation plane	-	70mm
h_3	Depth of sample holder center from second revolute joint's rotational axis	-	5mm

Table 3.11: Summary of nomenclature for 2-DOF RR Serial $\perp^{lr}$ axis Manipulator

3.2.2   2-DOF RR Serial $\perp^{lr}$ axis Manipulator: Kinematics Analysis

Position analysis of this 2-R series $\perp^{lr}$ mechanism is done with the help of Denavit-Hartenberg (D-H) parameters. D-H parameters are described as commonly used convention for selecting frame of reference in robotics application [47]. Based on transformation matrix described below, workspace of the mechanism is defined. The calculation of the homogeneous transformation matrices and obtaining the forward kinematics is very intensive so it is not feasible to perform it manually. So, MATLAB is used for computational purpose of the homogeneous transformation matrices.

3.2.2.1   Denavit-Hartenberg representation

A commonly used convention for selecting frames of reference in robotic applications is the Denavit-Hartenberg, or D-H convention [47]. In this convention, each homogeneous transformation A_i is represented as a product of four basic transformations as given below.

$$A_i = R_X(\alpha_i)D_X(a_i)R_Z(\beta_i)D_Z(d_i)$$

$$= \begin{bmatrix} 1 & 0 & 0 & 0 \\ 0 & c\alpha_i & -s\alpha_i & 0 \\ 0 & s\alpha_i & c\alpha_i & 0 \\ 0 & 0 & 0 & 1 \end{bmatrix} \cdot \begin{bmatrix} 1 & 0 & 0 & a_i \\ 0 & 1 & 0 & 0 \\ 0 & 0 & 1 & 0 \\ 0 & 0 & 0 & 1 \end{bmatrix} \cdot \begin{bmatrix} c\beta_i & -s\beta_i & 0 & 0 \\ s\beta_i & c\beta_i & 0 & 0 \\ 0 & 0 & 1 & 0 \\ 0 & 0 & 0 & 1 \end{bmatrix} \cdot \begin{bmatrix} 1 & 0 & 0 & a_i \\ 0 & 1 & 0 & 0 \\ 0 & 0 & 1 & 0 \\ 0 & 0 & 0 & 1 \end{bmatrix}$$

$$= \begin{bmatrix} c\beta_i & -s\beta_i c\alpha_i & s\beta_i s\alpha_i & a_i c\beta_i \\ s\beta_i & c\beta_i c\alpha_i & -c\beta_i s\alpha_i & a_i s\beta_i \\ 0 & s\alpha_i & c\alpha_i & d_i \\ 0 & 0 & 0 & 1 \end{bmatrix}$$

$$(3.20)$$

Where the four quantities α_i, a_i, d_i, and β_i are parameters associated with link i and joint i. The four parameters α_i, a_i, d_i, and β_i in equation 3.20 are generally given the names link twist, link length, link offset, and joint angle, respectively. Since the matrix A_i is a function of a single variable, it turns out that three of the above four quantities are constant for a given link, while the fourth parameter, β_i for a revolute joint and d_i for a prismatic joint, is the joint variable.

$$\begin{bmatrix} a_i c\beta_i \\ a_i s\beta_i \\ d_i \\ 1 \end{bmatrix}$$ indicates position of end-effector frame w.r.t. base frame.

$$
\begin{bmatrix}
c\beta_i & -s\beta_i c\alpha_i & s\beta_i s\alpha_i \\
s\beta_i & c\beta_i c\alpha_i & -c\beta_i s\alpha_i \\
0 & s\alpha_i & c\alpha_i \\
0 & 0 & 0
\end{bmatrix}
$$ indicates orientation of end-effector w.r.t. base frame.

3.2.2.2 Assigning the coordinate frames

For given robot manipulator, one can always select the frames 0, 1,..., n to find out the transformation matrix which gives translation and orientation of end-effector i.e. last link frame, with base frame and hence to derive forward kinematics of robot manipulator which is used for position analysis. Basic parameters involved in frame assignment are described in the following table 3.12.

Identifier	Description
Link twist (α_i)	The distance between z_{i-1} and z_i measured along x_{i-1}
Link length (a_i)	The distance between z_{i-1} and z_i measured along x_{i-1}
Link offset (d_i)	The distance between x_{i-1} and x_i measured along z_i
Joint angle (β_i)	The angle between x_{i-1} and x_i measured along z_i

Table 3.12: D-H parameters
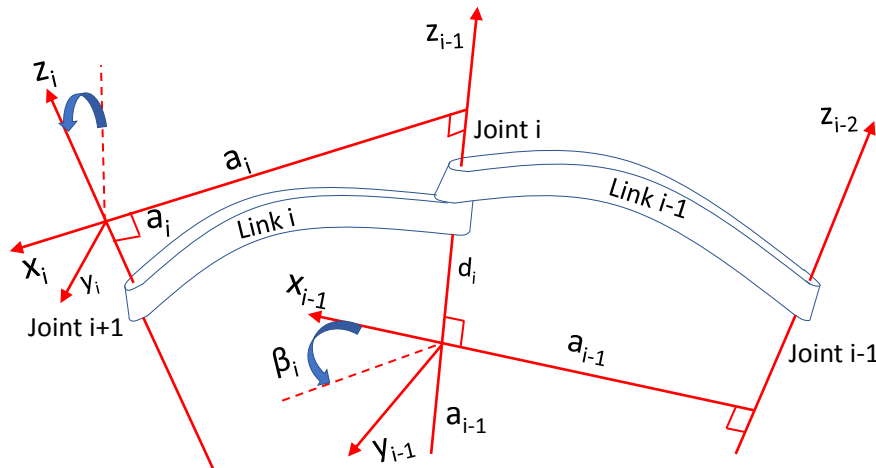
Figure 3.28: D-H Parameters frame assignment [8]

3.2.2.3 Procedure based on the D-H convention for deriving the forward kinematics for any manipulator

Below is the summary of the procedure to be followed for the D-H convention in order to derive forward kinematics for any manipulator [8]:

1. Identify and place the joint axis z_0.

2. Position the origin arbitrarily on z_0 axis after establishing the frame. Accordingly the x_0 and y_0 axis are chosen to form a right-hand frame. Repeat steps 3 to 5 in a loop from $i = 1$ to $i = n - 1$.

3. Select the point of intersection of common normal to z_i and z_{i-1} as the origin o_i. Position o_i at any place if z_i and z_{i-1} are parallel.

4. Along the common normal between z_{i-1} and z_i through o_i, establish x_i. If z_{i-1} and z_i intersects establish x_i in the direction normal to z_{i-1} - z_i plane.

5. In order to complete the right-hand frame establish y_i

6. Establish the end-effector frame $o_n x_n y_n z_n$. Assuming the nth joint is revolute, set $z_n = a$ along the direction z_{i-1}. Establish the origin o_n conveniently along z_n,preferably at the center of the gripper or at the tip of any tool that the manipulator may be carrying. Set $y_n = s$ in the direction of the gripper closure and set $x_n = n$ as $s \times a$. If the tool is not a simple gripper set x_n and y_n conveniently to form a right-hand frame.

7. Create a table of link parameters α_i, a_i, d_i, β_i.

8. Form the homogeneous transformation matrices A_i by substituting the above parameters into equation 3.20.

9. Form $T_n^0 = A_1 \cdots A_n$. Hence, giving the position and orientation of the end-effector frame expressed in base coordinates.

3.2.3 2-DOF RR Serial $\perp^{lr}$ axis Manipulator: Direct Kinematics

The goal of the direct kinematics is to obtain the final end-effector coordinates i.e. $^{P}E = \{x_E \quad y_R \quad z_E\}^T$ from the given input rotations to the revolute joints i.e. ϕ and ψ respectively. The direct kinematics for the 2-DOF RR Serial $\perp^{lr}$ axis Manipulator shall be carried out in four steps as shown in table 3.13 for the simplicity of understanding. Later on it will be merged for the homogeneous transformation from initial point $^{B}P = \{x_p \quad y_p \quad z_p\}^T$ to final control point $^{P}E = \{x_E \quad y_R \quad z_E\}^T$. The equation 3.21 gives the final transformation based on the intermediate transformation matrices generated by applying D-H parameters.

Step	From	To
1	Center of the moving platform $\{P\}$	1st revolute joint $\{1\}$
2	1st revolute joint $\{1\}$	2nd revolute joint $\{2\}$
3	2nd revolute joint $\{2\}$	Center of the sample holder $\{3\}$
4	Center of the sample holder $\{3\}$	End-effector (i.e. the target micro-particle on sample holder) $\{E\}$

Table 3.13: Steps for establishing coordinate frames for D-H Parameters
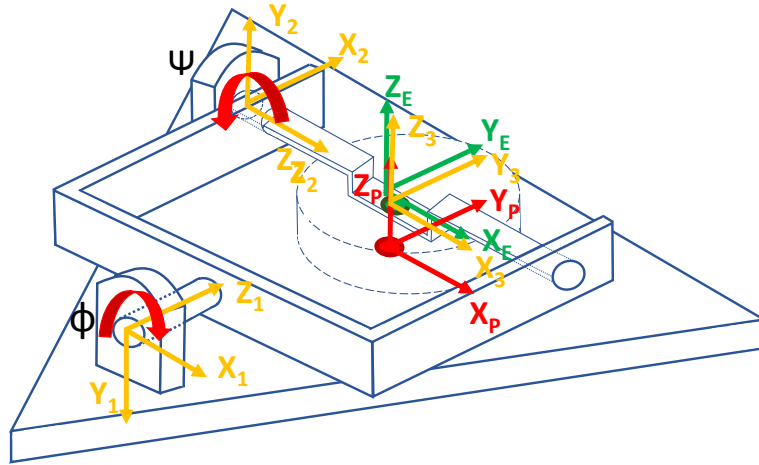
Figure 3.29: Establishing coordinate frames for D-H Parameters

$$T_E^P = A_1 A_2 A_3 A_4 \tag{3.21}$$

3.2.3.1 Homogeneous Transformation from the center of the moving platform to the 1st revolute joint

The first transformation of coordinates from the center of the moving platform to the 1st revolute joint can be broken down as shown in figure 3.30. D-H parameter table for the same is given in 3.14and the homogeneous transformation matrix A_{1H} for it is given in equation 3.22.
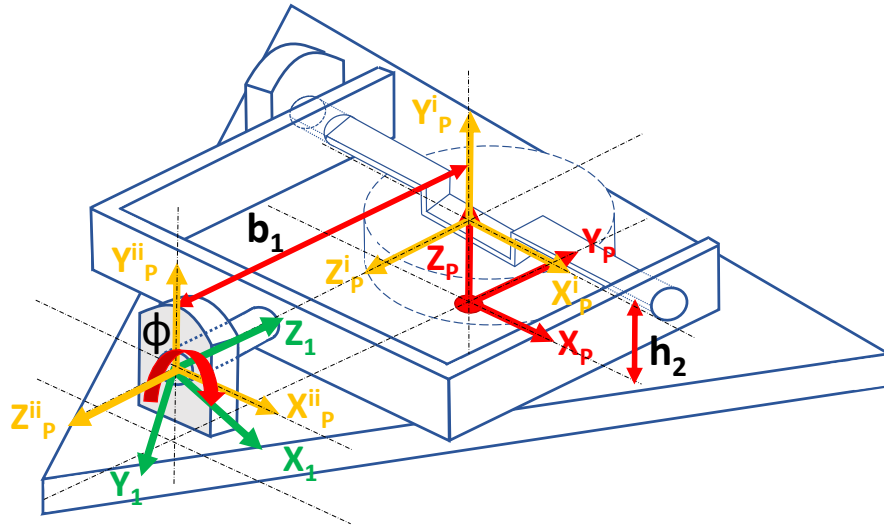
Figure 3.30: Establishing coordinates from the center of the moving platform to the 1st revolute joint

$i-1$	i	α_i	a_i	d_i	β_i
$\{P\}$	$\{P^i\}$	90	0	h_2	0
$\{P^i\}$	$\{P^{ii}\}$	0	0	b_1	0
$\{P^{ii}\}$	$\{1\}$	180	0	0	ϕ

Table 3.14: D-H Parameters: $\{P\}$ to $\{1\}$

$$A_{1H} = A_{Pi} A_{Pii} A_1$$

$$A_{1H} = \begin{bmatrix} c\phi & s\phi & 0 & 0 \\ 0 & 0 & 1 & -b_1 \\ s\phi & -c\phi & 0 & h_2 \\ 0 & 0 & 0 & 1 \end{bmatrix} \tag{3.22}$$

3.2.3.2 Homogeneous Transformation from 1st revolute joint to 2nd revolute joint

The second transformation of coordinates from 1st revolute joint to the 2nd can be broken down as shown in figure 3.31. D-H parameter table for the same is given in 3.15and the homogeneous transformation matrix A_{2H} for it is given in equation 3.23.
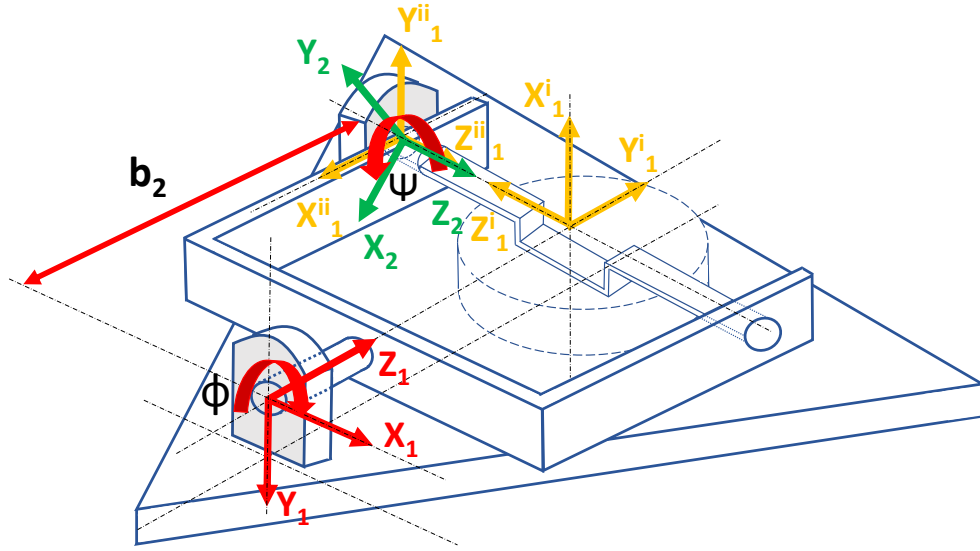
Figure 3.31: Establishing coordinates from from 1st revolute joint to 2nd revolute joint

$i-1$	i	α_i	a_i	d_i	β_i
$\{1\}$	$\{1^i\}$	90	0	b_2	-90
$\{1^i\}$	$\{1^{ii}\}$	180	0	a_1	90
$\{P^{ii}\}$	$\{2\}$	0	0	0	ψ

Table 3.15: D-H Parameters: $\{1\}$ to $\{2\}$

$$A_{2H} = A_{1^i} A_{1^{ii}} A_2$$

$$A_{2H} = \begin{bmatrix} 0 & 0 & 1 & -a_1 \\ -s\psi & -c\psi & 0 & 0 \\ c\psi & -s\psi & 0 & b_2 \\ 0 & 0 & 0 & 1 \end{bmatrix}$$

(3.23)

3.2.3.3 Homogeneous Transformation from 2nd revolute joint to the center of the sample holder

The third transformation of coordinates from 2nd revolute joint to the the center of the sample holder can be broken down as shown in figure 3.32. D-H parameter table for the same is given in 3.16 and the homogeneous transformation matrix A_{3H} for it is given in equation 3.24.
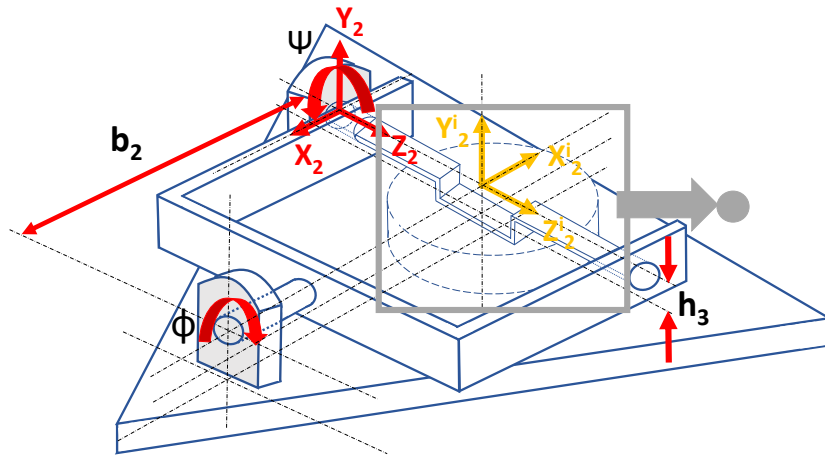
Figure 3.32: Establishing coordinates from 2nd revolute joint to the center of the sample holder: Part-1
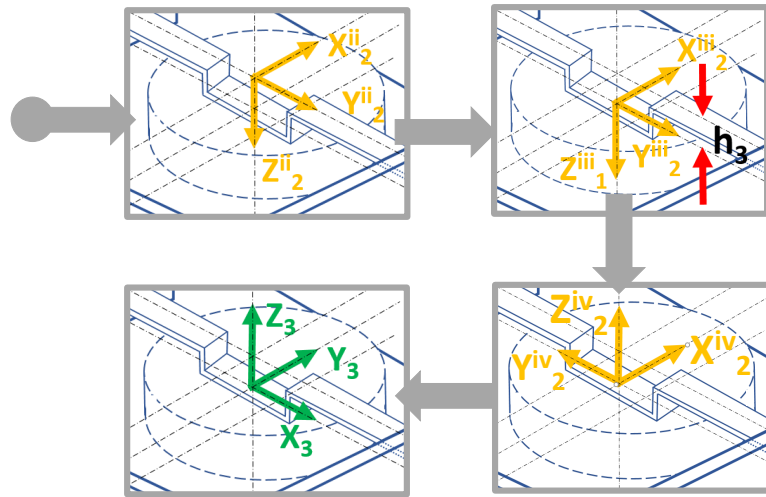
Figure 3.33: Establishing coordinates from 2nd revolute joint to the center of the sample holder: Part-2

$i-1$	i	α_i	a_i	d_i	β_i
$\{2\}$	$\{2^i\}$	0	0	a_2	0
$\{2^i\}$	$\{2^{ii}\}$	90	0	0	0
$\{2^{ii}\}$	$\{2^{iii}\}$	0	0	h_3	0
$\{2^{iii}\}$	$\{2^{iv}\}$	180	0	0	0
$\{2^{iv}\}$	$\{3\}$	0	0	0	-90

Table 3.16: D-H Parameters: $\{2\}$ to $\{3\}$

$$A_{3H} = A_{2^i} A_{2^{ii}} A_{2^{iii}} A_{2^{iv}} A_3$$

$$A_{3H} = \begin{bmatrix} 0 & 1 & 0 & 0 \\ 0 & 0 & 1 & -h_3 \\ 1 & 0 & 0 & a_2 \\ 0 & 0 & 0 & 1 \end{bmatrix} \tag{3.24}$$

3.2.3.4 Linear Translation from the center of the sample holder to the end-effector
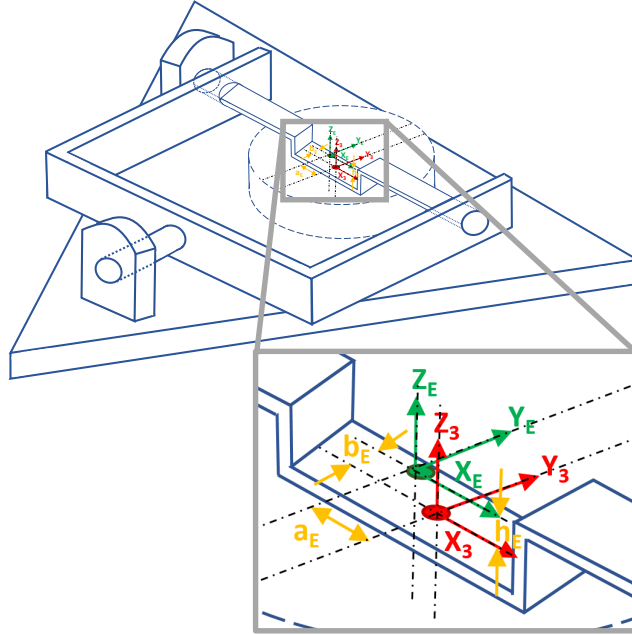
Figure 3.34: Establishing coordinates from the center of the sample holder to the end-effector

This is a simple translation as shown in figure 3.34 so a translation matrix given in equation 3.25 can be directly generated using a translation matrix from the parameters defined in the table 3.17.

$i-1$	i	d_x	d_y	d_z
$\{3\}$	$\{E\}$	a_E	b_E	h_E

Table 3.17: Translation Parameters: $\{3\}$ to $\{E\}$

$$A_{4T} = \begin{bmatrix} 1 & 0 & 0 & a_E \\ 0 & 1 & 0 & b_E \\ 0 & 0 & 1 & h_E \\ 0 & 0 & 0 & 1 \end{bmatrix} \tag{3.25}$$

3.2.3.5 Final transformation matrix: direct kinematics for 2-DOF RR Serial $\perp^{lr}$ axis Manipulator

Now from the equation 3.21 we can find out the final transformation matrix as shown in equation 3.26. This transformation matrix gives the direct kinematics for 2-DOF RR Serial $\perp^{lr}$ axis Manipulator.

$$T_E^P = A_{1H} A_{1H} A_{3H} A_{4T}$$

$$T_E^P = \begin{bmatrix} c\phi & -s\phi s\psi & -c\psi s\phi & (a_2 - a_1 + a_E)c\phi + (h_3 - h_E)c\psi s\phi - b_E s\phi s\psi \\ 0 & c\psi & -s\psi & b_2 - b_1 + b_E c\psi + (h_3 - b_E)s\psi \\ s\phi & c\phi s\psi & c\phi c\psi & h_2 + (a_2 - a_1 + a_E)s\phi - (h_3 - he)c\phi c\psi + h_E c\phi s\psi \\ 0 & 0 & 0 & 1 \end{bmatrix}$$

$$\tag{3.26}$$

3.2.4 2-DOF RR Serial $\perp^{lr}$ axis Manipulator: Inverse Kinematics

The goal of the inverse kinematics is to find the the rotations required at the revolute joints i.e. ϕ and ψ to achieve the given final end-effector coordinates i.e. $^PE = \{x_E \quad y_R \quad z_E\}^T$. From the final homogeneous transformation obtained in the previous section we can compare the given end effector coordinates as shown below:

$$
T_E^P = \begin{bmatrix}
c\phi & -s\phi s\psi & -c\psi s\phi & (a_2 - a_1 + a_E)c\phi + (h_3 - h_E)c\psi s\phi - b_E s\phi s\psi \\
0 & c\psi & -s\psi & b_2 - b_1 + b_E c\psi + (h_3 - b_E)s\psi \\
s\phi & c\phi s\psi & c\phi c\psi & h_2 + (a_2 - a_1 + a_E)s\phi - (h_3 - he)c\phi c\psi + h_E c\phi s\psi \\
0 & 0 & 0 & 1
\end{bmatrix}
$$

$$
= \begin{bmatrix}
R_{3\times 3} & {}^PE_{3\times 1} \\
0 & 1
\end{bmatrix}
$$

$$\tag{3.27}$$

Hence, we obtain the following three equations:

$$x_E = (a_2 - a_1 + a_E)c\phi + (h_3 - h_E)c\psi s\phi - b_E s\phi s\psi$$

$$y_E = b_2 - b_1 + b_E c\psi + (h_3 - h_E)s\psi \tag{3.28}$$

$$z_E = h_2 + (a_2 - a_1 + a_E)s\phi - (h_3 - he)c\phi c\psi + b_E c\phi s\psi$$

Rewriting the equation from y_E and comparing it with the following equation:

$$A_1 c\psi - B_1 s\psi = C_1 \tag{3.29}$$

where:

$$A_1 = (b_E), \qquad B_1 = h_E - h_3, \qquad \text{and} \qquad C_1 = y_e - b_2 + b_1$$

Also, another form of equation 3.29 is as follows,

$$A_1 c\psi - B_1 s\psi = C_1 = R_1 cos(\psi + \gamma_1) \tag{3.30}$$

where:

$$R_1 = \sqrt{A_1^2 + B_1^2}, \qquad \text{and} \qquad \gamma_1 = Atan\frac{B_1}{A_1}$$

Comparing the constants we get:

$$R_1 cos(\psi + \gamma_1) = C_1$$
$$\psi = (Acos\frac{C_1}{R_1}) - \gamma_1$$

(3.31)

where:

$$0 \leq \psi \leq 90°$$

Rewriting the other equations from x_E and z_E and comparing it with the equation similar to 3.29:

$$A_{2,3}c\phi - B_{2,3}s\phi = C_{2,3}$$

(3.32)

where:

$A_2 = a_2 - a_1 + a_E,$ $B_2 = (h_E - h_3)c\psi + b_E s\psi,$ and $C_2 = x_E$

$A_3 = h_E - h_3 c\psi + b_E s\psi,$ $B_3 = -(a_2 - a_1 + a_E),$ and $C_3 = z_E - h2$

Rewriting, another form of equation 3.32 similar to 3.30,

$$A_{2,3}c\phi - B_{2,3}s\phi = C_{2,3} = R_{2,3}cos(\phi + \gamma_{2,3})$$

(3.33)

where:

$$R_{2,3} = \sqrt{A_{2,3}^2 + B_{2,3}^2}, \qquad \text{and} \qquad \gamma_{2,3} = Atan\frac{B_{2,3}}{A_{2,3}}$$

Comparing the constants we get:

$$R_{2,3}cos(\phi + \gamma_{2,3}) = C_{2,3}$$
$$\phi = (Acos\frac{C_{2,3}}{R_{2,3}}) - \gamma_{2,3}$$

(3.34)

where:

$$0 \leq \phi \leq 90°$$

Thus, from equations 3.34 and 3.31 we can obtain the rotations required at the revolute joints i.e. ϕ and ψ respectively, in order to achieve the given final end-effector coordinates i.e. $^P E = \{x_E \quad y_R \quad z_E\}^T$.

3.3 Integrating 3-DOF RSR Parallel Delta Manipulator and 2-DOF RR Serial $\perp^{lr}$ axis Manipulator

After establishing both the manipulators individually, both the manipulators i.e. 3-DOF RSR Parallel Delta Manipulator and 2-DOF RR Serial $\perp^{lr}$ axis Manipulator are integrated. Both are connected in series with each other respectively as shown in figure 3.35. 3-DOF RSR Parallel Delta Manipulator provides the translation motion in 3D and 2-DOF RR Serial $\perp^{lr}$ axis Manipulator is responsible for the orientation of the end effector.
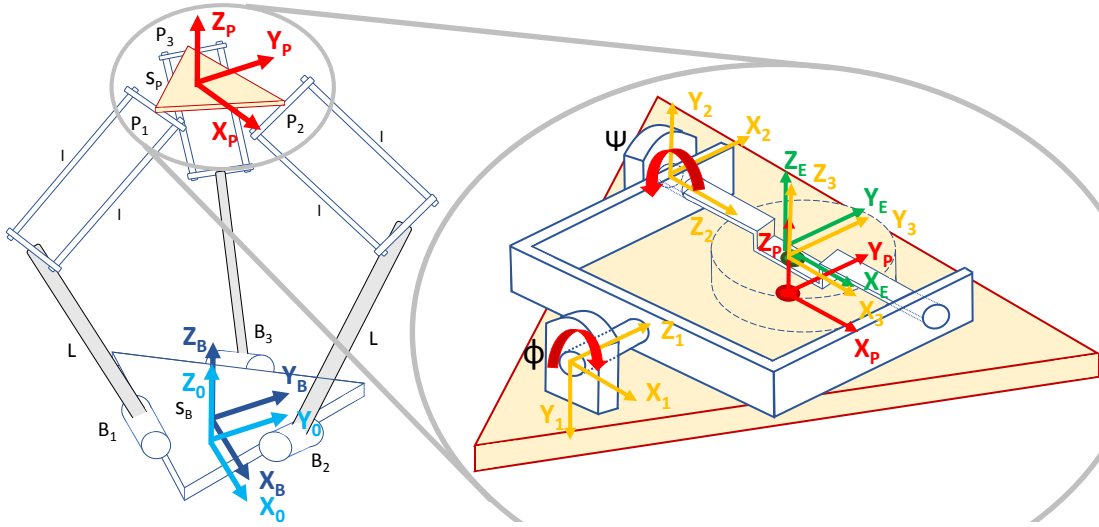
Figure 3.35: Integrating 3-RSR Parallel Delta manipulator and 2-DOF RR Serial $\perp^{lr}$ axis Manipulator

3.3.1 3-DOF RSR Parallel Delta Manipulator and 2-DOF RR Serial $\perp^{lr}$ axis Manipulator: Direct Kinematics

In order to derive the direct kinematics of the complete system an initial frame of coordinates is added at the top plane of the base plate to consider the elevation h_1 of the plane of actuation of the revolute joints in 3-DOF RSR Parallel Delta Manipulator.

The transformation of the initial coordinates from $^{B}O = \{x_0 \quad y_0 \quad z_0\}^T$ to final control point $^{P}E = \{x_E \quad y_R \quad z_E\}^T$ for the complete assembly can be described as follows:

Step	From	To	Method of Transformation	Section
1	Center of the top of the fixed base $\{O\}$	Center of the plane of motor actuation in fixed base $\{B\}$	Linear Translation	-
2	Center of the plane of motor actuation in fixed base $\{B\}$	Center of the moving platform $\{P\}$	Translation of coordinates by $\{x_P \quad y_P \quad z_P\}^T$	3.1.4
3	Center of the moving platform $\{P\}$	1st revolute joint $\{1\}$	Homogeneous Transformation	3.2.3.1
4	1st revolute joint $\{1\}$	2nd revolute joint $\{2\}$	Homogeneous Transformation	3.2.3.2
5	2nd revolute joint $\{2\}$	Center of the sample holder $\{3\}$	Homogeneous Transformation	3.2.3.3
6	Center of the sample holder $\{3\}$	End-effector (i.e. the target micro-particle on sample holder) $\{E\}$	Linear Translation	3.2.3.4

Table 3.18: Steps for establishing coordinate frames for integrated assembly of manipulators

From the above table we can derive the following equation for complete homogeneous transformation:

$$T_E^O = T_B^O T_P^B T_E^P$$

$$T_E^O = T_B^O T_P^B A_{1H} A_{1H} A_{3H} A_{4T}$$

$$T_E^O = \begin{bmatrix} c\phi & -s\phi s\psi & -c\psi s\phi & x_p + (a_2 - a_1 + a_E)c\phi + (h_3 - h_E)c\psi s\phi - b_E s\phi s\psi \\ 0 & c\psi & -s\psi & y_p + b_2 - b_1 + b_E c\psi + (h_3 - b_E)s\psi \\ s\phi & c\phi s\psi & c\phi c\psi & h_1 + z_p + h_2 + (a_2 - a_1 + a_E)s\phi - (h_3 - he)c\phi c\psi + h_E c\phi s\psi \\ 0 & 0 & 0 & 1 \end{bmatrix}$$

$$(3.35)$$

3.3.2 3-DOF RSR Parallel Delta Manipulator and 2-DOF RR Serial $\perp^{lr}$ axis Manipulator: Inverse Kinematics

The goal of the inverse kinematics is to find the the rotations required at the revolute joints i.e. ϕ and ψ for a particular linear translation $^B P_P = \{x_p \quad y_P \quad z_P\}^T$ to achieve the given final end-effector coordinates i.e. $^P E = \{x_E \quad y_R \quad z_E\}^T$. From the final homogeneous transformation 3.35 obtained in the previous section we can compare the given end effector coordinates as shown below:

$$T_E^O = \begin{bmatrix} R_{3\times3} & ^P E_{3\times1} \\ 0 & 1 \end{bmatrix} \tag{3.36}$$

Hence, we obtain the following three equations:

$$x_E = x_P + (a_2 - a_1 + a_E)c\phi + (h_3 - h_E)c\psi s\phi - b_E s\phi s\psi$$

$$y_E = y_P + b_2 - b_1 + b_E c\psi + (h_3 - h_E)s\psi \tag{3.37}$$

$$z_E = h_1 + z_P + h_2 + (a_2 - a_1 + a_E)s\phi - (h_3 - he)c\phi c\psi + b_E c\phi s\psi$$

Rewriting the equation from y_E and comparing it with the following equation:

$$A_1 c\psi - B_1 s\psi = C_1 \tag{3.38}$$

where:

$$A_1 = (b_E), \qquad B_1 = h_E - h_3, \qquad \text{and} \qquad C_1 = y_e - y_p - b_2 + b_1$$

Also, another form of equation 3.38 is as follows,

$$A_1 c\psi - B_1 s\psi = C_1 = R_1 cos(\psi + \gamma_1) \tag{3.39}$$

where:

$$R_1 = \sqrt{A_1^2 + B_1^2}, \qquad \text{and} \qquad \gamma_1 = Atan\frac{B_1}{A_1}$$

Comparing the constants we get:

$$R_1 cos(\psi + \gamma_1) = C_1$$
$$\psi = (Acos\frac{C_1}{R_1}) - \gamma_1 \tag{3.40}$$

Rewriting the other equations from x_E and z_E and comparing it with the equation similar to 3.38:

$$A_{2,3}c\phi - B_{2,3}s\phi = C_{2,3} \qquad (3.41)$$

where:

$$A_2 = a_2 - a_1 + a_E, \qquad B_2 = (h_E - h_3)c\psi + b_E s\psi, \qquad \text{and} \qquad C_2 = x_E - x_P$$

$$A_3 = h_E - h_3 c\psi + b_E s\psi, \qquad B_3 = -(a_2 - a_1 + a_E), \qquad \text{and} \qquad C_3 = z_E - h_1 - h_2 - z_p$$

Rewriting, another form of equation 3.41 similar to 3.39,

$$A_{2,3}c\phi - B_{2,3}s\phi = C_{2,3} = R_{2,3}cos(\phi + \gamma_{2,3}) \qquad (3.42)$$

where:

$$R_{2,3} = \sqrt{A_{2,3}^2 + B_{2,3}^2}, \qquad \text{and} \qquad \gamma_{2,3} = Atan\frac{B_{2,3}}{A_{2,3}}$$

Comparing the constants we get:

$$R_{2,3}cos(\phi + \gamma_{2,3}) = C_{2,3}$$
$$\phi = (Acos\frac{C_{2,3}}{R_{2,3}}) - \gamma_{2,3} \qquad (3.43)$$

where: $\quad 0 \le \phi \le 90°$

Thus, from equations 3.43 and 3.40 we can obtain the rotations required at the revolute joints i.e. ϕ and ψ respectively for a particular linear translation $^BP_P = \{x_p \quad y_P \quad z_P\}^T$, in order to achieve the given final end-effector coordinates i.e. $^PE = \{x_E \quad y_E \quad z_E\}^T$.

Chapter 4

Fabrication

As per the link lengths decide in the previous sections a CAD model is created in SOLIDWORKS for the analysis of the complete model and observe the working assembly of the model. During this phase of creating a CAD model many difficulties were identified and corrected in different versions. The final CAD model of the prototype is as shown in the figure 4.1. Furthermore, this section will discuss all the parts that were machined, fabricated and/or ordered. Also machines and tools used during this process will be described. For the parts of setup that were machined all the machining steps will be discussed.
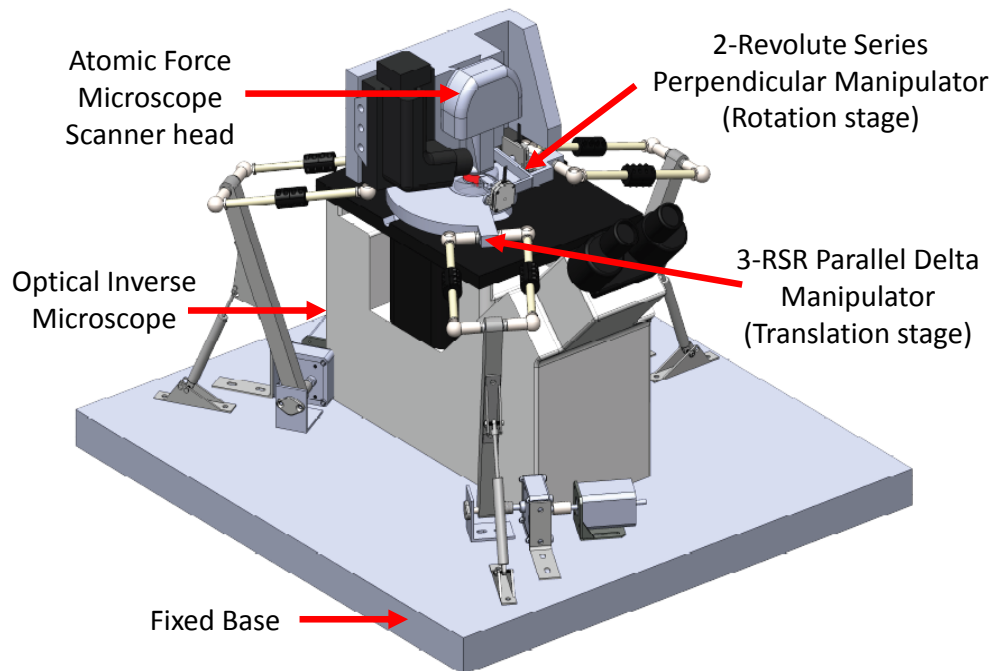
Figure 4.1: Final CAD Model for the setup

4.1 Fabrication: 3-DOF RSR Parallel Delta Manipulator

4.1.1 3-DOF RSR Parallel Delta Manipulator: CAD Model

The following figure 4.2 shows the CAD model for the 3-DOF RSR Parallel Delta Manipulator.
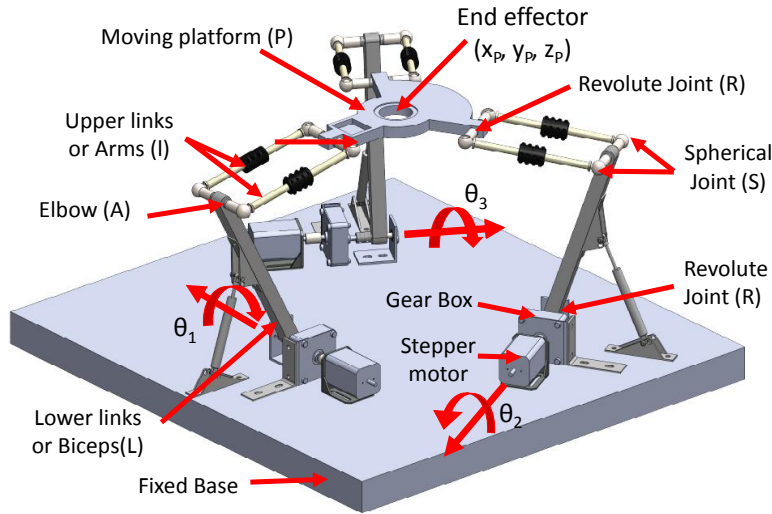
Figure 4.2: CAD Model for 3-DOF RSR Parallel Delta Manipulator

The link lengths chosen as described in the previous sections ensures the large range of motion as described by the workspace generated in the section 3.1.7.In order to increase the stability and robustness of the manipulator three gas springs were connected to the lower links. This cause a drastic reduction in the effects of vibrations induced internally and externally and increases the static stability. But, by doing so the range of the angular motion of the lower links is limited within the range of 55.12 ° to 87 °, as shown in figures 4.3 and 4.4. Hence the workspace is reduced because of that. Now the end-effector can reach -83.09 mm to 82.24 mm in X-axis direction, -90.45 mm to 77.26 mm in Y-axis direction and 236.1 to 402.8 mm in Z direction. Hence, we can say that the range of motion now available in X-axis is 165.33 mm , Y axis is 167.71 mm and Z axis is 166.7 mm. Hence, there is a reduction of 18.85 %, 18.75%, and 4.19% in X, Y, and Z-axis respectively.
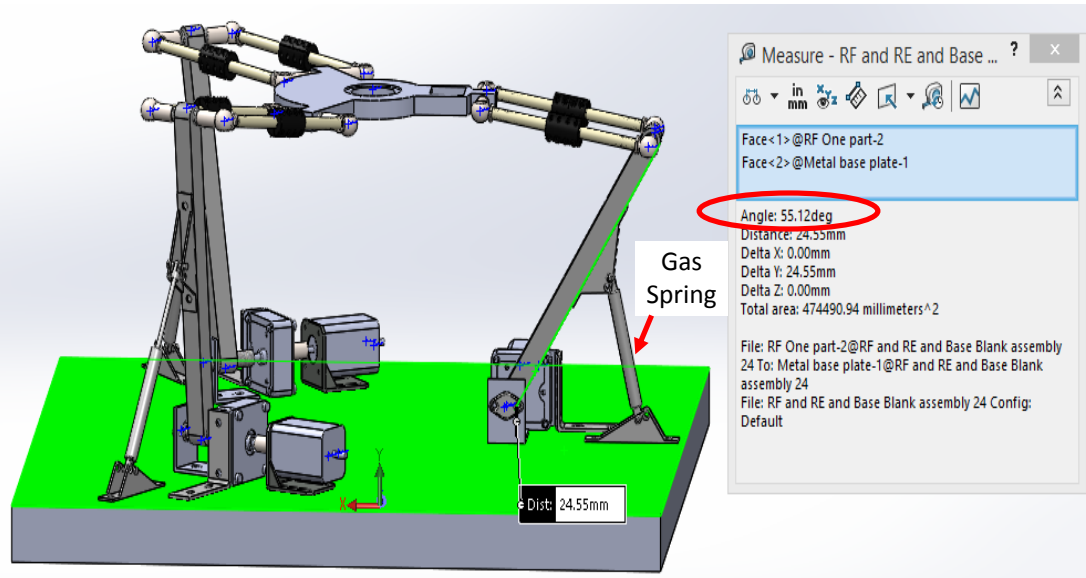
Figure 4.3: CAD Model showing minimum angle limit due to gas spring
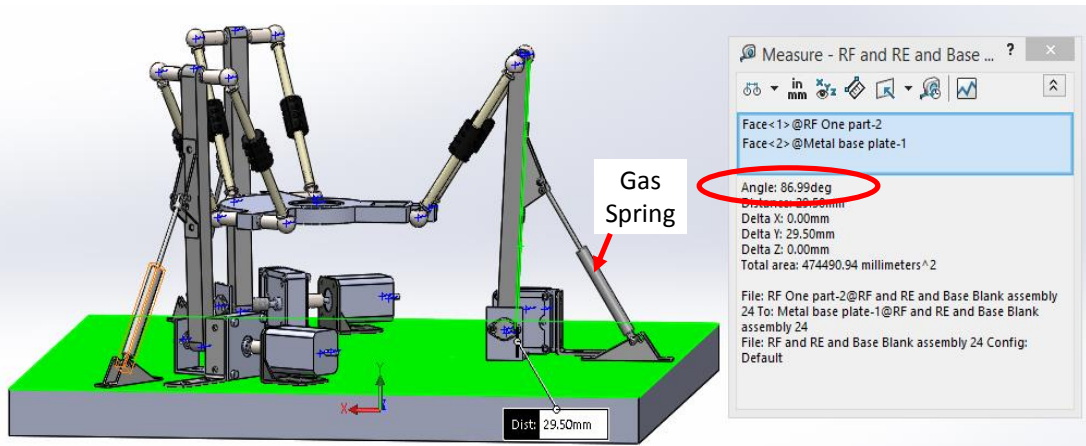
Figure 4.4: CAD Model showing angle maximum limit due to gas spring

In order to achieve high resolution in actuation the stepper motor is connected to a gearbox. In order to minimize any play and backlash in motion transmission precision coupling is used. And all the parts are selected with high precision and grade. Also, the parts fabricated in the machine shop were machined with precision up to two decimal points.

Moving platform have to accommodate a hole for the optical focus of OIM, and it is also necessary that it does not interferes with the AFM scanning head support

and camera setup. Hence, the moving platform have a distorted shape to satisfy all the requirements. It also have to be light-weight to prevent high payload at the end-effector of the assembly. So, it was decided to 3D print the part with plastic instead of fabricating it from metal.

The CAD model does not include the fasteners to prevent the computation time for SOLIDWORKS motion in the assembly. Various washers were used in the fabrication to hold the parts in place rigidly and for equal spacing. ePTFE washers were used to reduce the friction between the parts to prevent wear and tear and loss of motion transmission.

4.1.2 3-DOF RSR Parallel Delta Manipulator: Bill of Materials
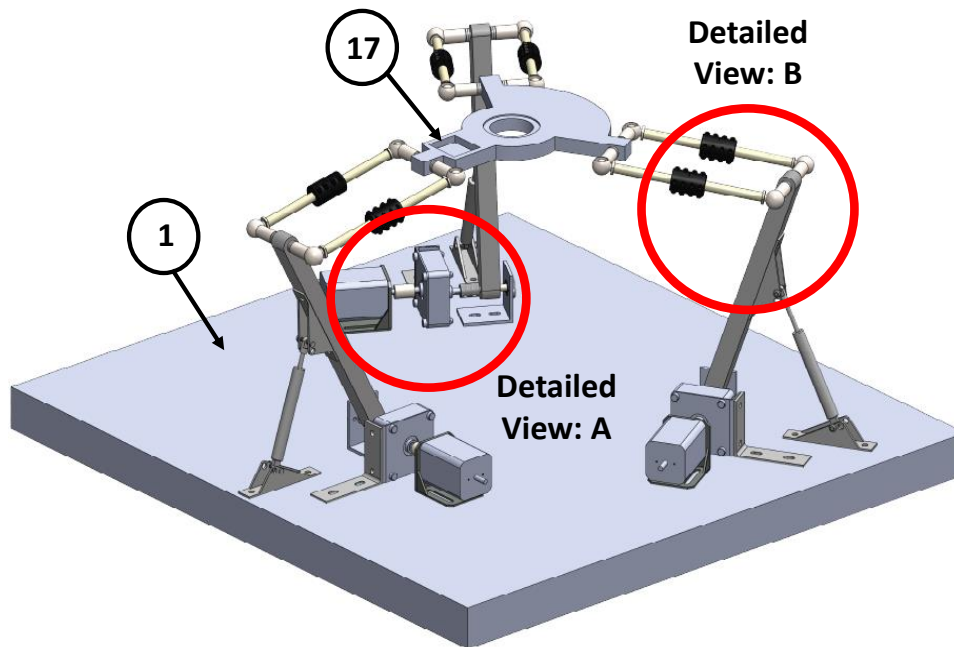
Figure 4.5: 3-DOF RSR Parallel Delta Manipulator:Bill of Materials

This subsection will describe the bill of materials required for the fabrication of the 3-DOF RSR Parallel Delta Manipulator. See table 4.1 for the components nomenclature, part name by vendor, name of the vendor and quantity required for the assembly. This section will cover all the parts that are purchased and that are machined after purchase.
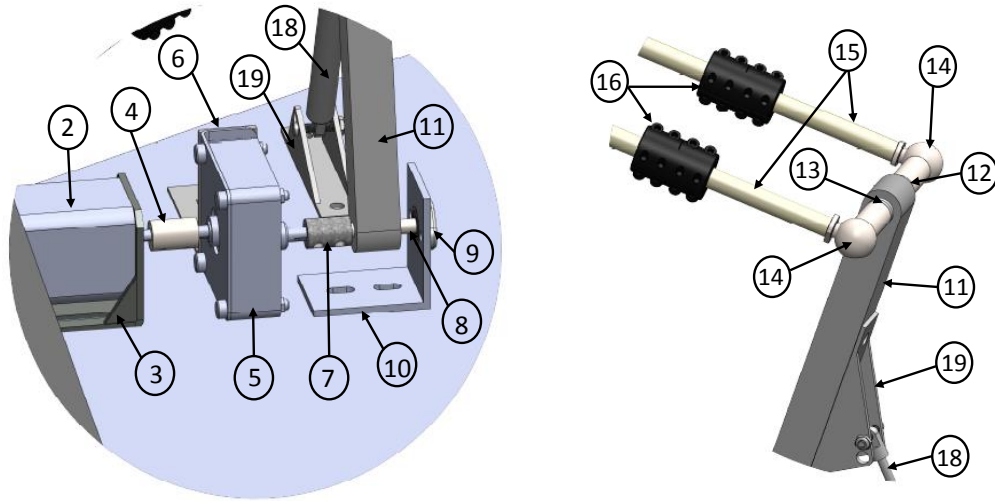
(a) Detailed view A: Scale 2:0.7   (b) Detailed view B: Scale 2:0.7

Figure 4.6: Detailed views for 3-DOF RSR Parallel Delta Manipulator

Label	Description	Part Name	Vendor	Qty.
1	Base Plate	Steel Plate 1-3/4" A-36 HR STEEL PLATE 26" × 28" Galvanized dipped	Metals Depot [51]	3
2	Stepper Motor	OMHT17-278	Omega Engineering [9]	3
3	Stepper Motor mount	3PCS Alloy Steel L Bracket for Nema 17 Stepper Motor	Amazon-Beauty Star [10]	3
4	Coupling A: Motor to gearbox	Shaft Couplings (metric)	Stock Drive Products Sterling Instrument SDP/SI [11]	3
5	Gearbox	Speed Reducer - Parallel Shaft	Stock Drive Products Sterling Instrument SDP/SI [12]	3
6	Gearbox mount	Corner machine bracket	McMaster Carr [13]	3

7	Coupling B: Gearbox to Dowel Pin	Shaft Couplings (metric)	Stock Drive Products Sterling Instrument SDP/SI [14]	3
8	Dowel Pin	Dowel Pin	McMaster Carr [15]	3
9	Ball Bearing	Light duty mounted ball bearing	McMaster Carr [16]	3
10	Ball Bearing mount	Corner machine bracket	McMaster Carr [17]	3
11	Lower Link(L)	-	-	3
12	Elbow (A)	Connecting Rod: External threads	McMaster Carr [18]	6
13	PTFE Washers	Abrasion-Resistant ePTFE Plastic Sealing Washer	McMaster Carr [19]	36
14	Ball Joints	Ball Joint: Right Hand thread	McMaster Carr [20]	12
15	Upper links	Connecting rod: Internal Threads	McMaster Carr [21]	6
16	Clamps	Two-piece shaft coupling	McMaster Carr [22]	6
17	Moving Platform	-	-	1
18	Gas Springs	Gas Spring 5 lbs. Force	McMasterCarr [23]	3
19	Gas Spring Mounts	Heavy Duty 0.16" ID Eyelet Mounting Bracket for Gas Spring	McMaster Carr [52]	6

Table 4.1: Bill of Materials for 3-DOF RSR Parallel Delta Manipulator

4.1.3   3-DOF RSR Parallel Delta Manipulator: Part Specifications

1. **Base Plate:**

   Hot Rolled A36 Steel Plate (L × W × H) = (28"× 26" × 1-3/4")

   Specifications: ASTM A36, AISI A-36 and Galvanized dipped for corrosion resistance.

   Applications: base plates, gussets, liners, road plates, trench covers, etc.

   Workability: Easy to Weld, Cut, Form and Machine

   Mechanical Properties: Magnetic, Brinell = 112, Tensile = 58,000 +/−, Yield = 36,000 +/− [51]

2. **Stepper Motor:**

   2-phase biploar high torque stepper motor **Optimized for microstepping**: It can achieve a stepping resolution of up to 51,200 steps/revolution (.007 ° per step) when operated by microstepping drives. [9] Following figure 4.7 shows all the specifications of the stepper motor purchased.

MODEL NO.	MOTOR CONNECTION 1 = SERIES 2 = PARALLEL 3 = UNIPOLAR	MOTOR LENGTH mm (in)	HOLDING TORQUE^2 (oz–in)	LEADS	STEP ANGLE (DEG)	VOLTS	AMPS	OHMS	MH	ROTOR INERTIA (oz-in^2/ g–cm^2)	MOTOR WEIGHT g (lb)
OMHT17-278	1	63 (2.47)	113	8	1.8	6.4	1.0	6.4	12.0	0.66/121	357 (1.32)
	2					3.2	2.0	1.6	3.0		
	3		79.0			4.5	1.40	3.2	3.0		
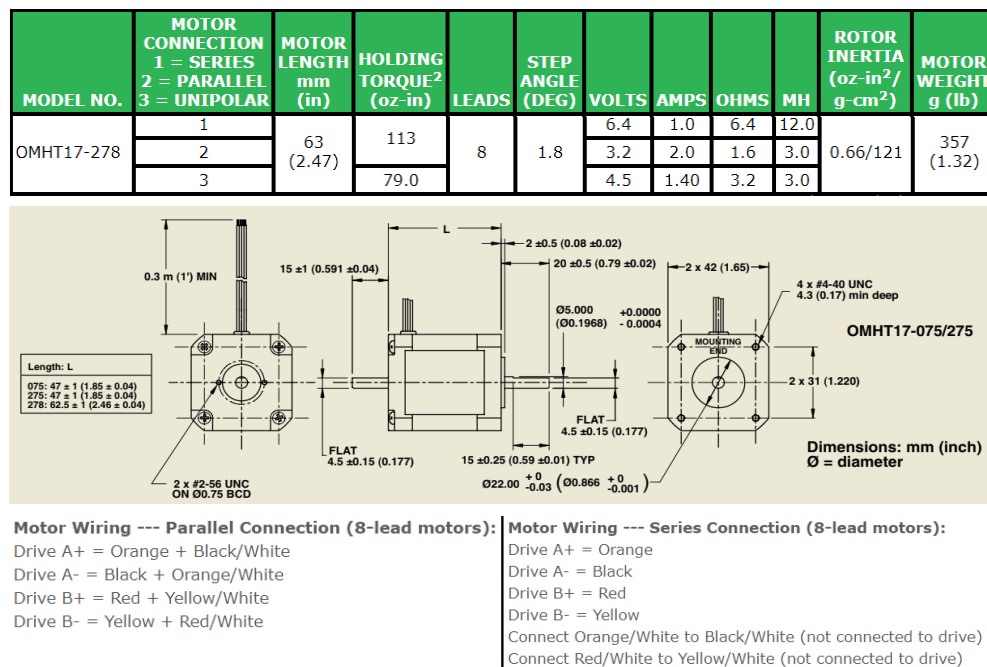
Figure 4.7: Stepper Motor: Specifications [9]

3. **Stepper Motor mount:**

3PCS Alloy Steel L Bracket for Nema 17 Stepper Motor with Screws and Inner Hexagon Spanner.

Material: Alloy steel with plastic spraying finish.

Following figure 4.8 shows the drawing of the part purchased.
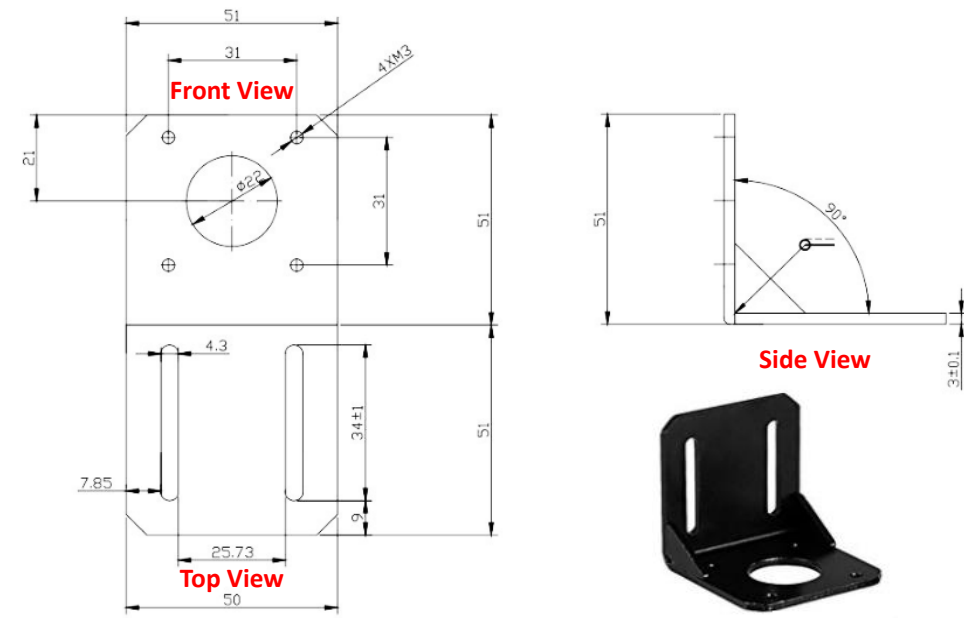
Figure 4.8: Stepper Motor mount: Specifications [10]

4. **Coupling A: Motor to gearbox:**

Material:303 Stainless Steel

Quality Class: Precision Tolerance [11] Following figure 4.9 shows all the specifications of the coupling purchased.

D Dia.	d Bore H7	d₁ Bore H7	l	A	L	T
13	5	6	10	5	20	M5
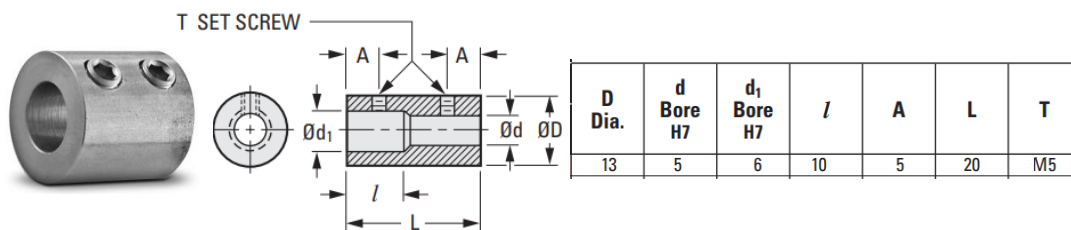
Figure 4.9: Coupling A: Motor to gearbox: Specifications [11]

5. **Gearbox:**

Material:Housing - Die Cast Aluminum;   Bracket - Steel, Black Enamel;

Shaft - Steel;   Gears - Steel and Phenolic;   Bearings - Input - Ball;

Output - Bronze;   Mating Motor Pinion - Brass

Operating Temperature:

-10°C to +60°C

Specifications:

Radial Play of Shaft: ≤ 0.1 mm;

Thrust Play of Shaft: ≤ 0.3 mm

Approx. weight: 0.026 kg (Speed Reducer) [12]

Following figure 4.10 shows the drawing of the part purchased.
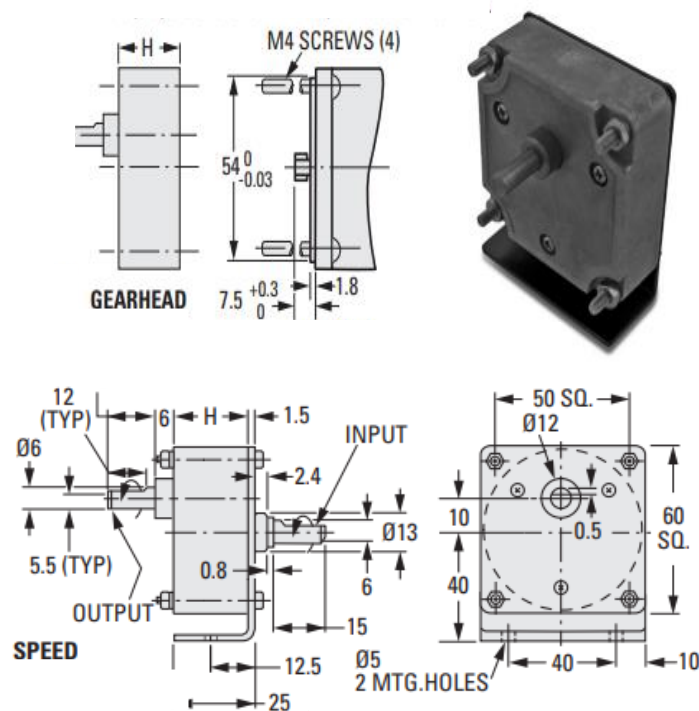
Catalog Number *		Gear Ratio to 1	Shaft Rotation	H	Efficiency %	Maximum Torque N • m (lb. in.)	
Speed Reducers	Gearheads Only					Continuous	Momentary
A 2Z25M0500	A 2G25M0500	500	Same	24	66	1 (8.9)	2.96 (26.2)

Figure 4.10: Gearbox: Specifications [12]

6. **Gearbox mount:** Corner Machine Bracket

   Material: 316 Stainless Steel

   Length: (A×B×C) = (75×60×75) [13]

   Following figure 4.11 shows the drawing of the part machined, from the part purchased.
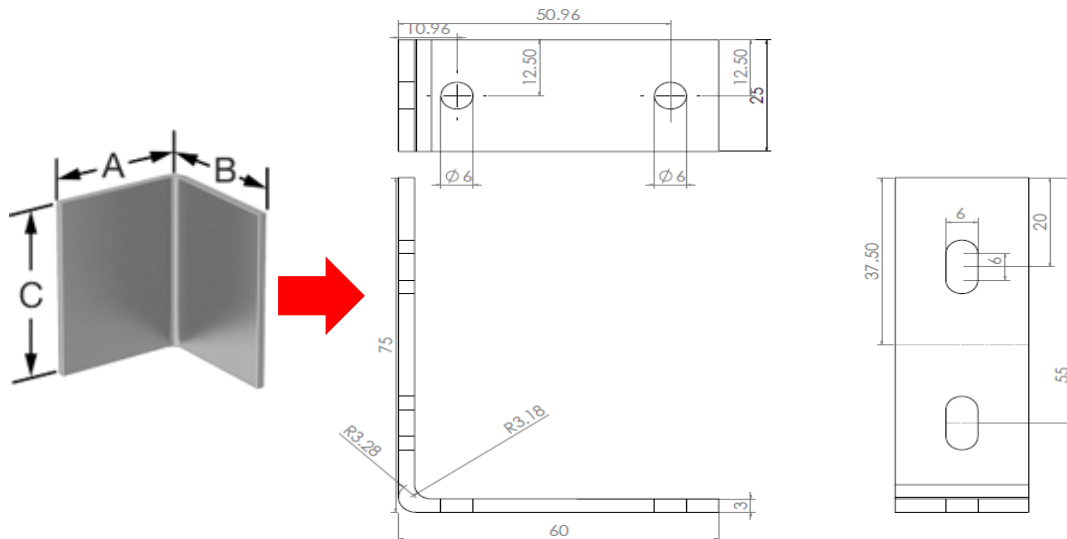
Figure 4.11: Gearbox mount: Specifications [13]

7. **Coupling B: Gearbox to Dowel Pin:**

   Material: Steel, Zinc Plated

   Quality Class: Commercial Tolerance [14] Following figure 4.12 shows all the specifications of the coupling purchased.

O.D.	B Bore +.002 -.000	D	L Length	Set Screw
1/2	.250	3/16	3/4	#10-24
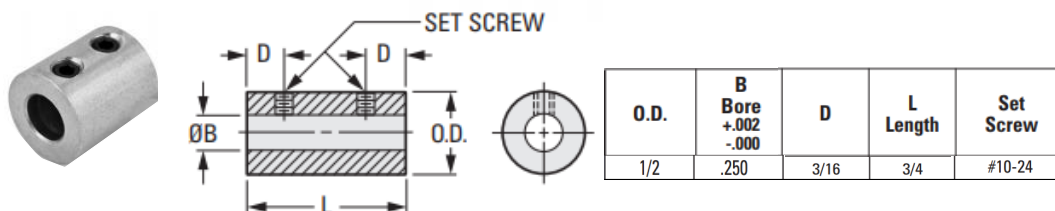
Figure 4.12: Coupling A: Gearbox to Dowel Pin: Specifications [14]

8. **Dowel Pin:**

1/4" Diameter, 2-1/2" Long

Material: 316 Stainless Steel [15]

Following figure 4.13 on page number 71 shows all the specifications of the part purchased.
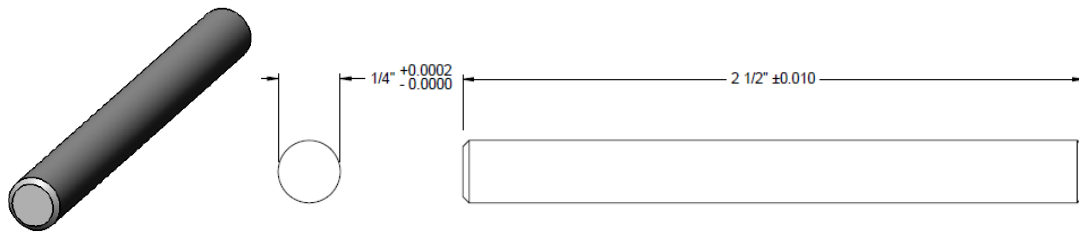
Figure 4.13: Dowel Pin: Specifications [15]

9. **Ball Bearing:**

Light Duty Mounted Ball Bearing with Two-Bolt Flange, Shielded, for 1/4" Shaft Diameter **Material**: 440C Stainless Steel

Radial Load Capacity: lbs. Dynamic 80 lbs.; Static 230 lbs.

Following figure 4.14 shows all the specifications of the part purchased.
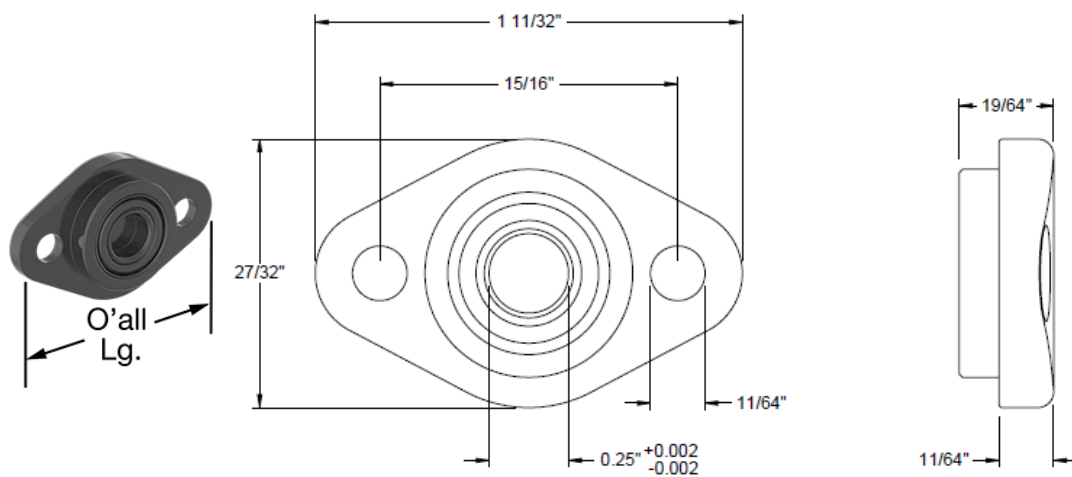
Figure 4.14: Ball bearing: Specifications [16]

10. **Ball bearing mount:**

Corner Machine Bracket

Material: 316 Stainless Steel

Length: $(A \times B \times C) = (2" \times 2" \times 1\frac{1}{2}")$ [17]

Figure 4.15 shows the drawing of the part machined, from the part purchased.
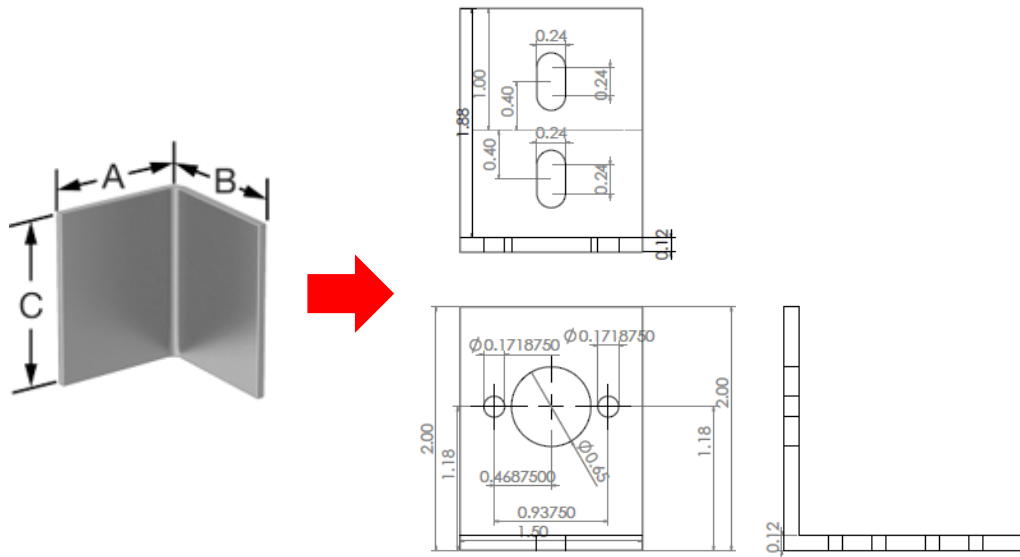

Figure 4.15: Ball bearing mount: Specifications [17]

11. **Lower link:**

Material: Poly Vinyl Chloride i.e. PVC plastic

Figure 4.16 shows the drawing of the part fabricated.
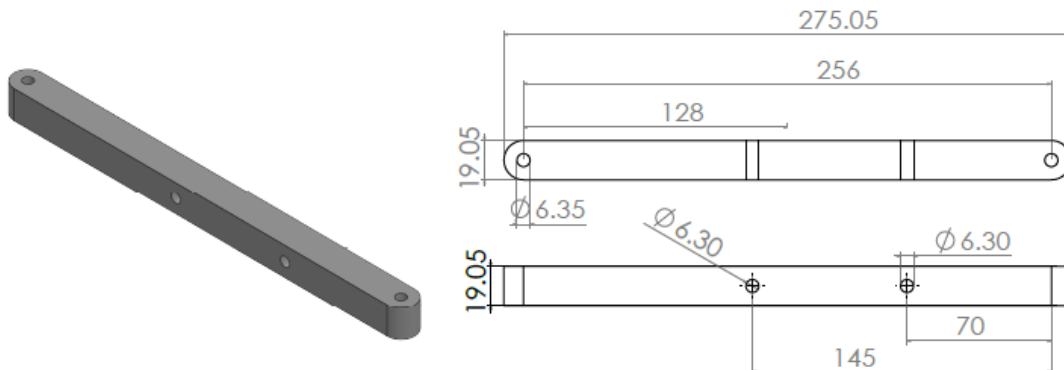
Figure 4.16: Lower link: Specifications

12. **Elbow:**

3" Overall Length, 1/4"-28 Thread

Material: Zinc-Plated Carbon Steel

Thread Direction: Right Hand [18]

Figure 4.17 shows the drawing of the part purchased.
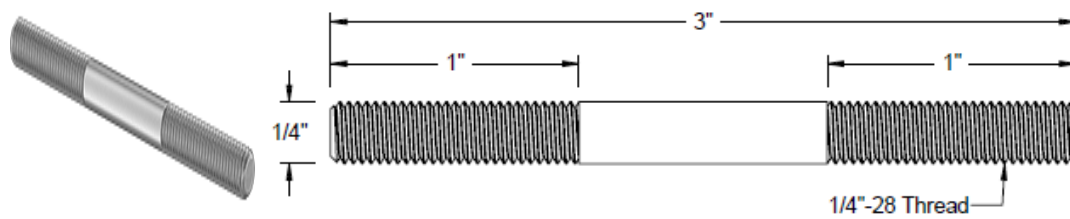
Figure 4.17: Elbow: Specifications [18]

13. **Washers:**

Abrasion-Resistant ePTFE Plastic Sealing Washer for 1/4" Screw Size, 0.25" ID, 0.5" OD Figure 4.18 shows the drawing of the part purchased.
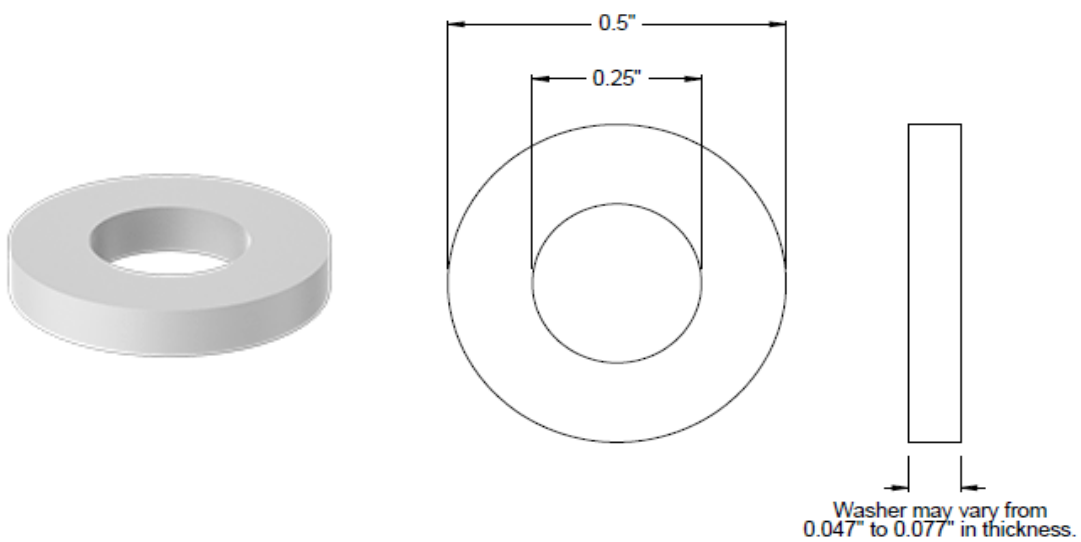
Figure 4.18: Washers : Specifications [19]

14. **Ball Joint:**

    Material: Zinc-Plated Alloy Steel; **Ball Stud Material**: Chrome-Plated Bearing Steel; **Insert Material**: Alloy Steel; **Liner Material**: PTFE Plastic

    Shank Thread Direction: Right Hand; **Ball Stud Thread Direction**: Right Hand

    Figure 4.19 shows the drawing of the part purchased.
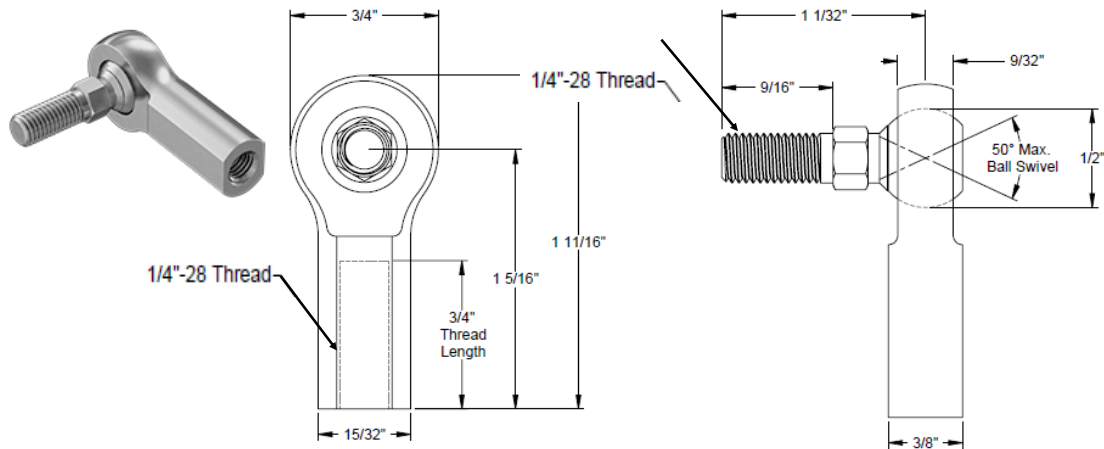
    Figure 4.19: Ball joint: Specifications [20]

15. **Upper Links:**

    Material: Zinc-Plated Carbon Steel; **Thread Direction**: Right Hand; Figure 4.20 shows the drawing of the part purchased.
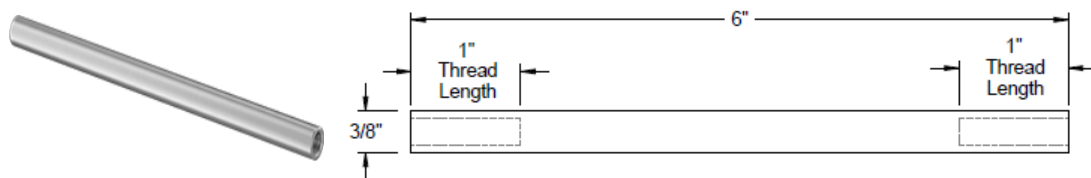

    Figure 4.20: Upper links: Specifications [21]

16. **Clamps:**

    Two-Piece Shaft Coupling Steel, for 3/8" x 3/8" Diameter Round Shaft **Material**: Steel;

Figure 4.21 shows the drawing of the part purchased.
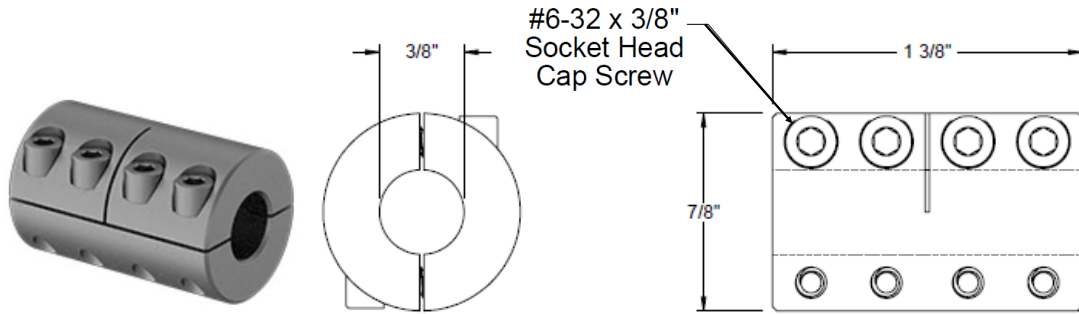
Figure 4.21: Clamps: Specifications [22]

17. **Moving Platform:**

3D Printed using Polyjet Printer; Figure 4.22 shows the drawing of the part that was 3D Printed
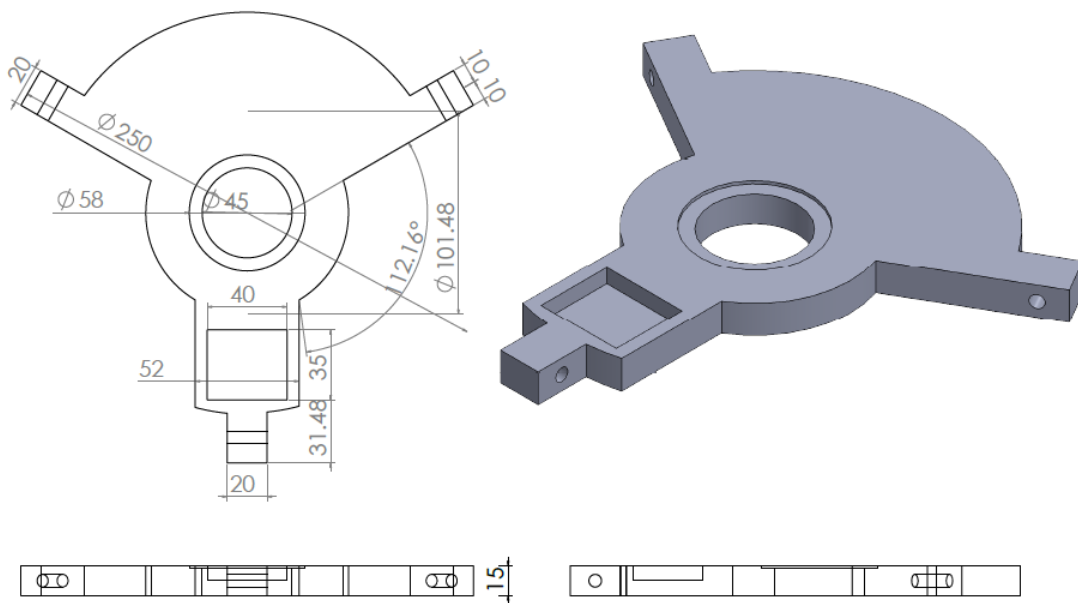
Figure 4.22: Moving Platform: Specifications

18. **Gas Springs:**

Extended Length: 7.08"; **Compressed Length**: 4.52"; **Stroke Length**: 2.56"; **Force Mechanism**: Compressed Nitrogen Gas; **Rod Material**: Chrome-Plated Steel; **Eyelet Material**: Aluminum Figure 4.23 shows the drawing of the
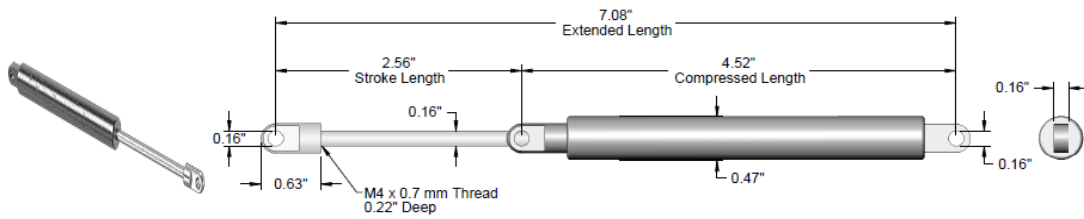
part purchased.

Figure 4.23: Gas Springs: Specifications [23]

19. **Gas Spring mounts:**

For Eyelet ID : 0.16"; **Material**: Zinc-Plated Steel Figure 4.24 shows the drawing of the part purchased.
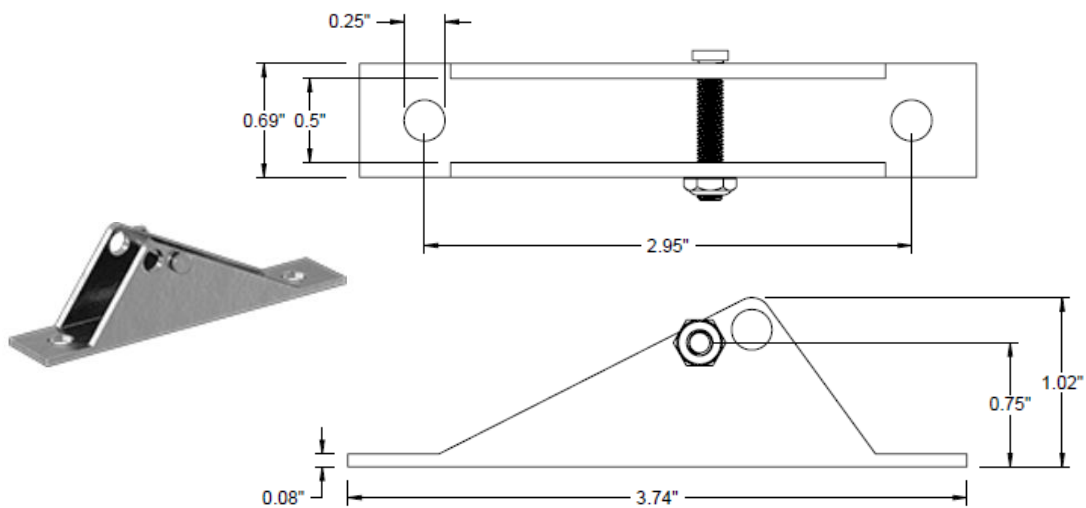
Figure 4.24: Gas Spring mounts: Specifications

4.2 Fabrication: 2-DOF RR Serial $\perp^{lr}$ axis Manipulator

4.2.1 2-DOF RR Serial $\perp^{lr}$ axis Manipulator: CAD Model

The following figure 4.25 shows the CAD model for the 2-DOF RR Serial $\perp^{lr}$ axis Manipulator. As shown in the figure the moving platform gives a base for the mounting of the first ultra-flat stepper motor. Ultra-flat stepper motors were used so that there is more space available on the platform for the wrist link to rotate without any interference. This first motor acts as an actuator for the wrist link and provides for the angle ϕ with respect to Y-axis. Both of them are connected by a wrist joint.

The second ultra-flat stepper motor is directly connected to the wrist link and indirectly connected to the sample holder by the means of a sleeve. This sleeve acts as a support for the sample holder. Two set of clips are added to the sleeve in order to prevent any motion besides desired revolute motion. The sample holder also have a depth so that the sample can remain submerged in the medium present in the Petri dish even when the sample holder is manipulated. this sample holder is 3D printed for the current studies, but it need to be transparent so that the cells can be viewed by the OIM from bottom.
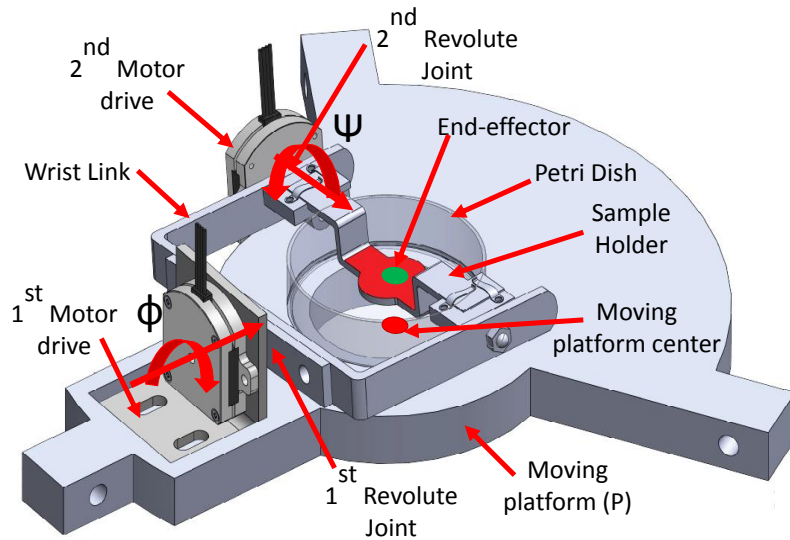
Figure 4.25: CAD Model for 2-DOF RR Serial $\perp^{lr}$ axis Manipulator

4.2.2   2-DOF RR Serial $\perp^{lr}$ axis Manipulator :Bill of Materials

(a) CAD Model: Top view

(b) CAD Model: Side view
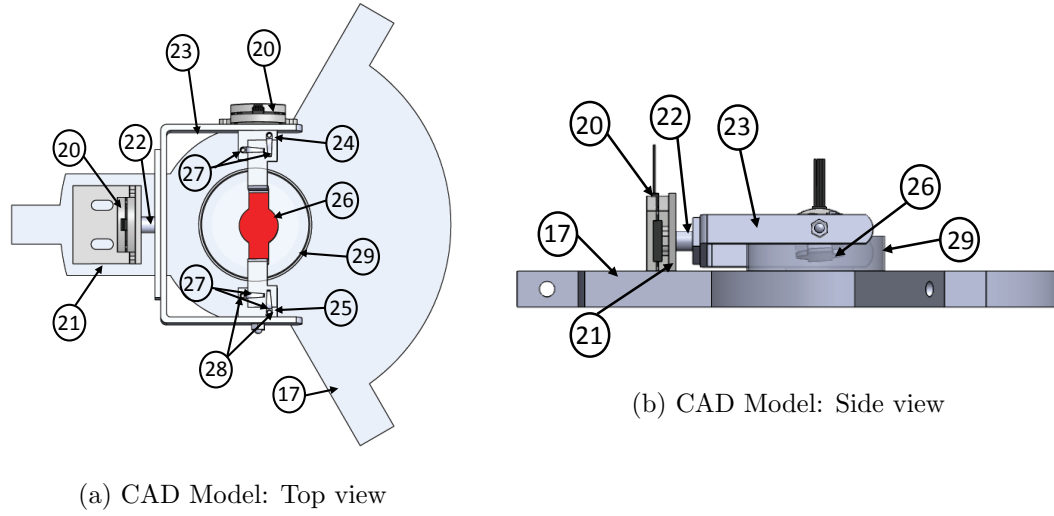
Figure 4.26: Top and Side views for 2-DOF RR Serial $\perp^{lr}$ axis Manipulator: Bill of materials

Label	Description	Part Name	Vendor	Qty.
20	Pancake Stepper Motor	Ultraflat Stepper Motor	Nanotec Electronics [24]	2
21	Pancake Stepper Motor mount	Corner machine bracket	McMaster Carr [25]	1
22	Wrist joint	-	-	1
23	Wrist link	Architectural 6063 Aluminum U-Channel	McMaster Carr [26]	1
24	Sleeve A	-	-	1
25	Sleeve B	-	-	1
26	Sample holder	-	-	1
27	Clips	PELCO SEMClip^{TM} Clips	Ted Pella, Inc. [27]	4
28	Screws	Screws, Brass M2 $\times$ 3	Ted Pella, Inc. [27]	4
29	Petri Dish	-	-	1

Table 4.2: Bill of Materials for 2-DOF RR Serial $\perp^{lr}$ axis Manipulator

4.2.3 2-DOF RR Serial $\perp^{lr}$ axis Manipulator: Part Specifications

20. **Pancake Stepper Motor:**

    Ultraflat high-torque stepper motor with 28 x 34 mm flange, 0.9 mm height, high torque and speeds up to 4500rpm. [24]

    Resolution 1.8 ° /step; **Holding Torque** 0.98 Ncm; **Rotor Inertia** 1.7 gcm^2; **Weight** 0.028 kg;

    Figure 4.27 shows the drawing of the part purchased.
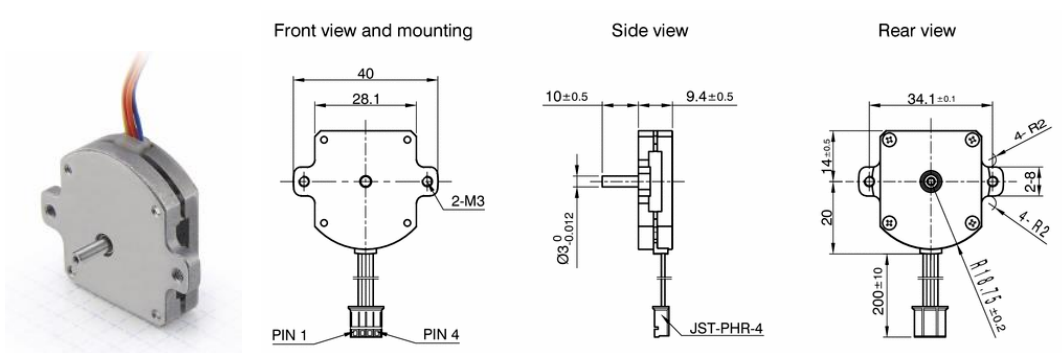
Figure 4.27: Pancake motors: Specifications [24]

21. **Pancake Stepper Motor mount:**
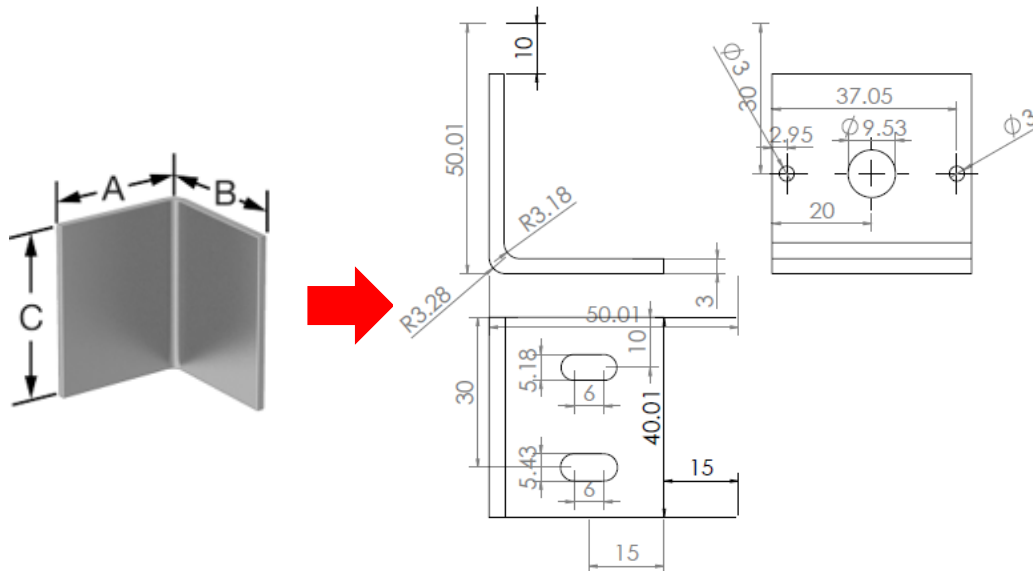
Figure 4.28: Pancake motor mount: Specifications [25]

Corner Machine Bracket

Material: 6061 Aluminum

Length: $(A \times B \times C) = (50 \text{ mm} \times 50 \text{ mm} \times 40mm\frac{1}{2}")$ [25]

Figure 4.28 shows the drawing of the part machined, from the part purchased.

22. **Wrist Joint:**

   Material: 6061 Aluminum

   Figure 4.29 shows the drawing of the part machined.
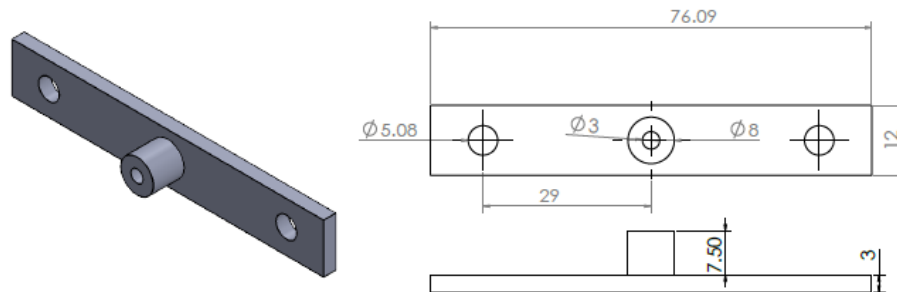
Figure 4.29: Wrist Joint: Specifications

23. **Wrist Link:**

   6063 Aluminum U-Channel; 1/8" Wall Thickness, 3" High x 4" Wide

   Figure 4.30 shows the drawing of the part machined from the part purchased [26].
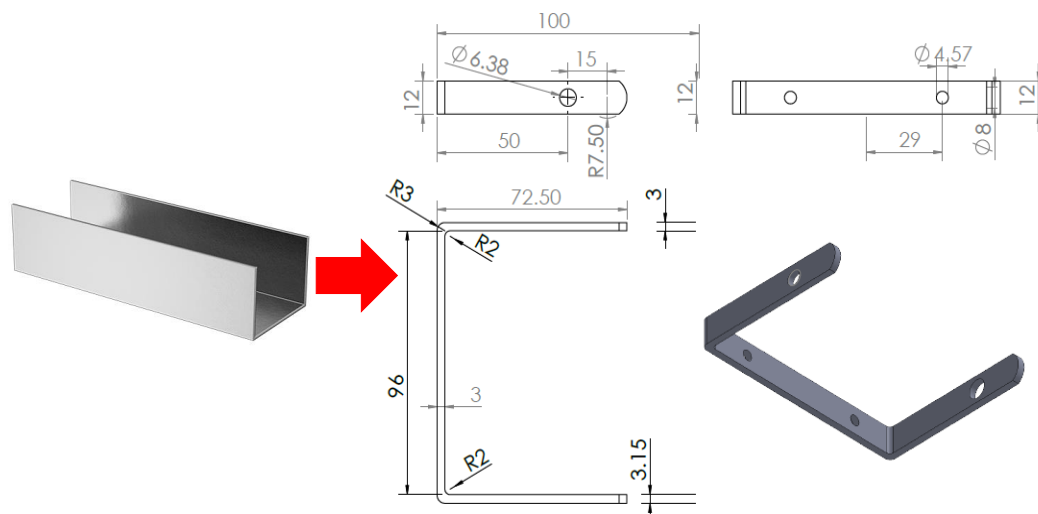
Figure 4.30: Wrist Link: Specifications [26]

24. **Sleeve A:**

Material: 6061 Aluminum

Figure 4.31 shows the drawing of the part machined.
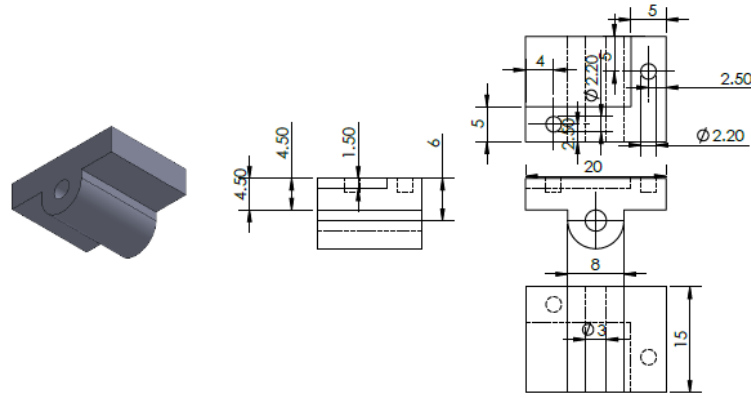
Figure 4.31: Sleeve A: Specifications

25. **Sleeve B:**

Material: 6061 Aluminum

Figure 4.32 shows the drawing of the part machined.
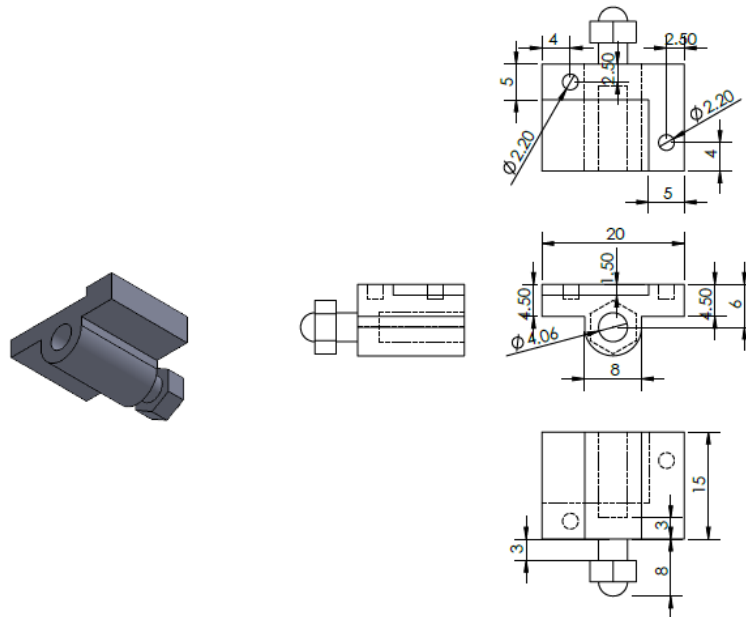
Figure 4.32: Sleeve B: Specifications

26. **Sample Holder:**

3D Printed using Polyjet Printer; Figure 4.33 shows the drawing of the part that was 3D Printed
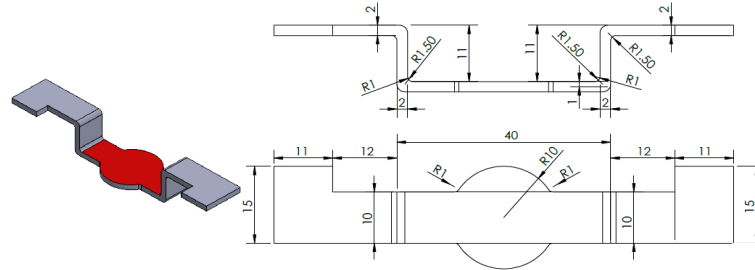
Figure 4.33: Sample holder: Specifications

27. **Clips and**

28. **Screws:**

PELCO SEMClip^{TM} Clips **Material:** spring grade beryllium-copper alloy;

Thickness: 0.25mm (0.01");

Overall length: 12.7mm (1/2");

Width at tip: 1.6mm (1/16");

Hole diameter: 2.2mm (0.087")

Figure 4.34 shows the image of the part purchased.

Figure 4.34: Clips and Screws : Product Image [27]

4.3   Machining: CAM Simulation, Process and Machine Tools

In this section the process of machining parts will be discussed briefly, along with the list of machine tools used for fabrication of components.

In order to figure out the steps required to machine a part Computer-Aided Manufacturing (CAM) simulation was performed in SOLIDWORKS using VisualCAMc by MecSoft Corporation [53]. Following lists the steps for the simulation

1. Initially, a part bounding box stock is created and controlled in VisualCAMc environment. This bounding box created shall be the same size of the component from which the final product is going to be machined. It depends on the availability of the sizes for a given component in the market. Further the component shall be selected to reduce machining-time,cost. Figure 4.35 illustrates the fabrication of lower links as shown in the figure 4.16 in section 4.1.3.
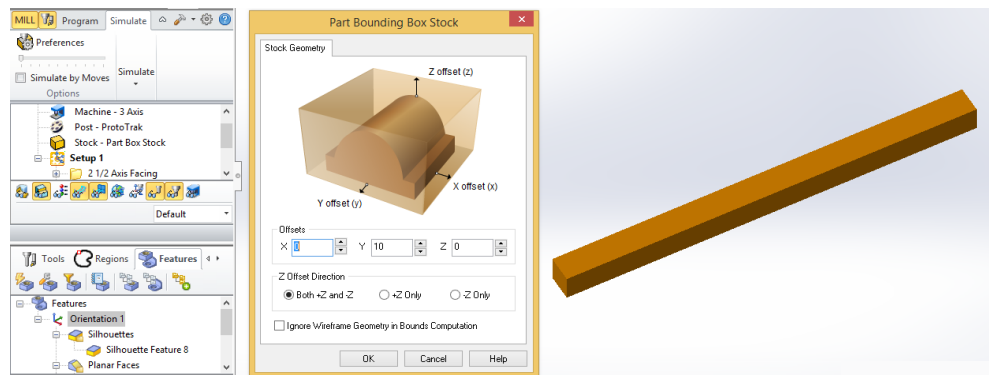
Figure 4.35: Part Bounding Box Stock

2. After, the bounding box stock is created, features are detected by automatic feature detection and/or interactive feature detection options. VisualCAMc provides an option to save the list of features that includes: (a) Feature type, (b) Feature name, (c) Feature parameters etc..

3. Once, all the features are identified on the part a machine knowledge base is created for milling features. This can also be done automatically and/or interactively. This knowledge base consists of all the machining steps required to fabricate the component.

   Since, machining holes is provided by VisualCAMc as a different set of options, a seperate knowledge base is generated for all the hole features on the component. The features detected for the part 4.16 are as shown in figure 4.36.
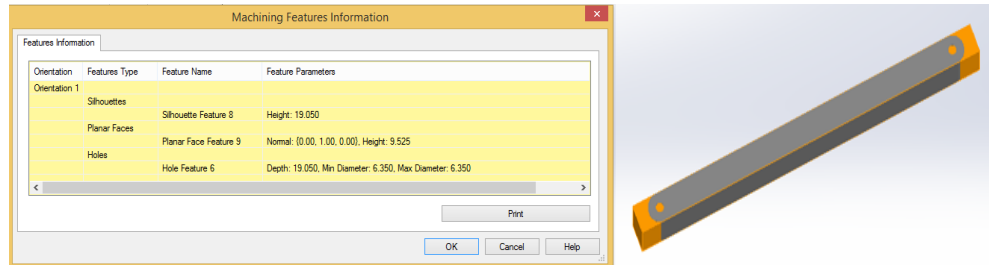
Figure 4.36: Feature Detection

4. Furthermore, the tools can be set by user depending on the machining process and availability of tool sizes and type.

5. Finally, based on all the machining steps provided in the knowledge base tool paths are created and they are custom for all the machines available in the Library. The change of tools automatically adjusts the tool path even at the later stage. Following figures 4.37, 4.38 shows the tool path for the facing and profiling operations respectively on the part bounding box stock. Also the figure 3.7 illustrates the drilling operations on the 4.16 part.
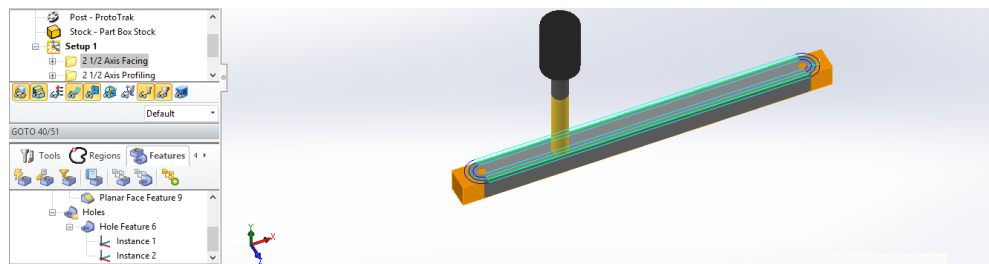
Figure 4.37: Tool Path for facing operation
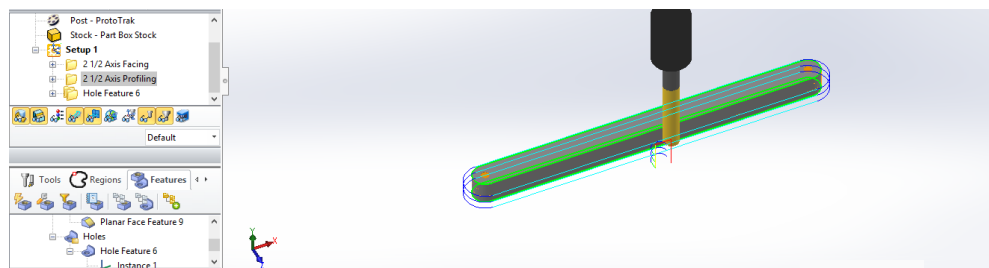
Figure 4.38: Tool Path for profiling operation
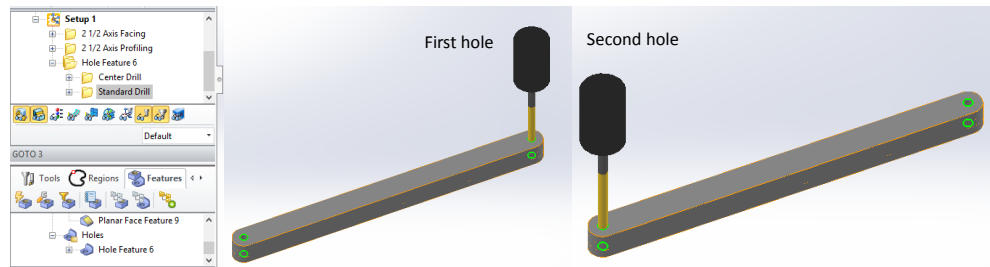
Figure 4.39: Steps:Drilling operation

Milling machine extensively used for the fabrication of all the components was Knee type milling machine controlled by ProtoTRAK SMX version-5.11 by Southwestern Industries, Inc. Other machines used were Lathe Machine, Drill Machines, Band Saw Machine, Grinding Machine. Various Hand tools were also used for machining purposes.

Following figure 4.40 shows the actual set up of the component on the Knee type milling machine controlled by ProtoTRAK SMX version-5.11 by Southwestern Industries, Inc.
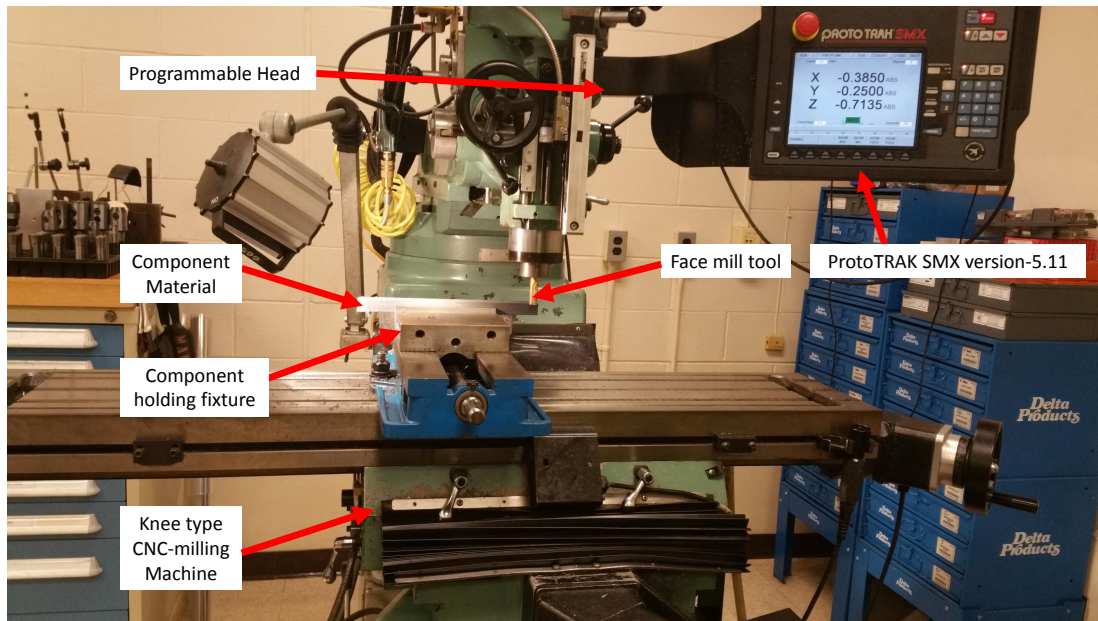
Figure 4.40: Machine setup for machining the lower links 4.16

4.4 Final Assembly

After the fabrication of all the components, they were assembled together for the 3-RSR Parallel Delta Manipulator and 2-DOF RR Serial $\perp^{lr}$ axis Manipulator. Assembly for the 3-RSR Parallel Delta Manipulator is shown in figure 4.41 and assembly of 2-DOF RR Serial $\perp^{lr}$ axis Manipulator is shown in the following figure 4.42. Figure 4.43 on page number 87 shows the final integrated assembly of both 3-RSR Parallel Delta Manipulator and 2-DOF RR Serial $\perp^{lr}$ axis Manipulator.
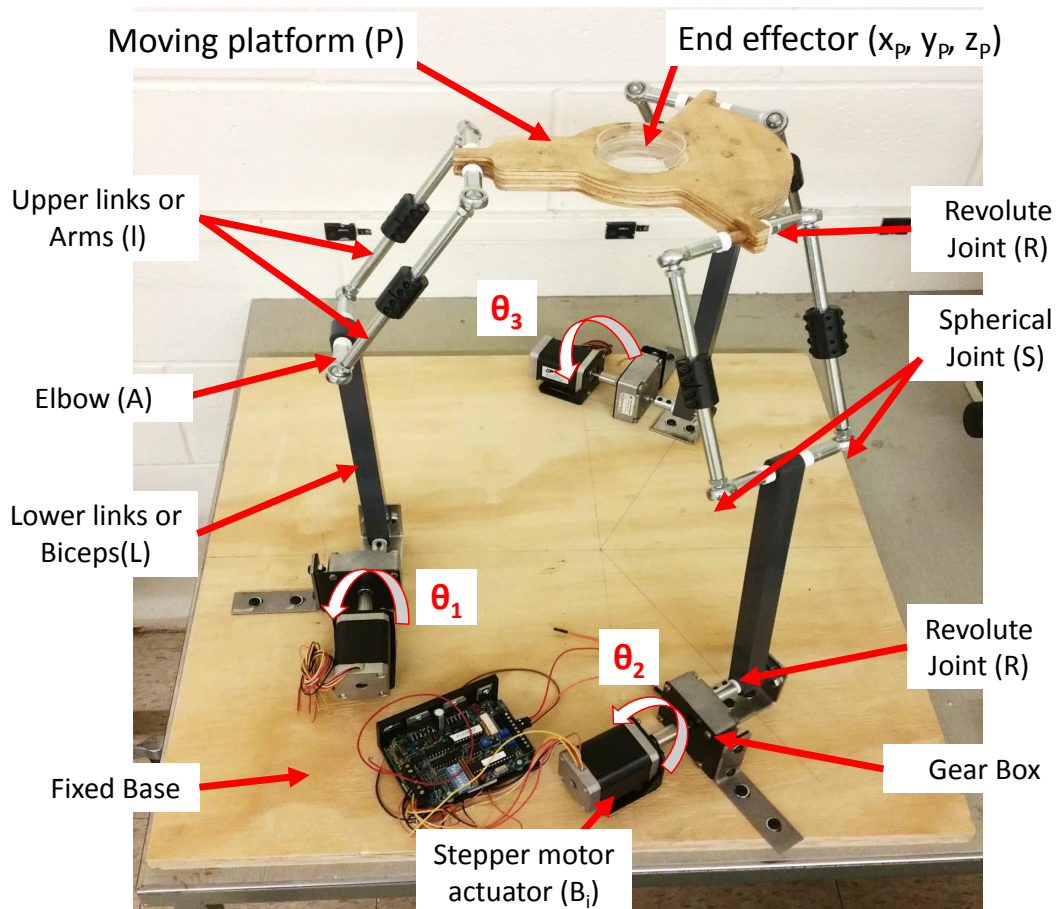
Figure 4.41: 3-RSR Parallel Delta Manipulator: Parts Assembly
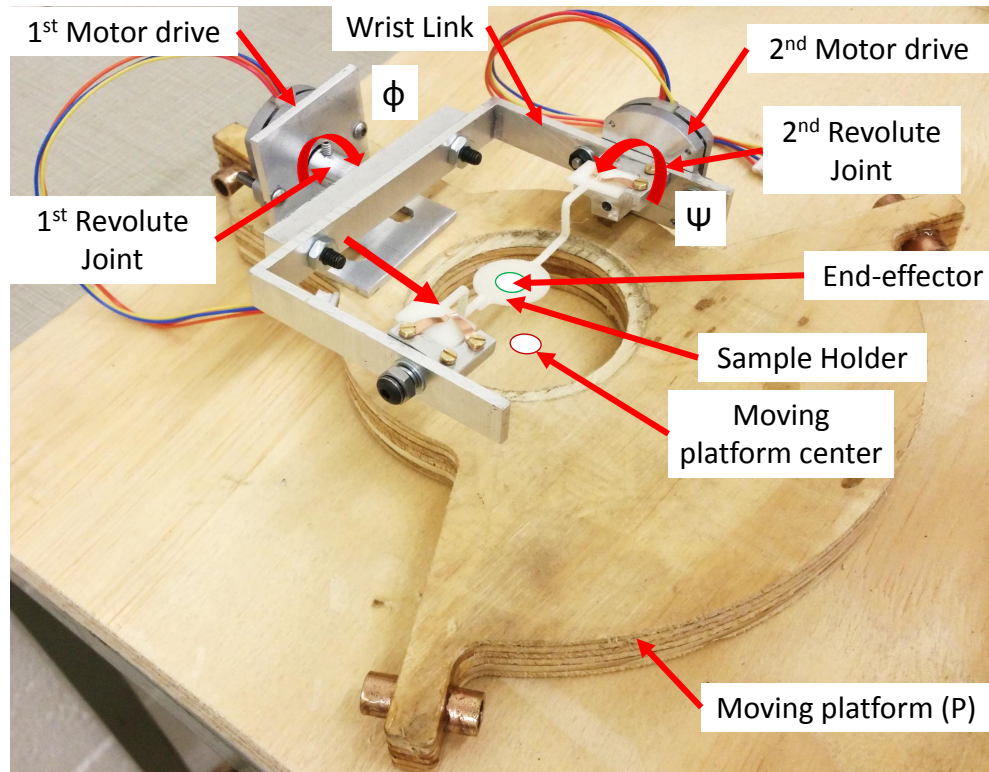
Figure 4.42: 2-DOF RR Serial $\perp^{lr}$ axis Manipulator: Parts Assembly
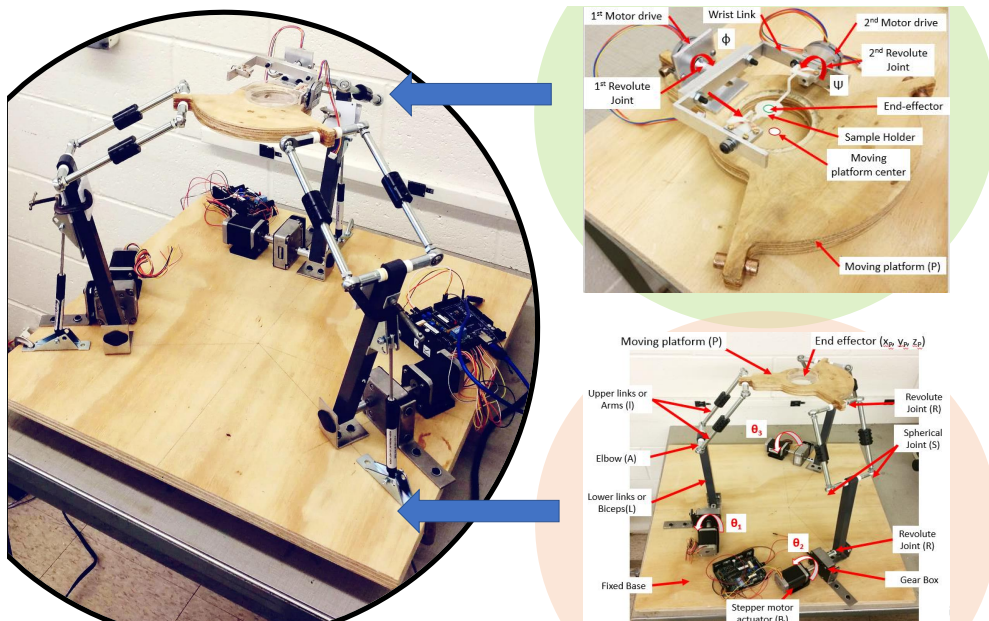
Figure 4.43: 3-RSR Parallel Delta Manipulator: Parts Assembly and 2-DOF RR

Serial $\perp^{lr}$ axis Manipulator: Parts Assembly

Following figure 4.44 shows the comparision of final integrated assembly of both 3-RSR Parallel Delta Manipulator and 2-DOF RR Serial $\perp^{lr}$ axis Manipulator with the CAD model of the same.
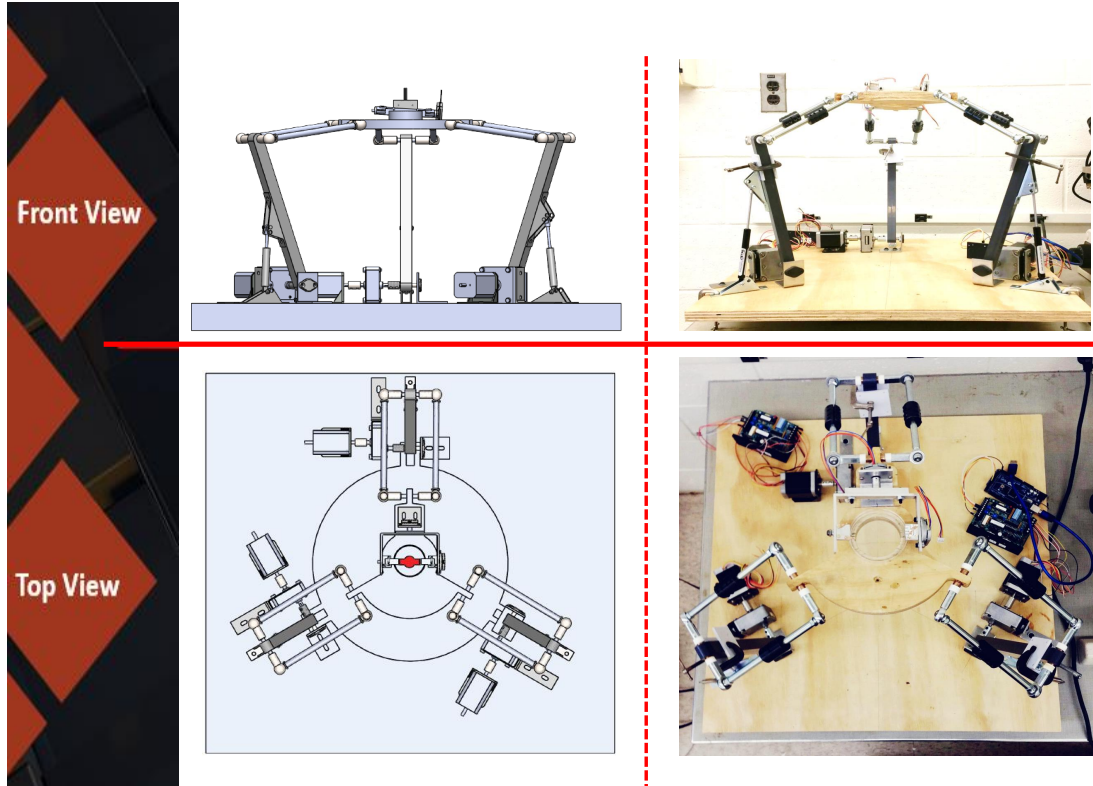
Figure 4.44: 3-RSR Parallel Delta Manipulator: Parts Assembly and 2-DOF RR Serial $\perp^{lr}$ axis Manipulator: Comparision between CAD assembly and Parts Assembly

Chapter 5

Manipulation and Control

As discussed in the inverse kinematics section for the 3-DOF RSR Parallel Delta Manipulator and 2-DOF RR Serial $\perp^{lr}$ axis Manipulator, 3.1.3 and 3.2.4 the desired coordinates of the manipulators can be obtained by finding the input angles and actuating controlling the motors. In order to achieve the tracking control of the active joint angles, which are generated from the motors mounted on the active joints, a controller shall be designed [54]. It is necessary to be able to measure the active joint angles with required accuracy (i.e. $0.012°$ for $10\mu m$ and $0.0005°$ for $5\mu m$ resolution) to control the motion precisely for the micro manipulation of the stage.

5.1 Control Block Diagram

Figure 5.1 shows the block diagram of the control system [54], where E_i are the voltages applied to the motors, and the subscript refers to reference signals. First block is the path planning (i.e. creating points for trajectory) (x_P, y_P, z_P). The second block converts the given trajectory points into an input angles. The third block is a controller, which computes voltage signals E_i of the motors based on the desired active joint angles. The last block is the direct kinematics, which can evaluates the actual coordinates (x_P, y_P, z_P) and/or (x_E, y_E, z_E).
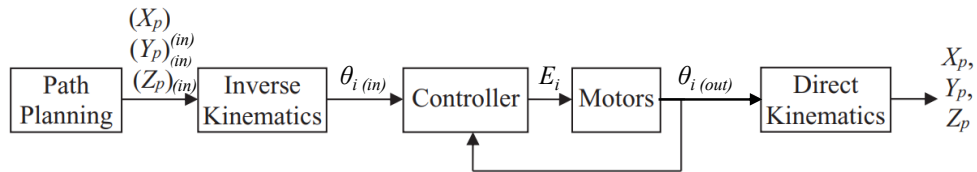
Figure 5.1: Position based control for the manipulator

Furthermore, the figure 5.1 can be separated in to three parts. The following figure 5.3 shows the actual implementation of the block diagram. This is explained as below:
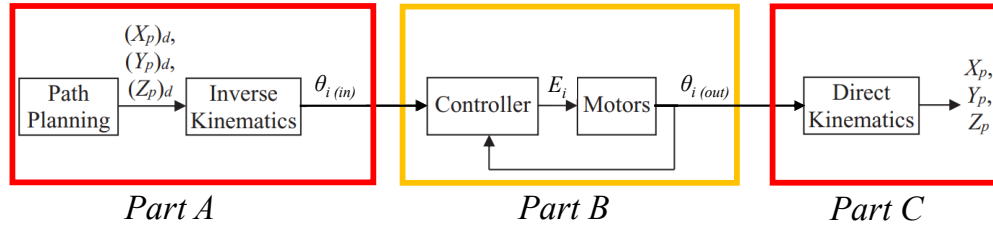
Figure 5.2: Position based control for the manipulator separated into parts
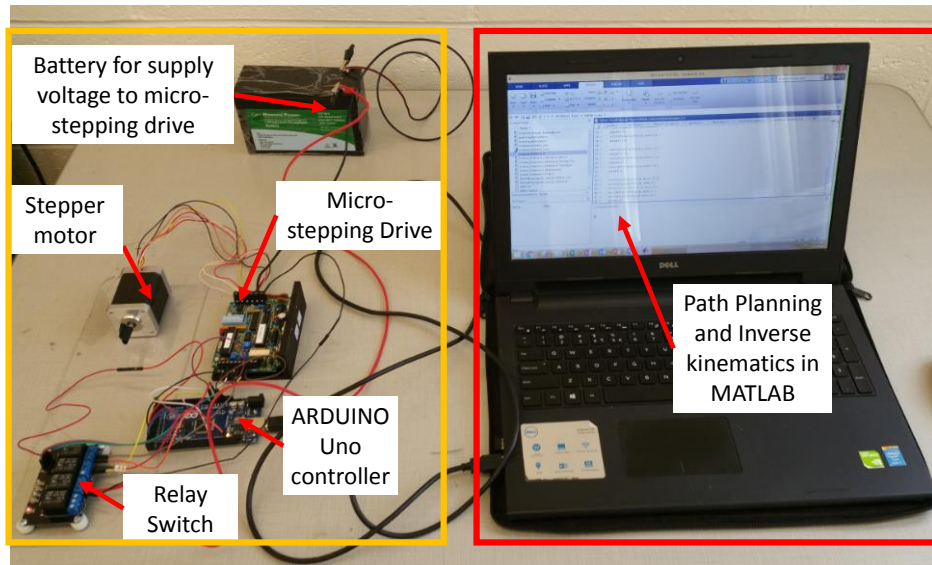
Figure 5.3: Control setup

1. **Part A**: Path planning and Inverse kinematics are achieved using MATLAB which consists of Part A. The input of Part A i.e. (x_P, y_P, z_P) and/or (x_E, y_E, z_E) are processed in the MATLAB code on the computer for a given trajectory to calculate required input angles i.e. $\{\theta_1, \theta_2, \theta_3\}$ and/or $\{\phi, \psi\}$ for the Part B.

2. **Part B**: For controlling the stepper motors microstepping drives [55] are used with Arduino Uno controller. In future, Arduino would be replace by a Data Aquisition card. MATLAB code converts the angle generated by part A into the signals to Arduino controller. The stepper motor drive receives these signal to run

the motors at a given speed (controlled by ARDUINO output analog voltage,which is controlled by MATLAB code). Once the motors are run the inclination sensors shall be used to check the $\theta_{i(out)}$

On the 3540MO, microstepping resolution is fixed at 12,800 steps/revolution, which is equal to 0.0028° resolution. Connecting a gearbox with the gear reduction increases its resolution further more.

3. **Part C**: In this part the Matlab code calculates the direct kinematics and checks the end effector coordinates for given the output angles

In order to make this motion controlled inclination sensors and position sensors shall be used in future to make this a closed loop system. From the inclination sensors we can check the actual output angles against the output angles required to achieve that given point. This can be corrected in a closed loop for the error reduction.

5.2   Matlab Simulation

5.2.1   3-DOF RSR Parallel Delta Manipulator: MATLAB Simulation

A simulation of the motion is created in MATLAB environment to understand the working of the 3-DOF RSR Parallel Delta Manipulator in terms of input angles and output target trajectory as a part of the control block diagram.
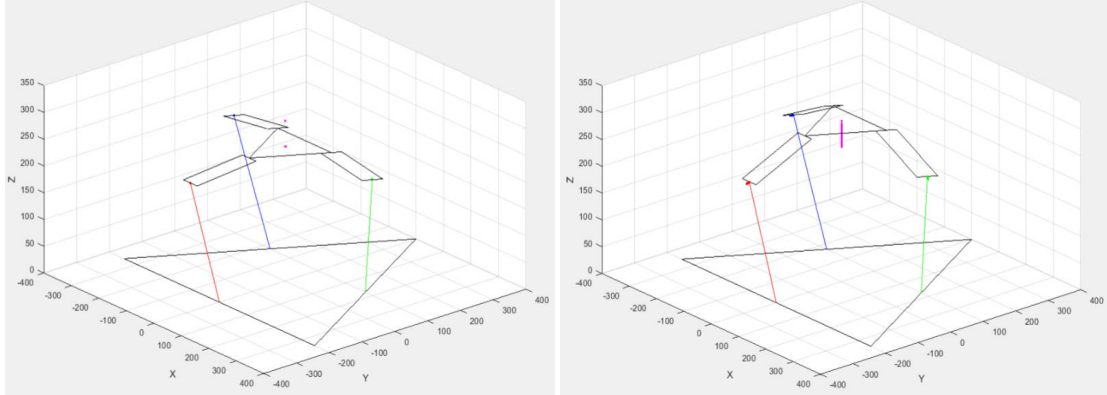
(a) Straight line trajectory simulation initial point $(0, 0, 250)$

(b) Straight line trajectory simulation Final point $(0, 0, 300)$

Figure 5.4: Straight line trajectory simulation from $(0, 0, 250)$ to $(0, 0, 300)$
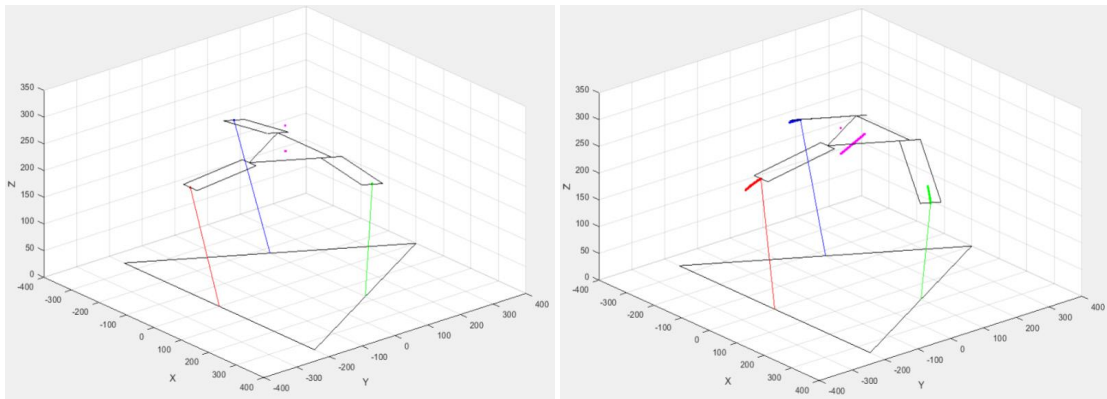
(a) Cross line trajectory simulation initial point $(0, 0, 250)$

(b) Cross line trajectory simulation Final point $(50, 50, 300)$

Figure 5.5: Cross line trajectory simulation from $(0, 0, 250)$ to $(50, 50, 300)$

The figure 5.4 and figure 5.5 on page number 92 shows the trajectory simulation of

the end-effector on a 3-DOF RSR Parallel Delta Manipulator following a straight and cross line respectively in 3-D. The figure 5.6 shows the simulation of the end-effector on a 3-DOF RSR Parallel Delta Manipulator following a circular trajectory of radius= 40 mm at z = 300 mm. It also shows the intermediate path followed by the end-effector and the passive spherical (i.e.elbow) joints. This gives a better idea of the performance of 3-DOF RSR Parallel Delta Manipulator by illustrating the links, joints and end-effector's motion.
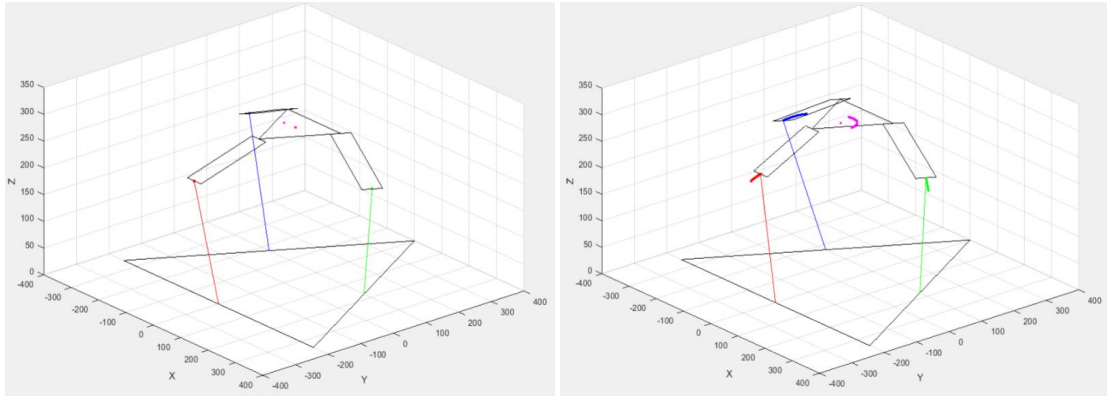
(a) Circular trajectory simulation initial point $(40, 0, 300)$

(b) Circular trajectory simulation intermediate point $(0, 40, 300)$
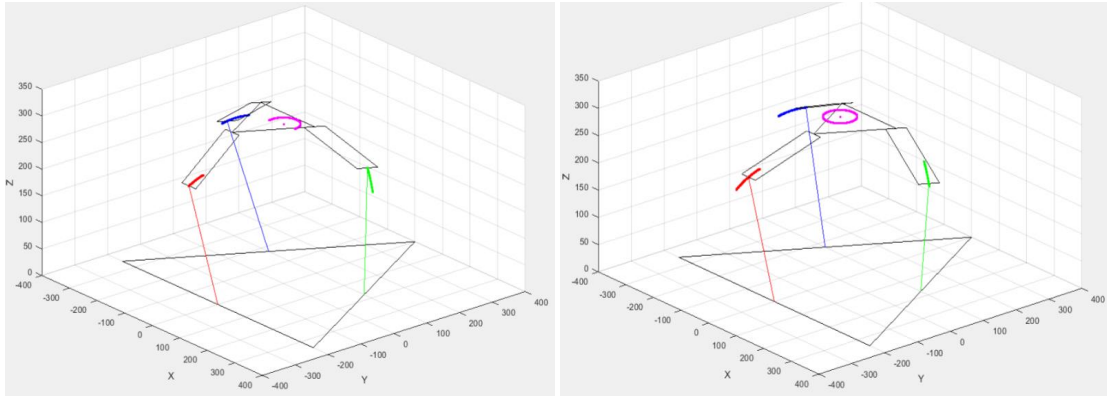
(c) Circular trajectory simulation intermediate point $(-40, 0, 300)$

(d) Circular trajectory simulation final point $(40, 0, 300)$

Figure 5.6: Circular trajectory simulation for circle with radius 40 mm @ z=300 mm

5.2.2   2-DOF RR Serial $\perp^{lr}$ axis Manipulator: MATLAB Simulation

After calculating the inverse kinematics a MATLAB simulation is created to understand the working of the 2-DOF RR Serial $\perp^{lr}$ axis Manipulator in terms of input angles and output target.

Following is the figure 5.7 which illustrates the Matlab simulation for the rotation of the first revolute joint by an input angle ϕ from 0 to 30 degrees. And the figure 5.8 illustrates the Matlab simulation for the rotation of the second revolute joint by an input angle ψ from 0 to 30 degrees.

(a) Initial position　　　　　　　　　　　　(b) Final position
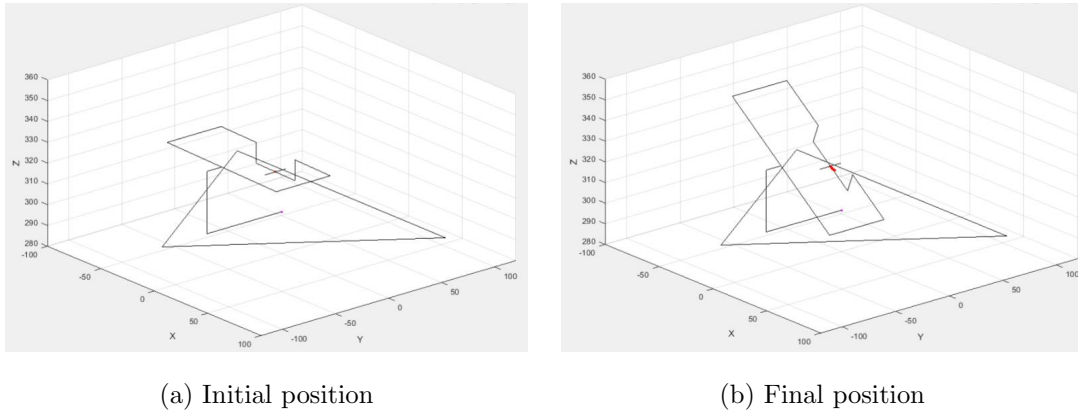
Figure 5.7: 1st Revolute joint actuation from 0 to 30°

(a) Initial position　　　　　　　　　　　　(b) Final position
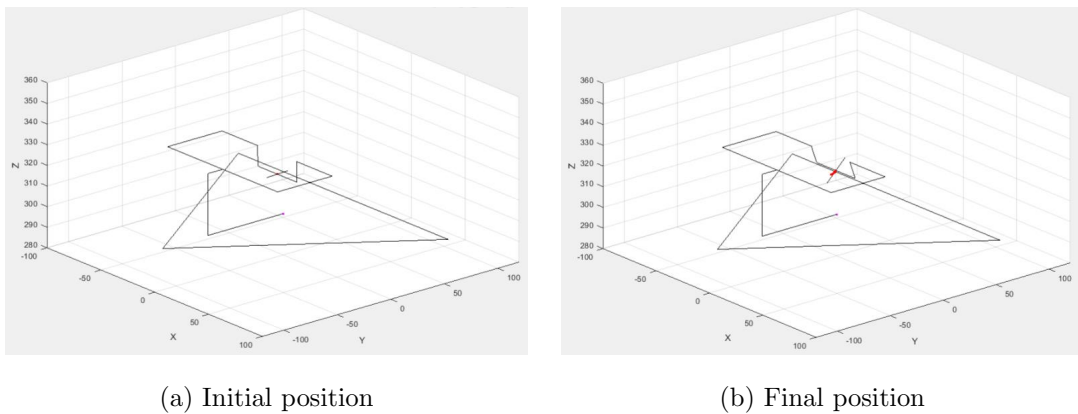
Figure 5.8: 2nd Revolute joint actuation from 0 to 30°

Finally, the figure 5.9 shows the Matlab simulation for the rotation of the first and

second revolute joint simultaneously by an input angle ϕ and ψ respectively from 0 to

30 degrees
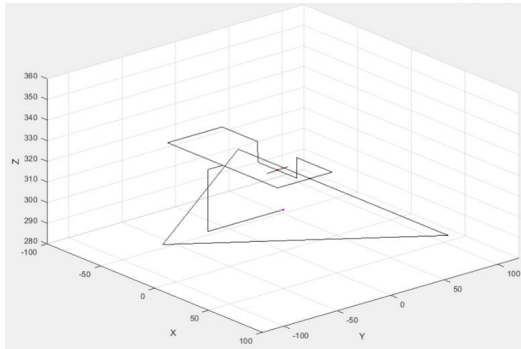
(a) Initial position
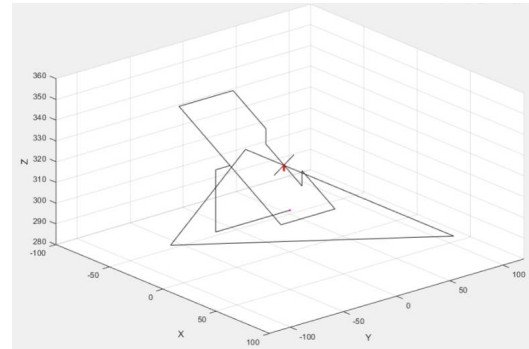
(b) Final position

Figure 5.9: 1st and 2nd Revolute joint actuation from 0 to $30°$

5.2.3 3-DOF RSR Parallel Delta Manipulator and 2-DOF RR Serial $\perp^{lr}$ axis Manipulator: MATLAB Simulation

MATLAB simulation is created to understand the working of the 3-DOF RSR Parallel Delta Manipulator and 2-DOF RR Serial $\perp^{lr}$ axis Manipulator as a combination in terms of input moving platform point $^{B}P_P = \{x_P \quad y_P \quad z_P\}^T$ and rotation angles ϕ and ψ. A MATLAB code was generated to create set of points which are given as an input to the inverse kinematics code. This then generated the required actuator angles and creates a diagram in a loop.

Figure 5.10a which illustrates the Matlab simulation for achieving position $^{B}P_P = \{0 \quad 0 \quad 300\}^T$ and rotation angles $\phi = 0°$ and $\psi = 0°$. And the figure 5.10b illustrates the Matlab simulation for reaching position $^{B}P_P = \{0 \quad 0 \quad 250\}^T$ and rotation angles $\phi = 30°$ and $\psi = 30°$.
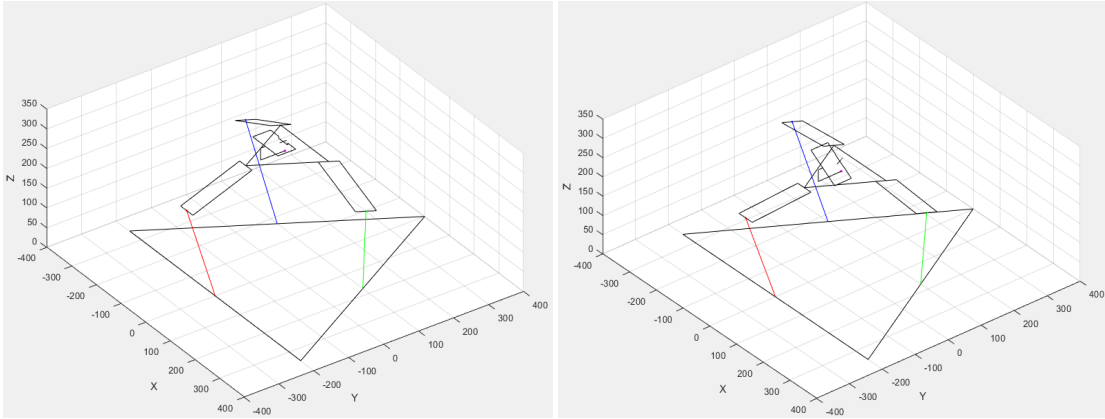
(a) Position $^{B}P_P = \{0 \quad 0 \quad 300\}^T$ and rotation angles $\phi = 0\circ$ and $\psi = 0\circ$

(b) Position $^{B}P_P = \{0 \quad 0 \quad 250\}^T$ and rotation angles $\phi = 30\circ$ and $\psi = 30\circ$

Figure 5.10: Matlab Simulation for combination of 3-DOF RSR Parallel Delta Manipulator and 2-DOF RR Serial $\perp^{lr}$ axis Manipulator

Chapter 6

Discussions and Conclusion

6.1   Discussion

Initially, two non-destructive methods of cell imaging i.e. atomic force microscopy and optical microscopy were discussed briefly. Their individual advantages and disadvantages are compared and reviewed. A need to combine both the technology was recognized and studied. Furthermore, the limitations were identified and research focus was defined. The main focus of this research was to develop a manipulator configuration for the large range and 3D manipulation of the sample holder so that both Optical Inverse Microscope and Atomic force microscope can access the sample for observation and carrying out micro-studies.

In the second section the OIM and AFM setup was identified, analyzed and several components critical for the manipulation were defined. This analysis of the setup helped in establishing the target specifications for the manipulator. Furthermore, various manipulators were studied and reviewed for their advantages and disadvantages. This proved to be critical in the selection of the manipulator configuration. The configuration finalized was a hybrid manipulator integrating parallel and series manipulator for the translation and rotation motion of the end-effector.

After, selection of concept both the 3-DOF RSR Parallel Delta Manipulator and 2-DOF RR Serial $\perp^{lr}$ axis Manipulator were described and studied for their kinematics. Both inverse and direct kinematics were performed. In this section all the critical link dimensions were selected based on the study of the workspace for 3-DOF RSR Parallel Delta Manipulator. Once, the link dimensions were finalized the workspace generated using the inverse and direct kinematics was compared to the target specified in the earlier chapter. After satisfactory results the link lengths were finalized for the

fabrication of the prototype. Kinematics study was also performed for the combination of both the manipulator.

In Chapter 4, the focus was to develop a prototype for the configuration proposed in the previous chapter. For which CAD models were created for system level design. This, CAD model helped a lot to identify all the difficulties and problems that might have aroused in future. Hence, creating a CAD model saved a lot of time and investment. Furthermore, these CAD system level designs were developed to a detailed level design by reiteration of market survey, parts and components availability, cost of machining etc.. This section provides a detailed Bill of Materials that was used for the assembly of the complete prototype. A brief description is provided on the use of CAM as an aided technology for machining and fabricating the parts. At the last, a complete assembly is compared with the CAD model for its completeness.

Chapter 5 briefly discusses the block diagram for the control of the entire configuration. The actual setups is compared with the block diagram. Finally, MATLAB simulation was performed to check the performance of the, manipulators for following a particular trajectory and achieving certain target point with a given orientation.

6.2 Conclusion and contributions

A 3-DOF RSR Parallel Delta Manipulator and 2-DOF RR Serial $\perp^{lr}$ axis Manipulator are combined together to form a hybrid configuration. In which the linear long range translation is provided by Parallel manipulator and the orientation of the end effector is given by Series revolute manipulator. Additionally, the focus was also to make sure that the manipulator is robust and less prone to vibrations induced internally and externally. To resolve this issue of vibrations three gas springs were attached to the lower links of the 3-DOF RSR Parallel Delta Manipulator. OIM was studied for its Optical focus and target workspace was defined and achieved on its basis. Furthermore, the space constraints due to the tight assembly of AFM and OIM moving parts were taken into the considerations while designing the CAD model and the prototype assembly.

6.3 Future Work

1. Velocity and acceleration studies shall be performed for the model based control of the complete setup with a GUI

2. A dynamic model can be created from the CAD model in MATLAB environment for better dynamic analysis of the combined manipulator setup.

3. Furthermore, compliance can be introduced to increase the manipulator's performance for stability, reliability and most importantly overall safety of the robot during human interaction.

4. A closed loop system control with the sensors would be critical for micro-manipulation for errors identification and reducing it.

5. Calibration and accuracy studies needs to be performed to confirm the resolution of the end-effector motion.

Bibliography

[1] Yangjie Wei, Chendong Wu, and Zaili Dong. State-of-the-art optical microscopy and afm-based property measurement of nanostructure materials. In Mahmood Aliofkhazraei, editor, *Handbook of mechanical nanostructuring, First Edition.*, pages 81–114. Wiley-VCH Verlag GmbH & Co. KGaA., 2015.

[2] Zoran Pandilov and Vladimir Dukovski. Comparison of the characteristics between serial and parallel robots. *Acta Technica Corvininesis - Bulletin of Engineering*, 7(1):143 – 160, 2014. ISSN 20673809. URL `https://login.proxy.libraries.rutgers.edu/login?url=https://search.ebscohost.com/login.aspx?direct=true&db=aph&AN=95030788&site=eds-live`.

[3] Yashavant Patel and P M. George. Parallel manipulators applications—a survey. *Modern Mechanical Engineering*, 2:57–64, 08 2012. doi: 10.4236/mme.2012.23008.

[4] Sameer A. Joshi. *A comparative study 3-DOF parallel manipulators.* PhD thesis, Graduate School of the University of Maryland, College Park, 2002. URL `https://search.proquest.com/docview/251769697?accountid=13626`. Copyright - Database copyright ProQuest LLC; ProQuest does not claim copyright in the individual underlying works; Last updated - 2016-05-12.

[5] Aqleem Siddiqui Swapnil S. Jogal, K. Jayarajan. Effect of link length ratio on the workspace of a delta robot. *International Journal of Engineering and Advanced Technology (IJEAT)*, 5(4):103–106, April 2016. ISSN 2249 – 8958.

[6] Image of afm parts with labelling, 2019. [Online] `http://mcf.tamu.edu/wp-content/uploads/2016/09/Icon-AFM-Instructions_Sep2012.pdf` [Last accessed: 18 March 2019].

[7] Steven M. Lavelle. Planning algorithms, 2006 cambridge university press, 2019. [Online] `http://planning.cs.uiuc.edu/node109.html` [Last accessed: 19 March 2019].

[8] Mark W Spong, Seth Hutchinson, Mathukumalli Vidyasagar, et al. *Robot modeling and control.* New York: Wiley, 2006.

[9] OMEGA Engineering. Stepper motor - omht17-278, 2018. [Online] `https://www.omega.com/pptst/OMHT_SERIES.html#order` [Last accessed: 4 May 2018].

[10] Amazon Beauty Star. Stepper motor mounting bracket, 2018. [Online] `https://www.amazon.com/dp/B071NWWB7Z/ref=sspa_dk_detail_0?psc=1` [Last accessed: 27 July 2018].

[11] Stock Drive Products Sterling Instrument SDP/SI. Shaft couplings (metric), 2018. [Online] `http://shop.sdp-si.com/catalog/product/?id=S51CYYM050060` [Last accessed: 6 July 2018].

[12] Stock Drive Products Sterling Instrument SDP/SI. Speed reducers - parallel shaft, 2018. [Online] `https://shop.sdp-si.com/catalog/Product.aspx?id=A_2Z25M0500` [Last accessed: 6 July 2018].

[13] McMaster Carr. Corner machine bracket, 2018. [Online] `https://www.mcmaster.com/2313n22` [Last accessed: 25 September 2018].

[14] Stock Drive Products Sterling Instrument SDP/SI. Shaft couplings (metric), 2018. [Online] `http://shop.sdp-si.com/catalog/product/?id=A_5C_9-0808` [Last accessed: 6 July 2018].

[15] McMaster Carr. Dowel pin, 2018. [Online] `https://www.mcmaster.com/97395a499` [Last accessed: 9 June 2018].

[16] McMaster Carr. Light duty mounted ball bearing, 2018. [Online] `https://www.mcmaster.com/4575n33` [Last accessed: 6 July 2018].

[17] McMaster Carr. Corner machine bracket, 2018. [Online] `https://www.mcmaster.com/2313n13` [Last accessed: 25 September 2018].

[18] McMaster Carr. Connecting rod, 2018. [Online] `https://www.mcmaster.com/6516k112` [Last accessed: 25 September 2018].

[19] McMaster Carr. Abrasion-resistant eptfe plastic sealing washer, 2018. [Online] `https://www.mcmaster.com/96371a201` [Last accessed: 8 November 2018].

[20] McMaster Carr. Ball joint, 2018. [Online] `https://www.mcmaster.com/60745k821` [Last accessed: 25 September 2018].

[21] McMaster Carr. Connecting rod: Internal threads, 2018. [Online] `https://www.mcmaster.com/6516k53` [Last accessed: 25 September 2018].

[22] McMaster Carr. Two-piece shaft coupling, 2018. [Online] `https://www.mcmaster.com/60845k32` [Last accessed: 25 September 2018].

[23] McMaster Carr. Gas spring 5 lbs. force, 2018. [Online] `https://www.mcmaster.com/9417k4` [Last accessed: 28 January 2019].

[24] Nanotec Electronics. Ultraflat stepper motor, 2018. [Online] `https://us.nanotec.com/products/597-stf2818x0504-a-ultraflat-stepper-motor/` [Last accessed: 4 November 2018].

[25] McMaster Carr. Corner mcahine bracket, 2018. [Online] `https://www.mcmaster.com/2313n43` [Last accessed: 4 November 2018].

[26] McMaster Carr. Architectural 6063 aluminum u-channel, 2018. [Online] `https://www.mcmaster.com/9001k94` [Last accessed: 4 November 2018].

[27] Inc. Ted Pella. Pelco semclip^{TM} clips, 2018. [Online] `https://www.tedpella.com/SEMmod_html/SEMmod3.htm#prod.no.15494` [Last accessed: 4 November 2018].

[28] Yves F. Dufrêne. Atomic force microscopy, a powerful tool in microbiology. *Journal of Bacteriology*, 184(19):5205–5213, 2002. ISSN 0021-9193. doi: 10.1128/JB.184.19.5205-5213.2002. URL `https://jb.asm.org/content/184/19/5205`.

[29] Nikolaj Gadegaard. Atomic force microscopy in biology: technology and techniques. *Biotechnic & Histochemistry*, 81(2-3):87–97, 2006.

[30] Ahmed Touhami, Manfred H. Jericho, and Terry J. Beveridge. Atomic force microscopy of cell growth and division in staphylococcus aureus. *Journal of Bacteriology*, 186(11):3286–3295, 2004. ISSN 0021-9193. doi: 10.1128/JB.186.11.3286-3295. 2004. URL `https://jb.asm.org/content/186/11/3286`.

[31] Ying Wu, Qingze Zou, and Chanmin Su. A current cycle feedback iterative learning control approach for afm imaging. *IEEE Transactions on Nanotechnology*, 8(4): 515–527, July 2009. ISSN 1536-125X. doi: 10.1109/TNANO.2009.2015051.

[32] Kristina Haase and Andrew E. Pelling. Investigating cell mechanics with atomic force microscopy. *Journal of the Royal Society, Interface, 12(104), 20140970.*, 12 (104), 2015. doi: 10.1098/rsif.2014.0970. URL `https://doi.org/10.1098/rsif.2014.0970`.

[33] Nicholas A. Geisse. Afm and combined optical techniques. *Materials Today*, 12(7):40 – 45, 2009. ISSN 1369-7021. doi: https://doi.org/10.1016/S1369-7021(09)70201-9. URL `http://www.sciencedirect.com/science/article/pii/S1369702109702019`.

[34] Bruker. Technical details for dimension icon head - atomic force microscope from bruker, 2019. [Online] `https://www.bruker.com/products/surface-and-dimensional-analysis/atomic-force-microscopes/dimension-icon/technical-details.html` [Last accessed: 16 March 2019].

[35] Nikon Corporation. Inverted microscope diaphot 200 from nikon corporation, 2019. [Online] `https://www.classe.cornell.edu/~hoff/LECTURES/09S_510/G10/G10_Microscope_Manual.pdf` [Last accessed: 16 March 2019].

[36] Dimension icon head - atomic force microscope from bruker, 2019. [Online] `https://www.researchgate.net/profile/Hf_Haghshenas/publication/309855179/figure/fig21/AS:427304796069899@1478888810579/15-Bruker-Dimension-Icon-Atomic-Force-Microscope_W640.jpg` [Last accessed: 17 March 2019].

[37] Inverted microscope diaphot 200 from nikon corporation, 2019. [Online] `https://www.spachoptics.com/DIAPHOT-200-p/nikon-diaphot-200-phase.htm` [Last accessed: 17 March 2019].

[38] Sébastien Briot and Ilian Bonev. Are parallel robots more accurate than serial robots? *Transactions of the Canadian Society for Mechanical Engineering*, 31: 445–455, 11 2007. doi: 10.1139/tcsme-2007-0032.

[39] Parth Patel, Palash Gala, Tanay Desai, and Abdul KadirBurhan. Development and control of shot – peening mechanism using industrial controller, 2015. Undergraduate Thesis.

[40] Vincenzo Parenti and Castelli Werner Schiehlen. Position kinematics of a 3-rrs parallel manipulator. In *ROMANSY 21 - Robot Design, Dynamics and Control*, pages 66–72, June 2016. doi: 10.1007/978-3-319-33714-2.

[41] R. Clavel. Delta, a fast robot with parallel geometry. In C. W. Burckhardt, editor, *Proc of the 18th International Symposium on Industrial Robots*, pages 91–100, New York, 1988. Springer-Verlag.

[42] M Pranav, A Mukilan, and Sundar Ganesh c s. A novel design of delta robot. *International Journal of Multidisciplinary Research and Modern Education*, 2:365–377, 11 2016. doi: 10.5281/ZENODO.168568.

[43] R.L. Williams II. "The Delta Parallel Robot: Kinematics Solutions", internet publication, April 2015. `www.ohio.edu/people/williar4/html/pdf/DeltaKin.pdf` [Last accessed: 19 March 2019].

[44] R.L. Williams II, J.S. Albus, and R.v. Bostelman. "3D Cable-Based Cartesian Metrology System". *Journal of Robotic Systems, 21*, 5:235–257, 2004.

[45] Abdolreza Gharahsofloo and Ali Rahmani. An efficient algorithm for workspace generation of delta robot. *International Journal of Robotics Theory and Applications*, 4:48–53, 08 2015.

[46] Anjan Kumar Dash, Song Huat Yeo, Guilin Yang, and I-Ming Chen. Workspace analysis and singularity representation of three-legged parallel manipulators. In *7th International Conference on Control, Automation, Robotics and Vision, 2002. ICARCV 2002.*, volume 2, pages 962–967 vol.2, Dec 2002. doi: 10.1109/ICARCV. 2002.1238554.

[47] John J. Craig. *Introduction to Robotics: Mechanics and Control (3rd Edition)*. Prentice Hall, 3 edition, August 2004. ISBN 0201543613. URL `http://www.amazon.com/exec/obidos/redirect?tag=citeulike07-20\&path=ASIN/0201543613`.

[48] George N Sandor and A. G. Erdman. *Advanced Mechanism Design: Analysis and Synthesis, Vol. II*. Prentice Hall, 1984.

[49] Richard M Murray. *A mathematical introduction to robotic manipulation*. CRC press, 2017.

[50] J Michael McCarthy and Gim Song Soh. *Geometric design of linkages*, volume 11. Springer Science & Business Media, 2010.

[51] Metals Depot. Steel plate, 2018. [Online] `https://www.metalsdepot.com/steel-products/steel-plate` [Last accessed: 7 September 2018].

[52] McMaster Carr. Heavy duty 0.16" id eyelet mounting bracket for gas spring, 2018. [Online] `https://www.mcmaster.com/9417k92` [Last accessed: 28 January 2019].

[53] Mecsoft Corporation. Visualcamc – production cam for onshape, 2019. [Online] `https://mecsoft.com/visualcamc/` [Last accessed: 24 March 2019].

[54] Yong-Lin Kuo and Peng-Yu Huang. Experimental and simulation studies of motion control of a delta robot using a model-based approach. *International Journal of Advanced Robotic Systems*, 14(6):1729881417738738, 2017. doi: 10.1177/1729881417738738. URL `https://doi.org/10.1177/1729881417738738`.

[55] OMEGA Engineering. Microsepping motor drives, 2018. [Online] `https://www.omega.com/pptst/3540M.html` [Last accessed: 25 March 2019].